Rajat Bajaj

STUDIES ON RARE EARTH DOPED LUMINESCENT MATERIALS FOR APPLICATIONS IN GENERAL ILLUMINATION AND BIO-P

Delhi Technological University

Document Details

Submission ID
trn:oid:::27535:96207970

Submission Date
May 16, 2025, 1:34 PM GMT+5:30

Download Date
May 16, 2025, 3:06 PM GMT+5:30

File Name
Rajat Bajaj Thesis R (1).docx

File Size
14.7 MB

179 Pages

35,120 Words

191,816 Characters

6% Overall Similarity

The combined total of all matches, including overlapping sources, for each database.

Filtered from the Report

- Bibliography
- Small Matches (less than 14 words)

Exclusions

- 404 Excluded Matches

Match Groups

- 68 Not Cited or Quoted 6%
  Matches with neither in-text citation nor quotation marks
- 0 Missing Quotations 0%
  Matches that are still very similar to source material
- 2 Missing Citation 0%
  Matches that have quotation marks, but no in-text citation
- 0 Cited and Quoted 0%
  Matches with in-text citation present, but no quotation marks

Top Sources

- 4% Internet sources
- 3% Publications
- 2% Submitted works (Student Papers)

Integrity Flags

2 Integrity Flags for Review

- Replaced Characters
  41 suspect characters on 27 pages
  Letters are swapped with similar characters from another alphabet.
- Hidden Text
  56 suspect characters on 7 pages
  Text is altered to blend into the white background of the document.

Our system's algorithms look deeply at a document for any inconsistencies that would set it apart from a normal submission. If we notice something strange, we flag it for you to review.

A Flag is not necessarily an indicator of a problem. However, we'd recommend you focus your attention there for further review.

Match Groups

- **68** Not Cited or Quoted 6%
  Matches with neither in-text citation nor quotation marks
- **0** Missing Quotations 0%
  Matches that are still very similar to source material
- **2** Missing Citation 0%
  Matches that have quotation marks, but no in-text citation
- **0** Cited and Quoted 0%
  Matches with in-text citation present, but no quotation marks

Top Sources

- 4% Internet sources
- 3% Publications
- 2% Submitted works (Student Papers)

Top Sources

The sources with the highest number of matches within the submission. Overlapping sources will not be displayed.

1	Internet	www.researchgate.net 2%
2	Internet	dspace.dtu.ac.in:8080 <1%
3	Submitted works	Visvesvaraya Technological University on 2015-08-17 <1%
4	Submitted works	Delhi Technological University on 2019-01-31 <1%
5	Publication	Ravita, Aman Prasad, Pooja Rohilla, Rajat Bajaj, Anu, Rajesh Punia, Allam Srinivas... <1%
6	Submitted works	Chaudhary Ranbir Singh University on 2025-05-13 <1%
7	Submitted works	Jawaharlal Nehru Technological University on 2022-07-23 <1%
8	Internet	www.encyclopedia.com <1%
9	Submitted works	University of the Free State on 2020-12-15 <1%
10	Internet	scholar.ufs.ac.za <1%

11	Submitted works	
IIT Delhi on 2013-10-25		<1%
12	Publication	
Mahamuda, Sk., K. Swapna, P. Packiyaraj, A. Srinivasa Rao, and G. Vijaya Prakash. ...		<1%
13	Publication	
R Rajaramakrishna, Jakrapong Kaewkhao. "Glass material and their advanced ap...		<1%
14	Submitted works	
University College London on 2021-05-22		<1%
15	Publication	
Nisha Deopa, A.S. Rao, Sk. Mahamuda, Mohini Gupta, M. Jayasimhadri, D. Haranat...		<1%
16	Submitted works	
The University of Wolverhampton on 2023-04-28		<1%
17	Submitted works	
Yeungnam University on 2022-05-23		<1%
18	Internet	
umpir.ump.edu.my		<1%
19	Submitted works	
Anna University on 2024-12-23		<1%
20	Publication	
R. Falihan, L. Hasnimulyati, N. A. Abdul-Manaf, W. Y. W. Yusoff, A. H. Azmi, A. Azur...		<1%
21	Internet	
www.x-mol.com		<1%
22	Submitted works	
Inter-University Accelerator Centre on 2017-07-05		<1%
23	Publication	
Ravita, Aman Prasad, Pooja Rohilla, Ankur Shandilya, A.S. Rao. "Photoluminescen...		<1%
24	Submitted works	
Indian Institute of Engineering Science and Technology on 2021-11-28		<1%

25 Publication
Sandeep Sharma, A.S. Rao, Kamal Kishore. "Energy transfer dynamics in thermall... <1%

26 Internet
ouci.dntb.gov.ua <1%

27 Submitted works
BML Munjal University on 2017-12-27 <1%

28 Internet
lib.buet.ac.bd:8080 <1%

29 Internet
www.eprint.iitd.ac.in <1%

30 Submitted works
Texas A&M University, Central Texas on 2025-05-11 <1%

31 Publication
Umer Mushtaq, Vijay Kumar. " Effect of Eu doping on the structural, optical, and ... <1%

32 Submitted works
Universiti Teknologi Malaysia on 2018-08-08 <1%

33 Submitted works
Higher Education Commission Pakistan on 2020-02-11 <1%

34 Submitted works
Indian School of Mines on 2019-06-14 <1%

35 Publication
Nisha Deopa, A.S. Rao. "Spectroscopic studies of Sm 3+ ions activated lithium lead... <1%

36 Publication
Rajat Bajaj, Pooja Rohilla, Aman Prasad, Ravita, Ankur Shandilya, Allam Srinivasa ... <1%

37 Submitted works
Universiti Teknologi Malaysia on 2017-01-29 <1%

38 Internet
www.akinik.com <1%

39 Internet

www.icomonline.org <1%

STUDIES ON RARE EARTH DOPED LUMINESCENT MATERIALS FOR APPLICATIONS IN GENERAL ILLUMINATION AND BIO-PHOTONICS

Thesis Submitted

in Partial Fulfillment of the Requirements for the

Degree of

DOCTOR OF PHILOSOPHY

in

Engineering Physics

by

Rajat Bajaj

Roll No. 2K18/Ph.D./AP/510

Under the joint Supervision of

Prof. A. S. Rao
Professor, Applied Physics
Delhi Technological University
Delhi, India

Prof. G. Vijay Prakash
Professor, Applied Physics
Indian Institute of Technology Delhi
(IITD) Delhi, India

Department of Applied Physics
DELHI TECHNOLOGICAL UNIVERSITY
(Formerly Delhi College of Engineering)
Shahbad Daulatpur, Main Bawana Road, Delhi-110042, India

May, 2025

DELHI TECHNOLOGICAL UNIVERSITY

(Formerly Delhi College of Engineering)

Shahbad Daulatpur, Main Bawana Road, Delhi-42

CANDIDATE'S DECLARATION

I, **Rajat Bajaj**, hereby certify that the work which is being presented in the thesis entitled "**Studies on Rare Earth Doped Luminescent Materials for Applications in General Illumination and Bio-photonics**" in partial fulfillment of the requirements for the award of degree of **Doctor of Philosophy** (Ph.D.) in Engineering Physics, submitted in the Department of Applied Physics, Delhi Technological University is an authentic record of my own work carried out during the period from January, 2018 to February, 2025 under the joint supervision of **Prof. A. S. Rao** and **Prof. G. Vijay Prakash.**

The matter presented in the thesis has not been submitted by me for the award of any other degree of this or any other Institute.

Candidate's Signature

This is to certify that the student has incorporated all the corrections suggested by the examiners in the thesis and the statement made by the candidate is correct to the best of our knowledge.

Signature of Supervisor (s) ***Signature of External Examiner***

DELHI TECHNOLOGICAL UNIVERSITY

(Formerly Delhi College of Engineering)

Shahbad Daulatpur, Main Bawana Road, Delhi-42

CERTIFICATE BY SUPERVISORS

This is to certify that **Mr. Rajat Bajaj** (enrollment No. 2K18/Ph.D./AP/510) has carried out their search work presented in the thesis entitled "**Studies on Rare Earth Doped Luminescent Materials for Applications in General Illumination and Bio-photonics**" for the award of **Doctor of Philosophy** in Engineering Physics discipline from Department of Applied Physics Delhi Technological University, Delhi, under our supervision. The thesis embodies result of original work, and studies are carried out by the student himself and the content of the thesis do not form the basis for the award of any other degree to the candidate or to anybody else from this or any other University/Institution.

Prof. A. S. Rao
Professor and Head
Department of Applied Physics
Delhi Technological University (DTU)
Shahbad Daulatpur, Delhi-110042

Prof. G. Vijay Prakash
Professor
Department of Physics
Indian Institute of Technology Delhi (IITD)
Hauz Khas, New Delhi, Delhi 110016

Date:

ACKNOWLEDGEMENTS

My study journey has been made possible by the invaluable assistance of numerous individuals. I feel sincerely grateful to acknowledge all those folks who have supported me either directly or indirectly through the finalization of my study effort. The fact that I can now thank each one of them is a pleasant feature. First and foremost, I want to express my gratitude to the goddess Saraswati, who has given me courage, guidance, and inspiration as I have traveled towards the research.

I would like to express my heartfelt gratitude and deep respect to my supervisor, ***Professor A. S. Rao****, Department of Applied Physics, Delhi Technological University, Delhi, for his exceptional guidance, unwavering support, and inspiring mentorship throughout the course of my research. His profound knowledge, insightful advice, and scientific intuition have been instrumental in shaping my growth as a researcher and in successfully completing this thesis. I am equally indebted to my co-supervisor,* ***Professor G. V. Prakash****, Department of Physics, IIT Delhi, for his consistent encouragement, valuable feedback, and critical insights that significantly enhanced the quality of my work. Their dedication, timely suggestions, and shared enthusiasm for research not only motivated me to tackle complex problems but also instilled in me a deeper appreciation for scientific inquiry. I feel truly privileged to have worked under such accomplished and supportive mentors, whose contributions have played a vital role in helping me achieve this academic milestone. I would also like to extend my sincere thanks to* ***Professor Prateek Sharma****, Vice Chancellor, Delhi Technological University (DTU), as well as* ***Professor Yogesh Singh*** *and* ***Professor J. P. Saini****, former Hon'ble Vice Chancellors of DTU, for their valuable support and encouragement. I am equally grateful to the university*

officials for providing excellent research facilities and a conducive academic environment that enabled the successful completion of my research work.

I would also like to express my heartfelt thanks to ***Professor Rinku Sharma****, Dean (Academic-PG), DTU, and* ***Professor Vinod Kumar****, Head of the Department od Applied Physics, DTU whose originality and insightful perspectives have significantly contributed to my intellectual growth and will continue to benefit me in the long term. Additionally, I extend my sincere appreciation to all the faculty and staff members of the Department of Applied Physics, DTU, for their unwavering support, assistance, and cooperation throughout the duration of my research.*

I express my gratitude to ***Dr. M. Jayasimhadri*** *of the Department of Applied Physics at DTU for providing the lab facilities necessary for the research. I express my gratitude to the chairman of the DRC, the members of the DRC, the SRC, and the other teaching and non-teaching personnel of the Applied Physics department.*

I would like to express my gratitude to my seniors, ***Dr. Nisha Deopa, Dr. Sumandeep Kaur, and Dr. Aman Prasad****, for their invaluable advice and help. My genuine gratitude goes out to my close friends, both past and present lab partners, and coworkers, whose encouragement enabled me to complete my work. To finish my research job, I would like to thank my fellow researchers,* ***Dr. Mukesh Sahu****,* ***Dr. Abhishek Bhardwaj****,* ***Dr. Mrityunjay Singh****,* ***Dr. Rajesh Kumar****,* ***Mr. Harender Mor****,* ***Mr. Lokesh*** *for their assistance whenever needed.*

I want to thank my family once again for their encouragement and support throughout my entire research period. My mother, ***Mrs. Indu Bala,*** *and father,* ***Mr. Janak Raj Bajaj,*** *have given me unwavering love and support throughout my life, and for that I am truly grateful. For their unwavering encouragement, support, nurturing, love, and belief in me throughout my life,*

*I am grateful to my wife **Mrs. Hitika Thakur**., have been my constant sources of inspiration, support, and motivation during this research project. I would like to express my gratitude to them for their unwavering support. I would also like to express my deep gratitude to my brothers, **Mr. Rajan Bajaj**, **Mr. Sajan Bajaj**, and **Mr. Rishav Bajaj**, for their unwavering spiritual support throughout the writing of this thesis and in all aspects of my life. Their understanding, cooperation, and sincere encouragement have been a constant source of strength and played a vital role in the successful completion of this work.*

I express my gratitude to everyone who assisted me in completing the thesis and realizing it successfully.

Thank you all!

(Rajat Bajaj)

New Delhi,

MAY-2025

ABSTRACT

STUDIES ON RARE EARTH DOPED LUMINESCENT MATERIALS FOR APPLICATIONS IN GENERAL ILLUMINATION AND BIO-PHOTONICS

Research in the field of luminescent materials doped with rare earth (RE) and transition metal (TM) ions has taken giant strides due to the rapid development of technologies such as solid-state lighting and other display technologies. RE ions doped glassy materials also find applications in lasers, optoelectronic devices, and civil-military applications such as infrared detectors, infrared fairings, nuclear imaging, and detection. Photo luminescent glass applies these distinctive properties to photonics, lighting, and photovoltaics by applying Downconversion light from UV to visible or near-infrared (NIR) light, and it is suitable for display devices, smart windows, lasers, and optical fibers & w-LEDs, among many other applications. RE doped glasses useful for optoelectronics devices have been fabricated and characterized by many researchers because of their high transparency, low production cost, ease of shaping, and relatively high thermal stability.

Rare earth activated glasses, and nanophosphor are important groups of engineering materials that can be used in a wide range of multifunctional and industrial applications. The advantages of glasses and glass ceramics have attracted a lot of attention. Inorganic glasses, which belong to the unique family of amorphous solid-state materials, are usually thermally stable and form over a wide range of glass-former concentrations. Since Snitzer first demonstrated the laser action of Nd^{3+} ions in barium crown glass in 1961, a great deal of work has been done on rare-Earth-doped glasses for solid-state lighting (SSL) applications, broadband optical amplifiers, up-conversion luminescence temperature sensors, and near-IR

lasers. Additionally, optical fibers that emitted infrared light were made using a variety of precursor glasses. In the current work, we have created a good glassy system (using the melt quench method) called alkali zinc alumino borosilicate (AZABS) glass doped with varying concentrations of europium ions. We have characterized them spectroscopically to gain insight into their suitability for general illumination such as w-LEDs and other related SSL device applications, all against the backdrop of the various scientific patronages of chemical species like H_3BO_3, SiO_2, Al_2O_3, ZnO, and Na_2CO_3. Also, the spectral properties of RE doped chlorides, oxides, fluorides and phosphate have been studied extensively to understand their suitability as potential luminescent applications. However, most of the systems are sensitive to moisture and thus are not quite suitable for bio labeling except the fluoride compounds with a formula such as $AREF_4$ (A = alkali, RE = rare earth F = Fluoride) [38,39]. Among $AREF_4$ host lattices, $KREF_4$ (K stands for potassium) especially have attracted much more attention because of the high reflective index and low phonon energy that make them excellent host matrix for both DS as well as UC processes

For the current thesis project, the rare earth-doped luminous material's industrial and multipurpose uses are chosen based on the previously described benefits. Enhancing the luminous qualities of rare earth ion-doped glasses and nanophosphors for use in biomedical and general illumination applications is the main goal of the research. Several chapters are meeting the research's objectives. Each chapter is meant to be read independently.

Chapter 1: A clearer introduction, the reason for the problem, the motivation for the research, and a review of recent literature are all included in the first chapter. This chapter starts with a brief introduction, the origin of the problem, the motivation of the research work, and an overview of the current literature. This chapter provides an introduction to different types of glasses and nanophosphors, the components involved in their formation, and their specific

properties. Furthermore, the importance of borosilicate glasses and nanophosphor are discussed in detail. Based on the characteristics required for glass host, $35B_2O_3.20SiO_2.15Al_2O_3.15ZnO.-15Na_2CO_3$ glass composition selected to synthesize, transparent, thermally mechanically stable glass with exceptional photonic properties, which can directly be applicable in general illumination. This approach has involved a thorough exploration of the properties of the many chemical components present in the host glass. The usefulness of RE ions doped in glasses for use in photonic devices has been studied further. Also, discussed the Eu doped KYF_4 (Potassium Yttrium Fluoride) nanophosphors as promising host material for biomedical application.

Chapter 2: The experimental process used for producing RE-doped glasses and nanophosphor and the methods for evaluating their luminous properties are the main topics of the second chapter. There is also a detailed discussion of the melt-quench process, which is used to create as-prepared glasses. This chapter describes the use of many sophisticated experimental techniques, such as X-ray diffraction (XRD), UV-VIS spectrophotometer, Temperature Dependent PL (TDPL) Spectroscopy, PL Decay Spectroscopy, SEM, and Up-conversion processes, to study various properties, including thermal, structural, photoluminescent, and colorimetric properties.

Chapter 3: In this chapter, Dy^{3+} doped Alkali Zinc Alumino Borosilicate (AZABS) glasses have been prepared via melt quenching technique. A series of AZABS glasses of varying concentrations of dysprosium (Dy^{3+}) (0.1 mol% -2.5 mol%) was prepared. It was found that under UV excitation, 0.5 mol% Dy^{3+} doped glass exhibited maximum luminescence intensity. Subsequent photoluminescence studies like emission/excitation spectra, temperature dependent photoluminescence and decay kinetics were also performed. Dexter theory was applied to study the energy transfer mechanism between the dopant ions in the glass matrix. Positive and

encouraging results from all the photoluminescence studies for Dy^{3+} doped AZABS glasses confirm that these as-prepared glasses can be used as prospective materials in general illumination. [Part of this work has been published in ***Journal of Materials Science: Materials in Electronic, 33 (2022) 4782–4793 (Impact Factor = 2.8)***]

Chapter 4: Samarium (Sm^{3+}) ions doped AZABS glasses were synthesized via quick melt quench technique. Various spectroscopic studies like optical absorption, photoluminescence (PL) emission, PL excitation, temperature-dependent PL and PL decay kinetics were performed on the as prepared glass system. Under 402 nm excitation, three sharp bands at wavelengths 563, 599 and 645 nm corresponding to transitions $^4G_{5/2} \rightarrow {}^6H_{5/2}$, $^6H_{7/2}$ and $^6H_{9/2}$ respectively can be seen in the PL emission spectra. The 0.25 mol% Sm3+ glass has the highest intensity for these emissions. The lanthanide interaction in the glass matrix is dipole-dipole in nature as was proven from Dexter's analysis. The direct bandgap of 0.25 mol% Sm^{3+} doped AZABS glass was calculated to be 2.88 eV. The lifetimes of the as prepared glasses range from 1.93 ms for the lowest concentration of Sm^{3+} to 0.75 ms for the highest. From temperature dependent PL studies, the activation energy for 0.25 mol% Sm^{3+} doped AZABS glass was found to be 0.19 eV which shows high thermal stability of this glass. We propose to utilize these Sm^{3+} doped AZABS glasses for general illumination such as w-LEDs and solid-state lighting (SSL) applications. [Part of this work has been published in ***Luminescence 28 (2023), 428-436, (Impact Factor = 3.2)***]

Chapter 5: In this chapter we discuss the synthesis of thermally stable borosilicate glasses doped with europium ions having chemical composition $35B_2O_3.20SiO_2.(15\text{-}x)Al_2O_3.15ZnO.15Na_2CO_3.xEu_2O_3$ (x = 0.5 to 2.5 mol%) using melt quench process. A broad hump without any sharp peaks observed in the XRD spectrum recorded for an undoped glass confirm its glassy

nature. The DSC & TGA has been conducted on an undoped glass to understand thermal stability and aggregate weight loss. The absorption spectral features recorded for the as prepared glasses are used to estimate optical band gap. In the process of understanding the effective usage of the as prepared glasses in visible red photonic device applications, the spectral features such as photoluminescence (PL) excitation, PL emission and PL decay were recorded and analyzed. Under 393 nm sharp excitation, all the glass samples are showing red emission corresponds to $^5D_0 \rightarrow {}^7F_2$ transition (612 nm) and whose intensity continuously increasing with Eu^{3+} ion concentration up to 2.5 mol%. The red to orange color ratio (R/O) estimated from the recorded PL spectral features varies from 3.62 to 3.92 within the variation limits of Eu^{3+} ions from 0.5 to 2.5 mol% indicates relatively low symmetry around Eu^{3+} ions in the as prepared glasses. Relatively higher R/O ratio also reveals that the nature of bonding between Eu^{3+} ions and the surrounding ligands as covalent. The Judd-Ofelt theory has been applied to the emission spectral features to understand the nature of bonding between the doped RE ion and its surrounding ligands along with the radiative properties of the doped RE ion. Activation energy (0.175 eV) and percentage loss (82%) in PL intensity estimated for 2.5 mol% of Eu^{3+} ions through temperature dependent PL (TDPL) studies reveal the superiority in thermal stability of the as prepared glasses. The PL, TDPL, PL decay studies conducted along with CIE coordinates estimated allows us to contemplate that, the as prepared glasses are quite useful in fabricating thermally stable visible red photonic devices. [Part of this work has been communicated in ***Journal of Non-Crystalline Solids 575 (2022) 121184 (Impact Factor = 3.2)***]

Chapter 6: This chapter deals with the synthesis of cubic phase $KYF_4:Eu^{3+}$ nanophosphors via wet chemical route. Morphological studies such as XRD, SEM and EDAX mapping were done to ascertain shape, size and composition of the as prepared nanophosphors. Debye Scherrer formula applied to the XRD spectral features of the as prepared nanophosphors reveals the

average size in the range 3 - 4 nm. The JCPDS data analysis for KYF4:Eu^{3+} nanophosphors confirm cubic structure with lattice constant a = b = c = 5.448Å and α = β = γ = 90°. The SEM image mapping clearly demonstrates the uniform distribution of all the constituent elements such as potassium, yttrium, fluorine and europium. Up-conversion (UC) studies carried out using 800 nm spitfire femtosecond laser produces peaks at 576, 590, 612, 650, 700 nm pertaining to the transitions 5D0 → 7Fj (J = 0, 1, 2, 3, 4) respectively. In addition to this, three higher order peaks are also observed at 523 531, 552 nm pertaining to $^5D_1 \rightarrow {}^7F_j$ (J = 0, 1, 2) transitions respectively. Down-shifting (DS) studies under 393 nm and 405 nm excitation were also recorded to understand the utility of the as prepared phosphors for lighting applications. These nanophosphors are capable of emitting visible emissions under UV/NIR excitations. The powder dependence studies conducted on UC and DS reveal the excitation process as two photons and single photon respectively. DS temperature dependent PL spectral revels good thermal stability for the as prepared phosphor. The interesting results obtained allow us to contemplate that the as prepared KYF4:Eu^{3+} nanophosphors are useful for bio-imaging (through UC) as well as lighting applications (through DS). [Part of this work has been published in ***Journal of Alloys and Compounds, 885 (2021), 160893, (Impact Factor = 5.8)***]

Chapter 7: An overview of the overall study effort and the particular conclusions drawn from the data are presented in sixth chapter of this dissertation. This chapter also looks at future directions and social impact for this study and how it could be used to inform future research directions.

LIST OF FIGURES

LIST OF TABLES

LIST OF PUBLICATIONS

- **Rajat Bajaj,** A.S. Rao, G. Vijaya Prakash**, "Linear and nonlinear photoluminescence from thermally stable $KYF_4:Eu^{3+}$ cubic nanocrystals",** ***Journal of Alloys and Compounds, 885 (2021), 160893 (Impact Factor = 5.8).***
- **Rajat Bajaj,** A.S. Rao, G. Vijaya Prakash, **"Photoluminescence down-shifting studies of thermally stable Eu^{3+} ions doped borosilicate glasses for visible red photonic device applications,"** ***Journal of Non-Crystalline Solids 575 (2022) 121184 (Impact Factor = 3.2).***
- ***Rajat Bajaj,*** Aman Prasad, A.V.S. Yeswanth, Pooja Rohilla, Sumandeep Kaur, A. S. Rao, **"Down-shifting photoluminescence studies of thermally stable Dy^{3+} ions doped borosilicate glasses for optoelectronic device applications"** ***Journal of Materials Science: Materials in Electronic, 33 (2022) 4782–4793 (Impact Factor = 2.8).***
- **Rajat Bajaj**, Pooja Rohilla, Aman Prasad, Ravita, Ankur Shandilya, Allam Srinivasa Rao, **"Thermally stable Sm^{3+}-doped alkali zinc alumino borosilicate (AZABS) glass for warm white light generation and w-LED applications",** ***Luminescence*** **28 (2023),** ***428-436 (Impact Factor = 3.2).***

TABLE OF CONTENTS

Page No.

Chapter 1

Introduction, Motivation, Literature Review and Objectives

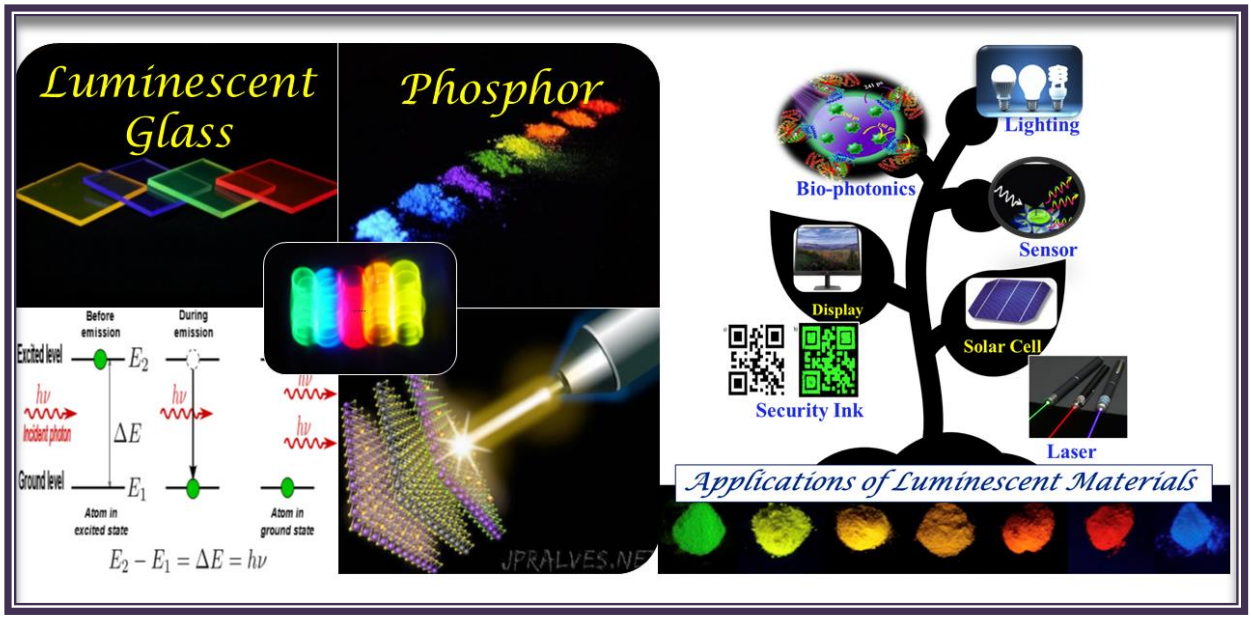

The first chapter starts with a brief introduction, the origin of the problem, the motivation of the research work, and an overview of the current literature. This chapter provides an introduction to different types of glasses and nanophosphors, the components involved in their formation, and their specific properties. Furthermore, the importance of borosilicate glasses and nanophosphor are discussed in detail. Based on the characteristics required for glass host, $35B_2O_3.20SiO_2.15Al_2O_3.15ZnO.15Na_2CO_3$ glass composition selected to synthesize, transparent, thermally mechanically stable glass with exceptional photonic properties, which can directly be applicable in general illumination. This approach has involved a thorough exploration of the properties of the many chemical components present

in the host glass. Also, discussed the Eu doped KYF_4 (Potassium Yttrium Fluoride) nanophosphors as promising host material for biomedical application.

1.1. Introduction

Optic spectroscopy has garnered a lot of interest lately and has shown itself to be an effective technique in the fields of material science, chemistry, and physics. Numerous spectroscopic techniques are available to address a broad spectrum of analytical issues. Spectroscopic techniques are frequently employed for both quantifiable and qualitative investigation since they are highly informative. Spectroscopy is concerned with the way electromagnetic radiation like X-rays, ultraviolet (UV), visible (Vis), infrared (IR), and radio waves, interacts with matter and aids to analyze the environment and structure of atoms and molecules. The basis of optical spectroscopy is the emission or absorption phenomenon. Absorption spectroscopy involves the excitation of an atom or molecule from an energy level that is lower to a higher one. In contrast, the transition from a higher energy level to a lower energy state occurs in emission spectroscopy, and the energy is released in the form of photon.

4

Over the past several decades, the luminescent spectroscopy studies of crystalline and non-crystalline materials have received much interest among the researchers in the field of science and technology. This may be due to enormous applications of luminescent materials, which are not only limited to physics, biology and chemistry but also extended to abundant fields such as astrology, agriculture, defense, optical communication, geology, forensic, medicine etc.

An inorganic material's atomic organization or translational periodicity can determine whether it is crystalline or amorphous. Amorphous materials, which include polymers, gels, thin films, and glass, are materials that are non-periodic in three dimensions and exhibit short-range order. All solid materials with atoms, molecules, or ions that display long-range order

and periodicity in three dimensions are referred to as crystalline materials [1,2]. A common example of an amorphous material having a solid-liquid transition is glass. The use of glasses, glass ceramics, and ceramics—three important classes of engineering materials—can be advantageous for a range of multifunctional and industrial applications. Amorphous materials have unique properties that distinguish them from crystalline liquids and solids, and they are crucial for numerous technological applications. Because they are versatile and adjustable, they can be used in materials science, engineering, and other fields [3,4].

1.2. Motivation of The Research Work

The main motivation for research into rare-earth-doped glass and phosphor is their distinct optical and electrical characteristics, which make them crucial for sophisticated photonic and optoelectronic applications. The sharp and consistent emission spectra, long luminescence lifetimes, and high quantum efficiency of rare-earth ions, like Eu^{3+}, Sm^{3+}, Dy^{3+}, Er^{3+}, Pr^{3+}, Yb^{3+}, Tm^{3+}, and Tb^{3+}, make them perfect for usage in lasers, fiber amplifiers, solid-state lighting, and display technologies. Biomedical imaging for high-resolution diagnostics, energy-efficient LEDs, and solar energy harvesting via upconversion phosphors have all advanced as a result of their capacity to increase light conversion efficiency. Further driving research in this area is the growing need for outstanding performance optical materials for use in nonlinear optics, security applications, and quantum computing.

Beyond technological developments, the search for ecologically sound and energy-efficient solutions is another factor propelling research in rare-earth-doped materials. White LEDs, for instance, use phosphors, which are essential in lowering world energy consumption by taking the place of traditional lighting systems as seen in the evolution of different generation light sources in Fig. 1.1. As lighting sources started with fire than the incandescent bulb, sodium

discharge comes under 2nd generation lighting source. The current era is phosphor converted LEDs comes under 4th generation illuminating devices. In order to increase overall efficiency, rare-earth-doped materials in solar cells allow unused infrared radiation to be converted into visible wavelengths. Additionally, the growing use of these materials in temperature sensing, medical diagnostics, and anti-counterfeiting has prompted the creation of novel materials with specialized optical qualities. The investigation of novel glass matrices and host materials broadens the possibilities of rare-earth-doped systems and opens the door for upcoming developments in sustainable technologies, photonics, and telecommunications.

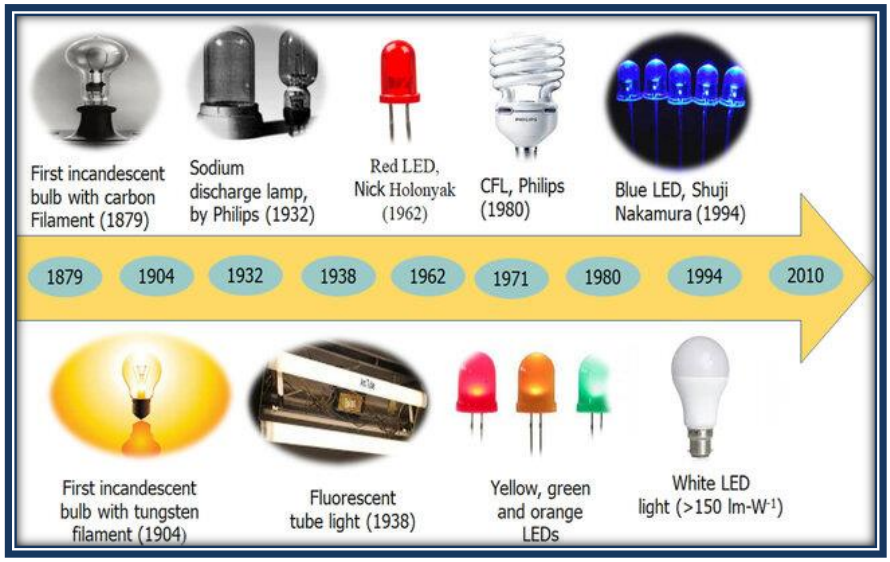

Figure:1.1 *Evolution of lighting devices.*

The simplicity of shaping any shape, reduced production costs, enhanced thermal stability, and—above all—a manufacturing process that eliminates the need for epoxy resin are the benefits of rare-earth ion-doped glasses over PC W-LEDs. Furthermore, a number of significant technical domains, including fibers, optical amplifiers, and optical detectors, use RE-doped glasses as an active medium. There are numerous applications for light-emitting materials [11–13]. Glasses and phosphors are thought to be the best hosts because they can display intriguing characteristics like significant doping capabilities, wavelength modification,

and wide inhomogeneous bandwidths. [14,15]. All this rare earth doped materials comes under the category of luminescent materials, which gives the radiative emission via process of luminescence mechanism having numerous applications in the field of science and technology.

In recent years, a growing body of research has demonstrated how phosphor materials, which can emit light when excited, find diverse applications in biophotonics, drug delivery, biosensing, including bioimaging, and therapy, leveraging their unique luminescent properties for noninvasive diagnosis and treatment. Biophotonics is multidisciplinary research field, which includes physical sciences, biology along with engineering as depicted in Fig1.2. Phosphor is used in biological research, particularly to analyze illness. investigations on oxygen distribution have been a major emphasis, with multiple research groups determining how phosphors might be employed in a variety of biological investigations as depicted in Fig1.2. Phosphors are also used extensively in cancer research. Cancer progression, treatment response, and aggressiveness are all thought to be linked to tumor hypoxia, in which tumor cells are deprived of oxygen.

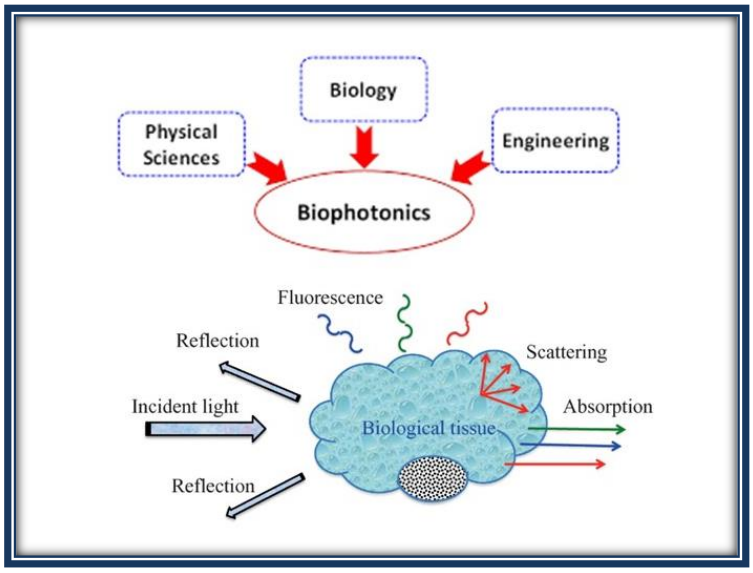

Figure:1.2 *Phosphor for Biophotonics applications.*

On the basis of rigorous literature survey, it has been identified that the phosphor lifetime imaging is a method that measures and maps oxygen gradients in biological tissues. Hence the phosphor materials have been prepared via chemical route and investigate their structural and optical upconversion characteristics for biophotonics applications.

1.3. Luminescence

Luminescence is the term used to describe a material or substance that emits light as a result of electrical energy, chemical reactions, or radiation exposure. After being absorbed by a substance, light is released by this mechanism. A condition involving cold body radiation is called luminescence, which occurs when energy is absorbed and subsequently released as light. Materials that have the ability to transform absorbed (invisible) energy into visible light: ultraviolet, x-rays, β, α, and so on, are known as luminescent materials as demonstrated in Fig.1.3 [27,28]. Although crystalline compounds such as phosphor are examples of luminous materials, luminescent glass is usually made of amorphous materials [29].

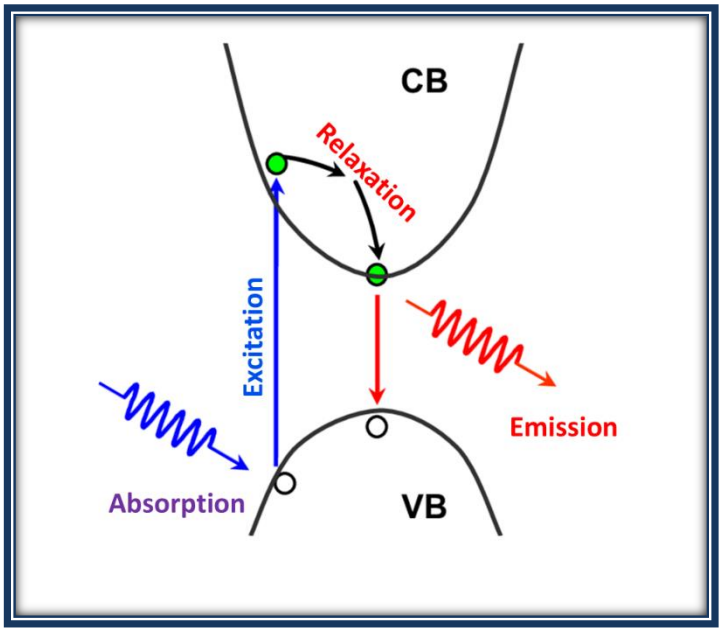

Figure:1.3 *Luminescence mechanism.*

1.3.1. Types of Luminescence

There are numerous types of luminescence on the basis of excitation source as mentioned in Fig.1.4. Based on kind of excitation source, luminescence is categorized as cathodoluminescence, electroluminescence, thermoluminescence, chemiluminescence, piezoluminescence, triboluminescence, radioluminescence, bioluminescence, sonoluminescence along with photoluminescence. All the excitation source for numerous categories of luminescence have been mentioned in Fig.1.4.

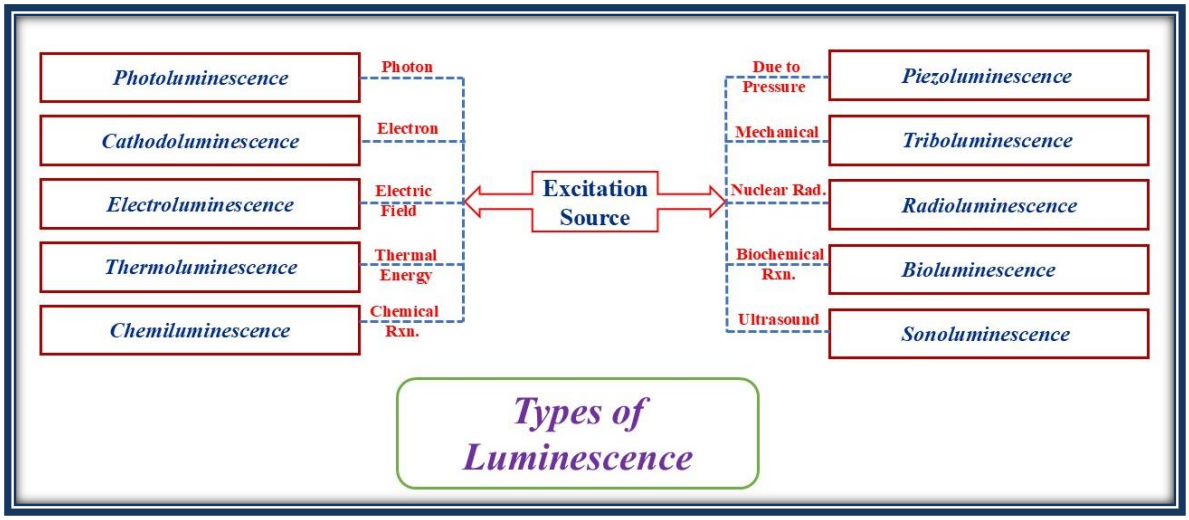

Figure:1.4 *Types of Luminescence on the basis of excitation source.*

1.3.2. Photoluminescence (PL)

PL refers to the process in which light emanates from atoms or molecules after they absorb photons. Photoexcitation causes electrons in the material to migrate into allowed excited states. When such electrons approach the lowest energy or ground states, they release the surplus energy as a phonon, a non-radiative process, or as visible light, a radiative process, as seen in Figure 1.5 [27,34]. The energy levels of the two-electron states involved in transitioning between the excited and equilibrium states determine the amount of light emitted. The emission or decay period of PL separates it into two categories.

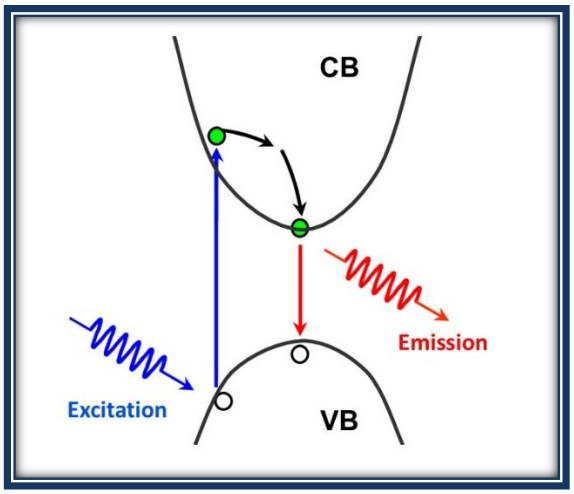

Figure:1.5 *Schematic representation of photoluminescence process.*

Stokes emission, also known as down-conversion, occurs when a photon is released with less energy than when it was incident, resulting in energy loss throughout the photoluminescence process. The Stokes shift is the energy difference between stimulated and emission photons. A substance may also be capable of absorbing two or more photons at the same time, so encouraging the generation of a higher energy photon. This process, known as "up-conversion," produces anti-Stokes emissions. [28,35]. Figures 1.6 (a) and (b) explain the down-conversion and up-conversion PL processes.

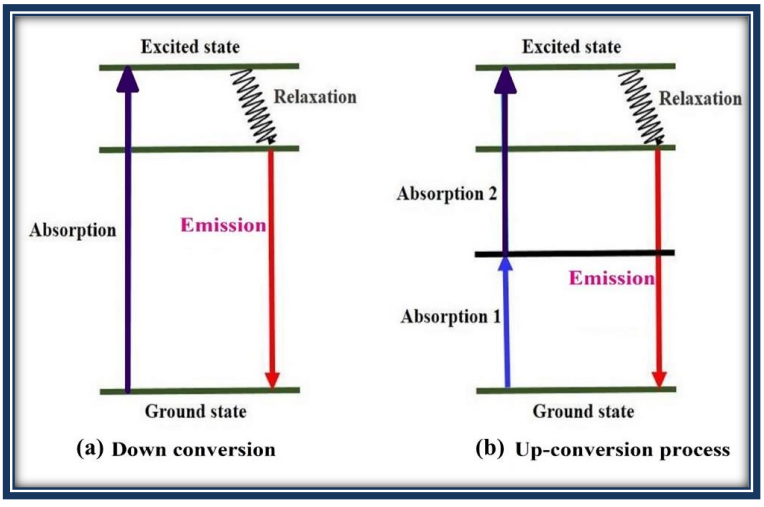

Figure:1.6 *Schematic process of* ***(a)*** *down-conversion and* ***(b)*** *up-conversion PL.*

Luminescence is used in many different industries, such as displays, forensics, medical diagnostics, environmental monitoring, lighting, and materials research. The ability to control and harness luminescence has proven beneficial for LED lighting, scientific research imaging techniques, and fluorescence microscopy [33].

1.4. Luminescent Materials

Luminescent materials emit light when excited, making them useful for lighting, displays, and bioimaging. Luminescent materials can be inorganic/organic and crystalline/amorphous, which can be illuminated using a number of luminescence processes.

1.4.1. Luminescent Glasses

Luminescent glass is glass that exhibits the phenomenon of luminescence, meaning it emits light after being exposed to a specific type of energy, often in the form of light or radiation. This is distinct from incandescence, where heat is the source of light emission. A substance that is translucent and glossy is referred to as "glass," and another word for glassy substances is "vitreous." Glass is a uniform, amorphous, inert solid that has no biological activity. In 1997, Shelby described glass as, "*an amorphous solid completely lacking in long range order, periodic atomic structure and exhibiting a region of glass transformation behavior. Any material, organic, inorganic or metallic formed by any of the stated processes which shows glass transition character can be categorized as glass*".

The durability, transparency, and brilliance feature of glass make them suitable for a wide range of modern applications. Machines were created to dope glasses with rare-earth ions in order to make them suitable for lasers. Furthermore, the glasses are intended to be used as telescope lenses for viewing astronomical objects. In the twenty-first century, glass produced by businesses for a range of uses is a component of growing economic growth in almost every

nation [5,6]. Glass's qualities and applications are substantially influenced by its components. Glass components, including glass or network formers, network modifiers, and intermediates, were classified into three categories depending on their bond strengths.

Oxides having bond strengths more than 80 kcal/mol are commonly used as glass and network formers. Notable and widely used glass formers were P_2O_5, SiO_2, V_2O_5, PO_4, As_2O_5, Sb_2O_5, B_2O_3, and GeO_2. The bulk of the four cations with oxygen coordination number create a tetrahedral shape [1]. Glass network modifiers are oxides with bond strengths ranging from 10 to 40 kcal/mol that do not integrate with the glass network formed. The fundamental goal of network modifiers is to change the properties of glass. The majority of glass modifiers are composed of alkali oxides. On the other side, more oxide materials can be used as network modifiers. Li_2O, SrO, ZnO, Na_2O, CaO, MgO, and BaO are major network modifiers. the proper choice of a cation-oxide modifier, which has a wide range of contemporary applications, including optoelectronic devices, conducting glasses, bioactive materials, and sensors [2,19]. Fig. 1.7 (i) represent structure of borosilicate glass former. As the Na_2O network modifier was added to borosilicate, can modify the glass network as symbolize in Fig. 1.7 (ii).

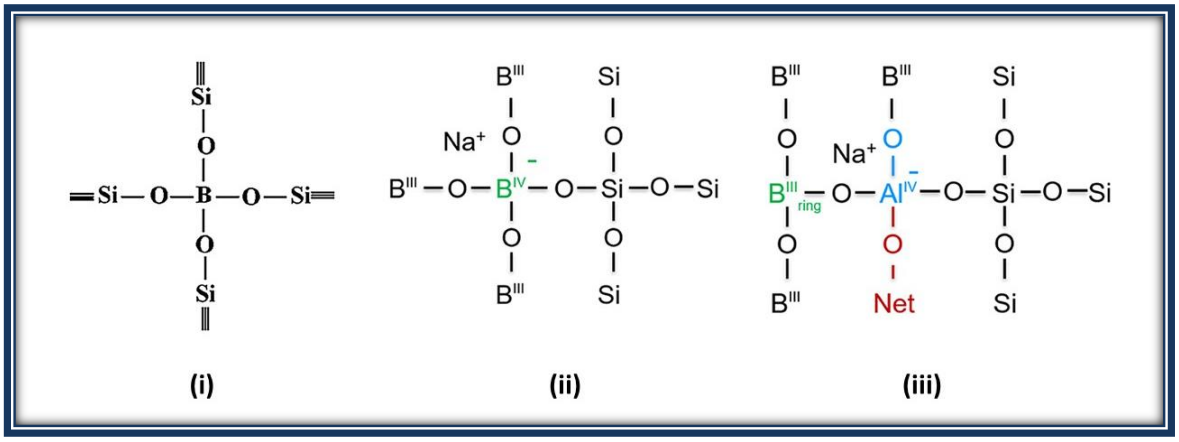

Figure: 1.7 *Glass compositions include glass formers, glass network modifier.*

Between the glass formers and the modifiers, there is a place for intermediates. TiO_2, ZnO, CdO, PbO, BeO, and Al_2O_3 are some important intermediates. Fig. 1.7 (iii) disclose the change in glass structure after addition of Al_2O_3 as intermediates in borosilicate glass. When characterizing the function of individual oxides in multi-component glasses, the terms glass formers, modifiers, and intermediates are popular. In certain situations, intermediate oxides can participate in the glass's network and operate as network modifiers, depending on the chemical makeup of the material [20–22].

Glass can be made from a variety of chemical components, including covalent, ionic, molecular, metallic, and hydrogen-bonded chemicals. Glasses can be made from elements, simple chemical compounds, complex organic molecules, salt combinations, or alloys. There is no especially beneficial way to group glass-forming materials. Almost any substance can be swiftly chilled into an amorphous solid, skipping the crystallization process and allowing the creation of glass [23,24] . Every substance imperturbable at a variable rate, resulting in unique glass. Glass forms when a material is rapidly cooled from a supercooled liquid. To form an amorphous solid, the substance is cooled below the glass transition point. Following that, the atoms start moving more slowly in a molecular pattern, leading the substance to change into glass. While the freshly produced amorphous structure is less ordered than a crystal, it is nevertheless more organized than a liquid [25].

To understand the glass transition process, the behavior of amorphous materials as they transition from supercooled to glass must be plotted on a V-T diagram, as shown in Figure 1.8. The y-axis of the V-T diagram shows the temperature, while the x-axis represents the volume and enthalpy. The letters Tg and Tm signify the temperatures at the glass transition and melting point, respectively [26].

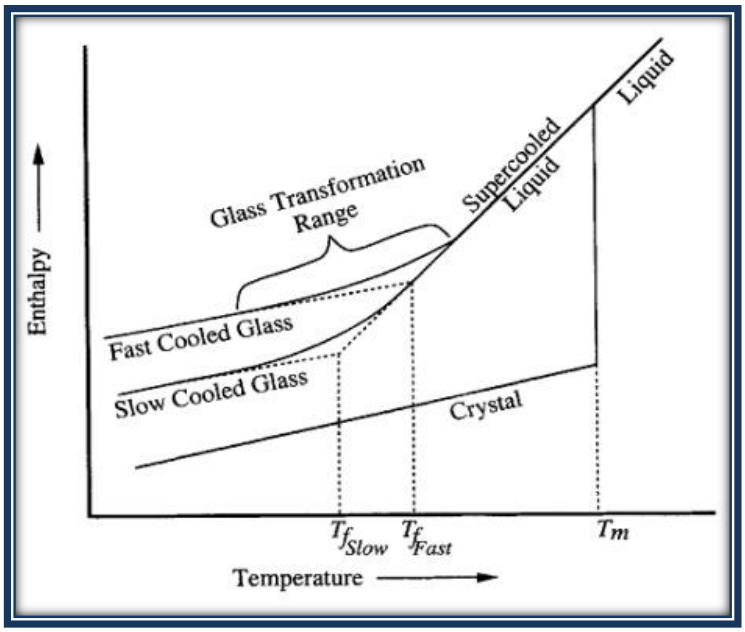

Figure:1.8 *Glass preparation V-T diagram.*

A supercooled liquid's volume does not abruptly change as it freezes into an amorphous solid at or near the glass transition temperature. At this point, the glass transition occurs [4]. The Tg of the crystalline material state is determined to be less than the Tm. A liquid can cool in one of two ways: converted to supercooled below Tm or crystallization at Tm. When the temperature drops more, the fluid thickens and crystallizes into glass. The glass transition is only produced by an increase in viscosity if the chemical composition remains unchanged, and Tg is determined by the rate of glass cooling [2]. The ideas that follow are the main theories behind the glass transition: When making glass, the cooling rate is increased to prevent crystal nucleation and growth. The glass is metastable. The V-T picture shows that glasses contain more free energy. Viscosity increases as temperature decreases.

1.4.2. Phosphor

The second kind of crystalline luminescent materials are known as phosphor. Phosphors are mainly inorganic, solid materials that emit visible light when subjected to radiation ranging

from gamma rays to near infrared. Phosphors are consisting a host lattice which provides the space to incorporate rare earth ions or transitional metals for a variety of display applications. Many research breakthroughs are directed at maximizing the features of rare earth doped phosphor materials for diverse applications such as display panels and field emission display detectors by increasing the luminescence efficiency.

Phosphors are highly tailored inorganic materials that require unique formulations for each use. This is a common oversight during the development of a new display, and it can lead to technical failure. Using phosphors developed for one technology in a different application is typically can be feasible for many advantageous photonic applications. Certain molecules labeled as activators may release energy instantaneously after being triggered by the appropriate sources. Sensitizers are a type of impurity that can form when activator ions do not absorb sufficient energy. Sensitizers absorb energy, which is subsequently transferred to activators. This method involves the transmission of energy through light materials. Figure 1.3 (a, b, c) displays the sensitizer and activator roles in the luminescence process. Dopant ions and/or other faults are purposefully introduced into an inert flawed host lattice to form luminous materials. Dopants play varied functions in host lattices based on their electrical configuration, solubility, and host lattice structure [30].

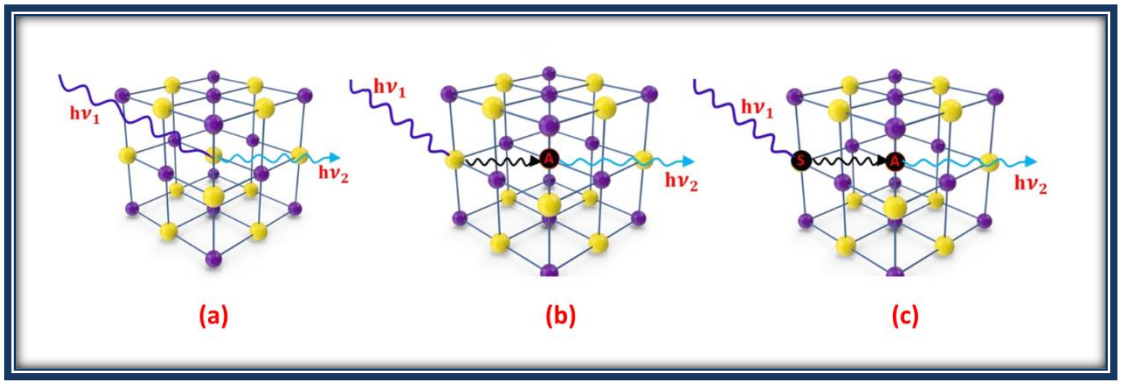

Figure:1.9 *Luminescence absorption and emission process.*

Activator: An activator (A), commonly referred to as a luminous center, is a dopant species ion atom that, after absorbing excitation energy, leaps into the excited state and, when returning to the ground state, releases the energy as radiation [29].

Sensitizer: Figure 1.9 (c) depicts two dopants, one of which is an activator (A) and the other a sensitizer (S) when present in a crystal lattice. Before energy is supplied to the "A" for emission, the "S" absorbs the majority of the energy.[28].

1.5. Rare Earth (RE) as Activator Ions

The essential features of 4f–4f electronic transitions make rare earth elements activated luminous and photonic materials highly sought after in a variety of applications, including solid-state lasers, lighting, optical fiber amplifiers, and small microchip lasers. Because they were only sporadically found in nature, the lanthanide group elements of the periodic table are known as rare earth elements. Because of their distinctive quality, they draw the attention of researchers and are important to the investigation. The fifteen elements in the RE element group, which range in atomic number from Z = 57 to Z = 71, are lanthanum through lutetium [27,36]. Because of their comparable properties, yttrium and scandium elements are likewise categorized as rare earth elements. In practically every field of research and technology, rare earth elements are used extensively. Rare earth elements are primarily found as trivalent state (RE^{3+}) RE_2O_3 oxide, while a very small number can also be found in the divalent state (RE^{2+}). Electronically, RE elements are configured as $[Xe]4f^n$ (n = 0–14), where [Xe] is the xenon configuration. Fig.1.5 displays the electrical arrangement of RE components with respect to their ground state and various excited states. From these configurations, several energy levels can be obtained, which are defined by the spectral expression ($^{2S+1}L_J$), where the three quantum numbers L, S, and J resulted from the spin-orbit coupling. Dieke's energy level diagram for trivalent rare-earth ions,

shown in Fig. 1.5, provides a clear definition of these energy levels, which have specified energies [27,28].

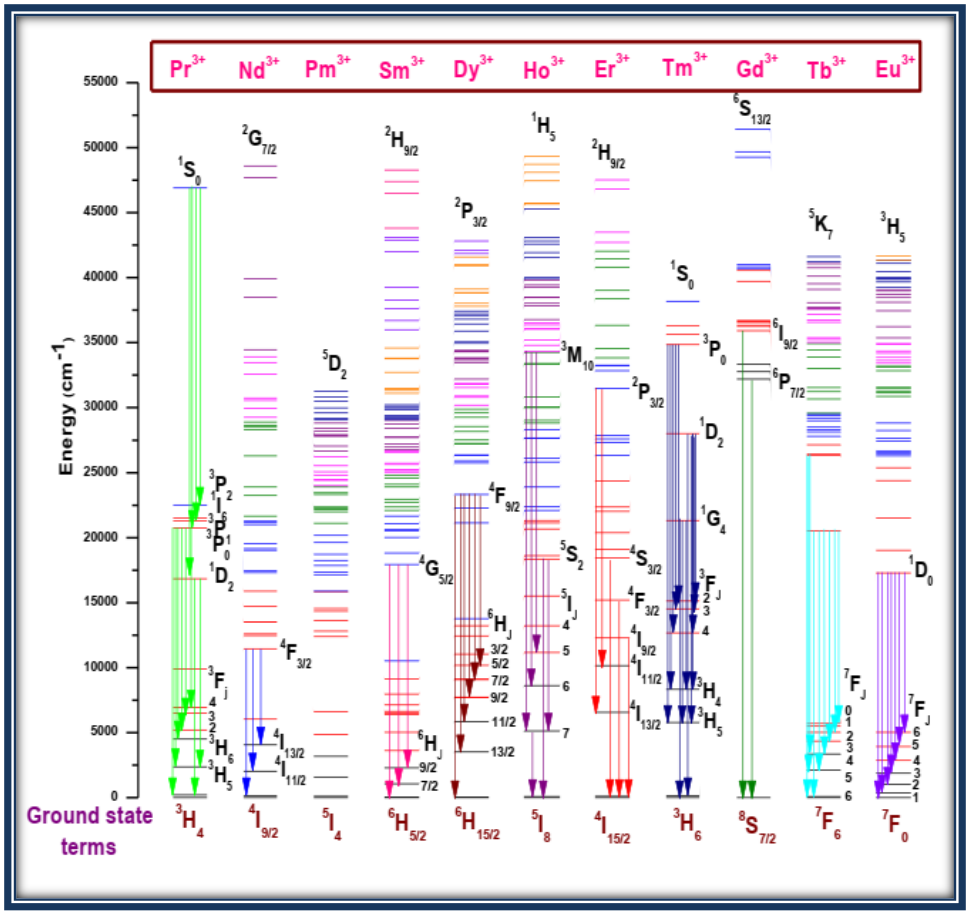

Figure:1.10 *Energy level diagram of numerous rare earth ions.*

1.5.1. Types of Transitions in RE ions

Three types of optical transitions are generally used to classify the interaction between the various levels of RE ions. These transitions include charge transfer transitions, transitions between multiple 4f levels, and characteristic transitions between multiple $4f^{n-1}5d^1$ -$4f^n5d^0$ levels. These transitions are explained below[37,38]:

Discrete $4f^n$– $4f^n$ transitions: Discrete Transitions between electronic states within the f orbitals of lanthanides or rare-earth elements are referred to as $4f^n$–$4f^n$ transitions. After absorbing or releasing photons, the partially filled *f* orbitals of these elements can change in energy.

Lanthanide ion 4f electronic energy levels are not significantly affected by their surroundings because the outer $5s^2$ and $5p^6$ electrons shield the *4f* electrons from external electric fields. It is strictly forbidden to transition within 4f shells since Laporte's criteria is not met by parity. The RE ion's interaction with the crystal field or the lattice vibrations, which can combine states of different parities into *4f* states, is what causes the observed forbidden transitions. Conversely, when spin-orbit contact occurs, such transitions are allowed. The luminous lifetime resulting from *4f -4f* transitions is usually in the millisecond range because the luminescence transition is prohibited [38,39]. There are three ways to understand the proper interpretation of *4f -4f* transitions.

- An electric quadrupole occurs when a charge exhibits quadrupole behavior or a zero-dipole moment. Electric quadrupole transitions are weaker than induced ED and MD transitions, and even parity follows them. Quadrupole transitions in RE ions have not yet been experimentally verified. The quadrupole transitions' selection principles apply to some transitions, referred to as hypersensitive transitions [40].
- The incoming source electromagnetic radiation's electric field vector component interacts with the activator (RE) ions to produce induced electric dipole transitions. In RE ions, the induced electric dipole type transitions account for most of the transitions, according to the literature review. Essentially, the electric dipole (ED) transition is caused by linearly moving charges. Odd parity exists in the ED transition because of the odd transformation that comes after it and relates to the inversion center [37,41].
- When activator (RE) ions interact with the magnetic dipole caused by the electromagnetic radiation, an induced magnetic dipole (MD) transition occurs. A charge forms a magnetic dipole when it travels along a curved path. The MD transition is

believed to have a low intensity rotating displacement of charge in comparison to the ED transition [42].

1.5.2. Energy Transfer in RE ions

This section will provide a comprehensive analysis of the energy transfer (ET) in RE ions. Luminescent glasses are mostly composed of inorganic glass compositions that have been doped with RE or transition metal ions, or weakly activated. The electromagnetic radiation is absorbed by either the sensitizer or the glass host lattice. However, only in the vicinity of the activator ions does radiation emission occur. Consequently, the sensitizer has been sensitizing the activator by providing electromagnetic energy, which ideally creates light in the visible range[10,43]. Very rarely, a small amount of the excitation energy can be transferred from one activator to another. The following distributions of excited state energy and electron transit from the bright center to excited states are frequently observed: Via phonon emission or other energy transfer from the sensitizer to the activator, the activator can be directly excited to produce a photon of visible light, as shown in Fig. 1.6 (a), or indirectly stimulated to emit a photon of visible light (ii), as shown in Fig. 1.6 (b).

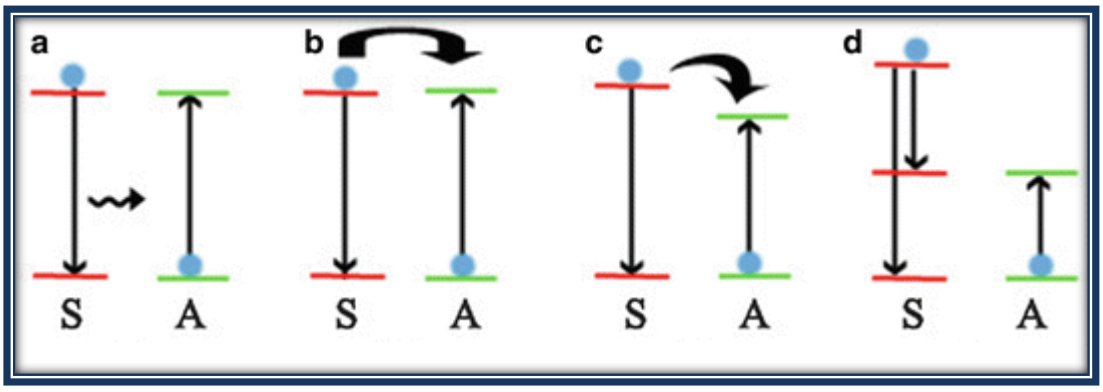

Figure:1.11 *Energy exchange processes among the doped RE ions.*

It is possible to compute radiative ET efficiency based on the sensitizer emission's ability to activate the activator, as seen in Fig. 1.6(a). There should be a noticeable overlap between

the activator's and sensitizer's excitation spectra in their emission spectra. The activator concentration has no effect on the lifetime of the sensitizer fluorescence if radiative energy transfer takes place primarily. With an increase in activator concentration, Figure 1.6(b) illustrates a non-radiative energy transfer with a significant reduction in the sensitizer fluorescence decay period. The excited states of the sensitizer and activator have an energy differential of the same magnitude, which drives the energy transfer process[44,45]. It is possible for a phonon to aid in non-resonant ET if there is a significant distance between the ground and excited states of the sensitizer and activator. The ET process in luminous materials is largely dependent on the potential contacts, characteristic transitions, and energy differential between the sensitizer and activator. For phonon-assisted non-radiative transitions (Fig. 1.6(c)), where the two ions are in different excited states, there is little chance of energy transfer. The term "cross-relaxation" refers to any kind of down conversion energy transfer between ions or similar luminous centers that are adjacent to one another. When the first ion, which is originally excited—trades energy with the second ion, which is initially in the ground state cross-relaxation, a straightforward potential energy level scheme takes place. As a result, inside the energy between the two beginning states, both ions lie in some state of intermediary concurrently[46].

1.5.3. Quenching phenomena in RE ions

When materials are doped with RE ions, the intensity of luminescence grows to a specific point and then declines. We refer to this process as quenching concentration. Increases in absorption efficiency generate an increase in luminescence intensity, which is greatest at a specific doping ion concentration known as the critical concentration [47,48]. In any RE ions doped phosphor host lattice, concentration quenching is mostly caused by energy transfer between activator ions. Concentration quenching occurs when the distance between the donor

and acceptor atoms gets smaller to such an extent that the energy exchange between them is induced. Two explanations exist for the concentration quenching process [49].

i. In the first kind of mechanism, dominant energy transfer allows the excitation energy to be spread into several luminescent centers prior to emission. Multi-phonon relaxation returns these excited luminous centers to their ground state. These centers have the potential to function as energy sinks in the transfer chain, leading to the quenching of emission intensity [50,51].

ii. The second type of mechanism uses a cross-relaxation process to utilize the excitation energy from the emitted state. This process is caused by resonant energy transfer between the two neighboring activator ions [52,53].

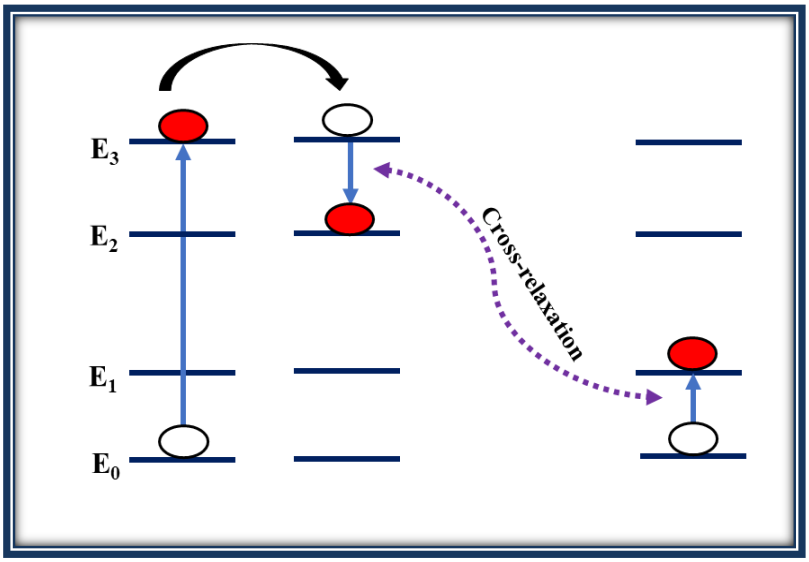

Figure:1.12 *Cross-relaxation between pairs of centers.*

Fig. 1.7 shows the energy level diagram with cross-relaxation. Resonant energy transfer occurs when the energy difference (E_0-E_1) of one nearby center (acceptor) and the energy difference (E_3-E_2) of another luminous center (donor) are equal. This largely depends on the type of energy level. The excited electron moves from E_3 to E_2, acting as a donor center, and releases energy that was absorbed by another electron at E_0, moving from E_0 to E_1 levels, acting as an acceptor,

in a process known as cross-relaxation. The emission intensity is quenched because of the non-radiative energy transfer between the closest activator ions.

1.5.4. Lifetime of RE Ions

The process of excitation and de-excitation is initiated by the intra $4f - 4f$ electronic transition of the RE ion, provided that the required energy is present. In Fig. 1.7, a time-resolved intensity spectrum shows the excitation and de-excitation process. Through radiative transition, energy exchange between nearby RE ions, cross relaxation channels, or other mechanisms, the excited RE ion can return to its ground state. At low RE ion concentrations, RE ions are not able to interact with one another, hence a single exponential function fits the intensity decay curve against time. The PL intensity can be expressed using the following equation [54,55].

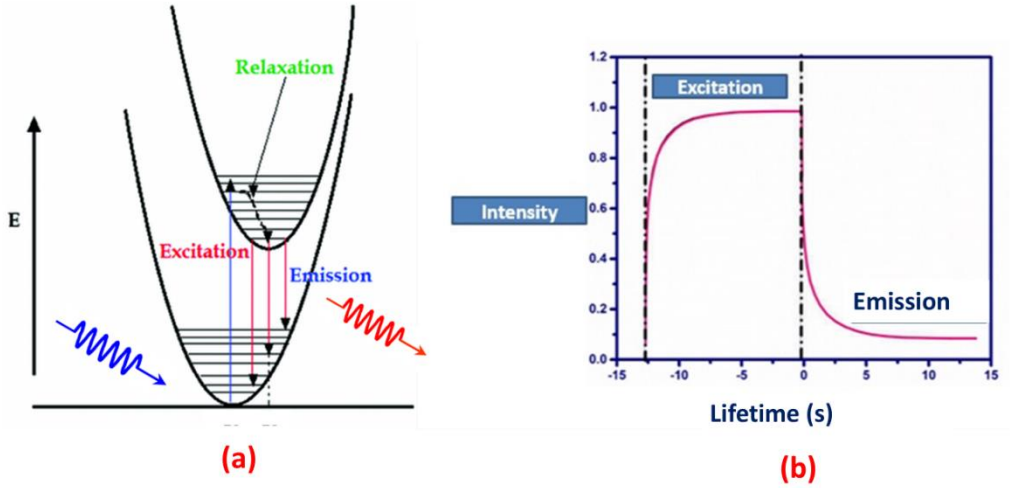

Figure:1.13 *Excitation and emission lifetime process of RE ions.*

$$I_t = I_0 + A_1 \exp\left(-\frac{t}{\tau}\right) \tag{1.1}$$

In this instance, the PL intensity at time zero is denoted by I_0. The logarithmic plot of intensity against time can be used to determine the excited RE ion's lifespan, represented by τ. The

excited state's intensity steadily decreases with time as 1/e, as seen in Fig. 1.8. The experimental lifetime of an excited RE ion can be predicted using the following formula[56].

$$\tau_{exp} = \frac{\int tI(t)dt}{\int I(t)dt} \quad (1.2)$$

However, at higher concentrations of RE ions, the decay profiles suit the bi-exponential function quite well. For a bi-exponential fit, the PL intensity can be represented by an equation[57,58].

$$I_t = I_0 + A_1 \exp\left(-\frac{t}{\tau_1}\right) + A_2 \exp\left(-\frac{t}{\tau_2}\right) \quad (1.3)$$

To find the average lifespan (τ_{avg}) in this case, apply the following formula[59].

$$\tau_{avg} = \frac{A_1\tau_1^2 + A_1\tau_2^2}{A_1\tau_1 + A_2\tau_2} \quad (1.4)$$

In this case, the lifespan components τ_1, τ_2 are exponential, and A_1, A_2 are fitting constants.

1.6. Current Glass Composition and Phosphor Host

Glasses activated with RE ions recommended numerous remarkable properties, including the ability to accept high concentrations of RE ions, wide inhomogeneous bandwidths, low production costs, and simple manufacturing techniques. The bands of emission transitions, and thus the luminescence efficacy of a doped RE ion in a host matrix, are determined by the host's and ligand field's inherent structures. To achieve the highest luminous efficiency, it is critical to select an appropriate host with relatively low phonon energies. According to the literature, B2O3 is one of the best glass formers due to its outstanding properties, including good thermal stability, low melting point, and high solubility of RE ions. [14]. Aside from the aforementioned advantages, pure borate hosts exhibit self-control due to their relatively high phonon energies (1300 cm^{-1}) [25-26]. It is generally recognized that a host glass with relatively high phonon energy is not ideal for luminescence applications, as much of the input excitation energy is

wasted inside the host due of its high phonon energy. [26]. A combination of borate (B2O3) and silicate (SiO_2) creates a network of borosilicate glass with favorable features such as mechanical strength, low melting point, high thermal stability, and corrosion resistance. For the reason that of their beneficial properties, borosilicate glass systems have proven acceptable and valuable for a wide range of optical applications. Because network-forming oxides stretch when vibrated, borosilicate glasses have a high phonon energy, which accounts for nonradiative losses. Borosilicate glass has favorable qualities such as mechanical strength, low melting point, and great thermal stability.

As a result, the host matrix has a lower quantum efficiency, which makes it less effective as a luminous material. Typically, metal oxides such as SiO_2 or Al_2O_3 are blended with borate glass to reduce its superfluous high phonon energies and transform it into a good luminous material best suited for various optoelectronic device applications [26]. The structure of a glass is determined by two factors: the network former and network modifier. A glass former, also known as network formers, consists of oxides such as SiO_2 and B_2O_3, which are indispensable in the creation of the glass [27]. Network modifiers given to a network glass former affects the internal structure of the host and produces a holistic environment around the doped RE ions, allowing them to have relatively high luminescence efficiency [28]. Borosilicate glasses can be advantageously used for illuminating purposes by inducing them with RE ions for applications in a number of industries ranging from pharmaceutical industry to nuclear waste immobilization, in addition to their usual use in photonic devices [27, 29]. Controlled heat treatment of these glasses improves a variety of qualities, including chemical and physical stability and crystal nucleation strength. BO_3 triangles in borosilicate glass interact with SiO¬2 to generate silicate groups. Adding Na_2O as a flux to borosilicate glass can lower the dispensing temperature and change the characteristics of the glass [29,30].

Aluminum oxide (Al_2O_3) is added to a borosilicate glass to increase the physical properties and chemical stability of the host glass [30]. The AlO_4 structural units present in Al_2O_3 crosslinks with borate and silicate chains present in a borosilicate host glass and builds the glass more resistive to the attacks of alkali metals [19,31,32]. Addition of zinc oxide (ZnO) to borosilicate glass can increase its glass forming composition range along with other noble features such as low glass transition temperature and high chemical stability. Apart from this, the glasses with ZnO are non-toxic, non-hygroscopic and are used vigorously for the development of optoelectronic devices [19-21,25]. Most of lanthanides (Ln3+) ions gained much attention due to its unique optical properties such as high brightness and high chemical stability. All RE ions are well-known spectroscopic agents for intense through down-conversion process in wide variety of materials such as glasses, phosphorus, nanophosphors and organic-inorganic hybrid materials [33]. In the backdrop of aforementioned various scientific patronages offered by the chemical species such as H_3BO_3, SiO_2, Al_2O_3, ZnO and Na_2CO_3 in the present work we have fabricated a good glassy system (using melt quench method) by name alkali zinc alumino borosilicate (AZABS) glass doped with different concentration of europium ions and characterized them spectroscopically to have an insight into their suitability for general illumination such as w-LEDs and other related SSL device applications.

In bio-photonics, up-conversion (UC) processes are essential. UC involves the conversion of low-energy NIR radiation into high-energy visible light through the absorption of multiple photons. This process has applications in solid-state lasers, 3D displays, white LEDs, solar cells, photodynamic therapy, temperature sensing, optical imaging, and biological labeling [34-36]. Unlike conventional luminescent probes like quantum dots (QDs) and organic dyes, upconversion nanoparticles (UCNPs) offer unique advantages, including multiple absorption

and emission centers, superior photostability, narrow emission bandwidths (<10 nm), long excitation lifetimes, low cytotoxicity, and large anti-Stokes shifts (up to 500 nm). These properties, combined with deep tissue penetration and minimal autofluorescence under NIR excitation, make UCNPs highly suitable for bio-imaging and targeted drug delivery [37-47]. Most of the UC materials use rare earth (RE) ions as active ions. Most of the trivalent RE ions (Ln^{3+}) in which 14 electrons are filled in the 4f inner shell, presenting a great similarity in electron configurations $4f^n5s^25p^6$ (n = 1 - 14). The 4f shell is partially filled and exhibits similar physical, chemical, optical and magnetic properties. These properties are dependent on various things like crystals structure, morphology as well as on chemical composition which are very sensitive to the bonding states of RE ions [48]. The absorption, as well as emission transitions produced by RE ions are very sharp as such transitions are produced between 4f energy levels [49]. Spectral properties of RE doped chlorides, oxides, fluorides and phosphate have been studied extensively to understand their suitability as potential luminescent applications [50]. However, most of the systems are sensitive to moisture and thus are not quite suitable for bio labeling except the fluoride compounds with a formula such as $AREF_4$ (A = alkali, RE = rare earth F = Fluoride) [38,39]. Among $AREF_4$ host lattices, $KREF_4$ (K stands for potassium) especially have attracted much more attention because of the high reflective index and low phonon energy that make them excellent host matrix for both DS as well as UC processes [50-56]. The KREF4 exhibits two polymeric forms of crystal structures, namely cubic and hexagonal phases depending upon the methodology and synthesis conditions as shown in Fig.1.14 [57-61]. Apart from this, relatively less phonon energy, non-hygroscopic nature, ability to convert NIR & UV radiations into visible (through UC & DS processes), good dissolving nature in solvents and relatively higher chemical stability makes the fluoride based nano crystals as promising host lattices for various luminescent applications when doping with

RE [62-63]. Trivalent rare-earth (RE^{3+}) doped with luminescent materials have gained so much attention due to their applications in the field of white LEDs as red emitting phosphors, plasma screens and so on [64].

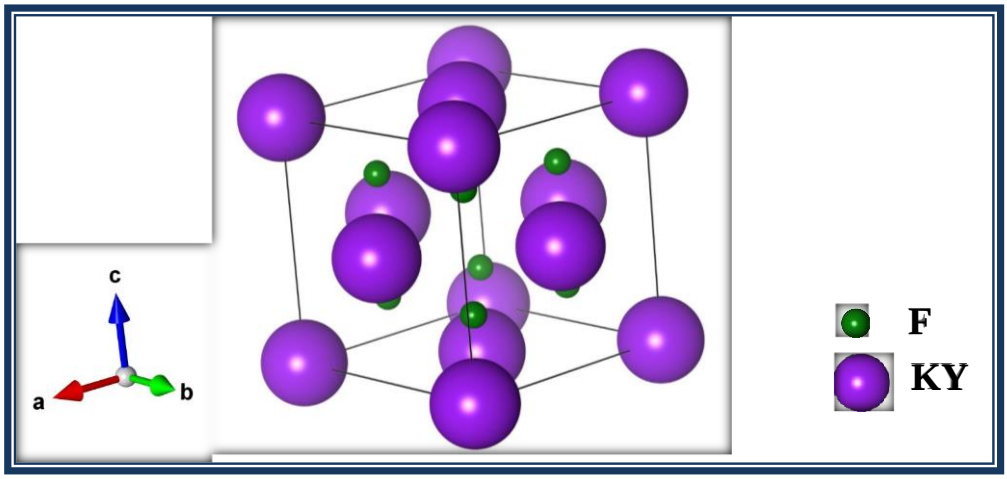

Figure: 1.4 *Crystal structure of* KYF_4.

1.7. Objectives of The Research Work

With the advent of science and technology, an overwhelming contribution has been made by any researchers in developing pc-wLEDs. However, there are certain major challenges to overcome and achieve high luminous efficiency, high chromatic stability, brilliant color-rending properties, and price competitiveness with fluorescent lamps. The main objectives of the present doctoral work are:

- To prepare optical glasses and upconverting nanophosphors doped with RE ions having low phonon energy.
- To perform Structural and morphological studies like XRD, SEM, TEM and EDAX
- To optimize RE doped ions in the glass and phosphor lattices for better Luminescence Efficiency.

- To understand the spectral characteristics of the as prepared glasses and nanophosphors by using photoluminescence (PL) excitation, emission and decay.
- To perform surface modification of the RE doped UCNPs.
- To check whether as prepared glasses and UCNPs can be used in lasers, optical amplifiers, white light LEDs and bio-medical applications by associating with concerned research laboratories and medical institutes

Chapter 2

Experimental Work and Characterization Techniques

Characterization methods and experimental activities are essential to scientific study and technical development. This chapter examines the several experimental techniques used to create the luminous materials (glass and phosphor) as well as the various characterizations for their potential use in optoelectronic devices. X-ray diffraction (XRD), TGA-DSC, scanning electron microscopy (SEM), and spectroscopic methods are also highlighted as important characterization techniques that offer vital information about structural, morphological, electrical, and optical characteristics. In order to comprehend material behaviour, maximize performance, and guarantee dependability in real-world applications,

it is imperative to choose the right characterization methodologies. Using a variety of characterization approaches, the properties of RE ions doped luminous were examined in order to investigate their optical, structural, vibrational, and morphological properties for potential usage in cutting-edge optoelectronic devices. The operating principles, device descriptions, and operational controls of the characterization tools employed in the current research project are explained in the current chapter to help readers better comprehend the instruments.

2.1. Experimental Work

Innovation in technology and the advancement of scientific knowledge depend heavily on experimental activity. By offering empirical support for or opposition to theoretical forecasts, it guarantees that concepts are based on observable reality. Researchers can investigate unidentified events through testing, which can result in fresh ideas and discoveries. Through the development of new technologies, process improvement, and testing and optimization of solutions, it also plays a critical part in solving real-world problems. Experiments push the boundaries of disciplines, inform evidence-based decision-making, and promote society and industry by linking theory and practice. A thorough understanding of various synthesis processes and adequate characterization techniques are necessary for the creation of effective multifunctional materials.

Throughout the thesis study, characterization approaches and a full experimental protocol are covered in this chapter. Redox-ion-doped glass and nanophosphor synthesis and characterization methods for its application in cutting-edge optoelectronic devices. Covered are the principles of optimizing the statistical method used for analysis and the experimental procedures learned.

Nanophosphors are made by synthesizing luminous materials at the nanoscale, which have special optical characteristics because of their small size and large surface area. One of the most important steps is the nanophosphor synthesis methods and material analysis process. Various synthesis methods such as hydrothermal, solvothermal sol-gel, co-precipitation, and combustion have been used to synthesize nanophosphors.

A rare earth-doped glass study's experimental and instrumentation section covers the techniques and tools used to look into the optical and spectroscopic characteristics of the glass substance. Glass is enhanced optically and luminescent by the addition of rare earth dopants, which makes it suitable for a variety of uses, including amplifiers, sensors, and lasers [69]. Here's an outline of the experimental and instrumentation aspects:

- Melt quenching
- Sol-gel method
- Electrochemical methods
- Pyrolysis
- Solid state methods (Radiation damage, intense shock-waves, diffusion effects)
- Vapor quenching Sputtering (evaporation, sputtering and reactive deposition)

Among all listed techniques, melt quenching is the oldest and easiest technique for preparing amorphous material. This technique is widely used commercially.

2.1.1. Melt quenching techniques

The technique of quickly cooling molten precursor material to convert amorphous materials into the proper shape is known as melt quenching. One distinctive feature of the melt quenching process is the constant hardening of the uniformly melted material, which produces

amorphous solids. Depending on the host glass system, different cooling rates are required to produce glassy states. The melt can be rapidly cooled after being taken out of the temperature-controlled electric furnace and then poured onto heated conductive surfaces like copper or brass plates. This will accomplish necessary cooling. [70].

2.1.2. Synthesis of Rare Earth Activated AZABS Glass

Quick melt quenching technique was used to synthesis the rare earth (Dy^{3+}, Sm^{3+}, Eu^{3+}) ions doped AZABS glasses with the composition details as given below:

$$\mathbf{35B_2O_3\text{-}20SiO_2\text{-}(15\text{-}x)Al_2O_3\text{-}15ZnO\text{-}15Na_2CO_3\text{-}xRe_2O_3}$$

(x = 0.0, 0.5, 1.0, 1.5, 2.0, 2.5 mol%). Starting powders like H_3BO_3 (99.5%), SiO_2 (99.9%), Al_2O_3 (99.9%), ZnO (99%), Na_2CO_3 (99.9%) and Re_2O_3 = Dy_2O_3, Sm_2O_3, Eu_2O_3 (99.99%) were purchased from sigma -aldrich and in total 8 grams of sample weighed in stoichiometric ratio. The powder was mixed in an agate mortar until to get a homogeneous mixture as mentioned in schematic flowchart at Fig 2.1.

Further the powder was placed in a alumina crucible in an electric furnace at 1250^{o}C for 2 hrs. Thereafter, the melt was poured in between two pre-heated brass plates and further annealing is done at ~350^{o}C for another two hours to avoid the flaws caused by thermal and mechanical stress. Finally, the glass obtained was transparent and circular in shape with uniform thickness 2.2 mm and diameter about 1.5-2.0 cm

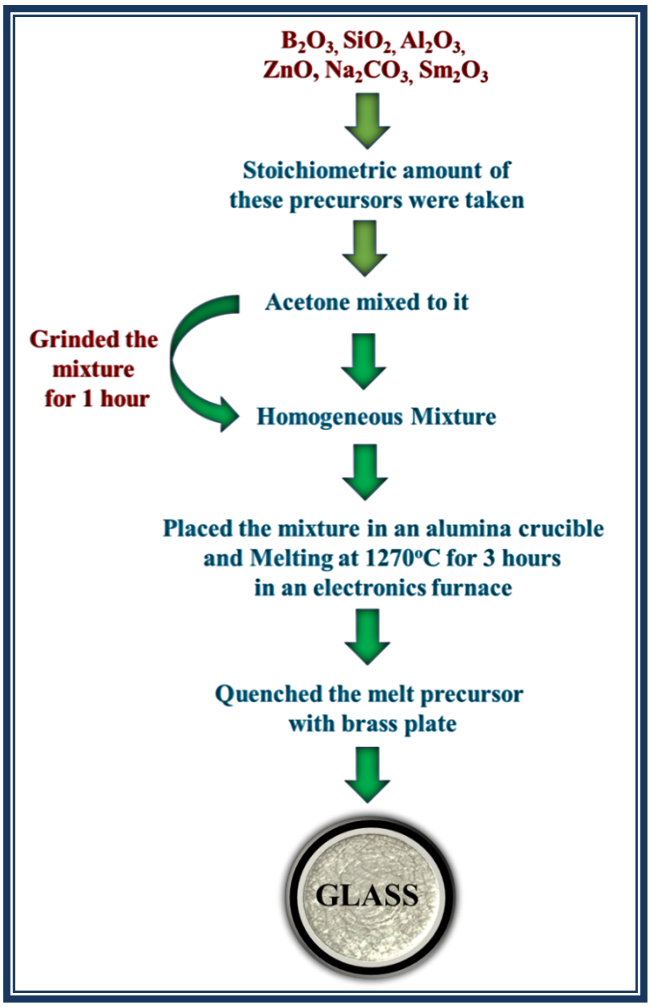

Figure:2.1 *Flowchart for RE doped* AZABS *glass preparation.*

2.1.3. Synthesis of KYF_4 Nanophosphor

KYF_4 host lattices were prepared by employing wet chemical route. For the manufacture of oxide-based phosphor/nanophosphor, co-precipitation is a straightforward, economical, industrially feasible, and quick method. Co-precipitation is a chemical process in which solid particles form from a solution containing ions or precursor molecules. These ions are incorporated into the solid through physical frame-up in the pore spaces and adsorption on the surfaces of the growing particles. Adsorption is one of the primary strategies used in the co-precipitation method. During this procedure, a solution containing additional ions, called

adsorbates, is mixed with the solid species, or adsorbent. In this case, the adsorbates are bound to the solid's surface by physical or chemical interactions between one adsorbate and the adsorbent. The coprecipitation method's primary benefits are its high yield, low cost, excellent product purity, and ease of reproducibility.

In mentioned method, yttrium acetylacetonate [$Y(acac)_3$. xH_2O] (Sigma Aldrich 99.0%, 1.0 *mol%*)], potassium fluoride [KF (Fisher Scientific, 4.0 *mol%*)] and the dopant europium chloride hexahydrate [$EuCl_3.6H_2O$ (Sigma Aldrich 99.0%, 1 to 5 *mol%*)] were first dissolved in 5ml of methanol independently. The Y solution was added drop wise to KF solution first and after 5 minutes the combined solution was added with Eu solution drop wise. The final solution was subjected to magnetic stirring for three hours at RT followed by four hours stirring at 65°C. After completing the whole reaction, the solution could cool down to the room temperature on its own. After that, the samples were centrifuged at 10,000 rpm after being washed three times with methanol. The final precipitation was dried for 12 hours in a vacuum oven at 50°C.

2.2. Characterization's Techniques

Materials characterization techniques are methods used to analyze and measure the physical, chemical, mechanical, and structural properties of materials. These techniques help researchers and engineers understand material behavior, composition, and performance, which is essential for material selection, quality control, and failure analysis.

2.2.1. Thermogravimetric analysis (TGA) and differential scanning calorimetry (DSC)

TGA is a perfect characterization method for studying the thermal properties of any material at high temperatures in a specific environment. Changes in the % weight loss of

materials are interpreted in TGA procedures as a result of an increase in temperature. Thermal stability, compositional changes, and kinetic parameters for the chemical reaction in materials are all shown by the weight loss plot that was recorded. A thermobalance, a programable temperature-controlled furnace, an inlet/outlet facility for various gas atmospheres, and a computer for processing and storing the results make up the high precision TGA apparatus. Initially, the crucible containing the sample was placed in the sample platform's groove and heated to capture TGA data. In the second step, a sample's temperature is progressively increased in a furnace while its weight is recorded on an analytical balance that is kept outside the furnace. Lastly, if a volatile component is lost during a thermal event, the mass changes are noted [71,72].

When compared to a known reference sample or empty crucible, DSC is the perfect tool for thermal inquiry since it records the heat flow into or out of a precursor material as a function of higher temperature over a set period of time in a controlled gas atmosphere. Many material properties, such as melting, specific heat capacity, oxidation nature, crystallization, thermal, etc., are assessed for the crystallization process of any metals or compounds using the DSC curve. DSC detected a heat quantity at a high temperature that, depending on the temperature difference between the precursor and reference material, the precursor sample may absorb or radiate [73].

In the current thesis, SETARAM LabsysEvo obtained simultaneous TGA-DSC data. as shown in Figure 2.2. At a high, regulated temperature in an argon environment, weight changes and heat flow in the precursor material were recorded simultaneously.

Figure: 2.2 *Picture of TGA instrument (Perkin Elmer TGA 4000).*

The TGA-DSC curve's synchronized data recordings can increase production and make the results easier to understand. Additionally, exothermic and endothermic actions—which do not result in weight loss or loss during calcination—can be distinguished using the free data.

2.2.2. X-ray diffraction

One of the best instantaneous analytical and characterization methods is X-ray diffraction (XRD), which is mostly used to determine if a material is crystalline or amorphous. XRD can give information on any crystalline sample's atomic spacing, preferred orientation, unit cell dimensions, thermal expansion and contraction, and crystal structures. When monochromatic X-rays strike crystalline materials, Bragg's law creates constructive interference and meets the diffraction laws, which is the basis for X-ray diffraction. When the incident radiation wavelength is similar to the atomic spacing sample and experiences constructive interference according to Bragg's law, a diffraction peak appears. The incident radiations in the crystalline powder sample were dispersed from several lattice planes and

separated by d. When each wave's travelled path length is equal to an integer multiple of its wavelength, constructive diffraction patterns are found. This results in the state for constructive interference from successive planes of the crystalline sample, which is defined by Bragg's law [74].

$$n\lambda = 2dsin\theta \tag{2.1}$$

An integer is represented by n in this case, the wavelength of the incident radiation by λ, and the angle between the incident ray and the scattering planes by θ. The ceramic's crystallite size was assessed using XRD pattern data, including full width at half maximum (FWHM) at diffraction angle [75].

$$D = \frac{K\lambda}{\beta cos\theta} \tag{2.2}$$

here, β denotes FWHM at Bragg angle θ, K denotes shape factor, λ represents the wavelength of X-rays ($CuK\alpha$= 1.54 Å).

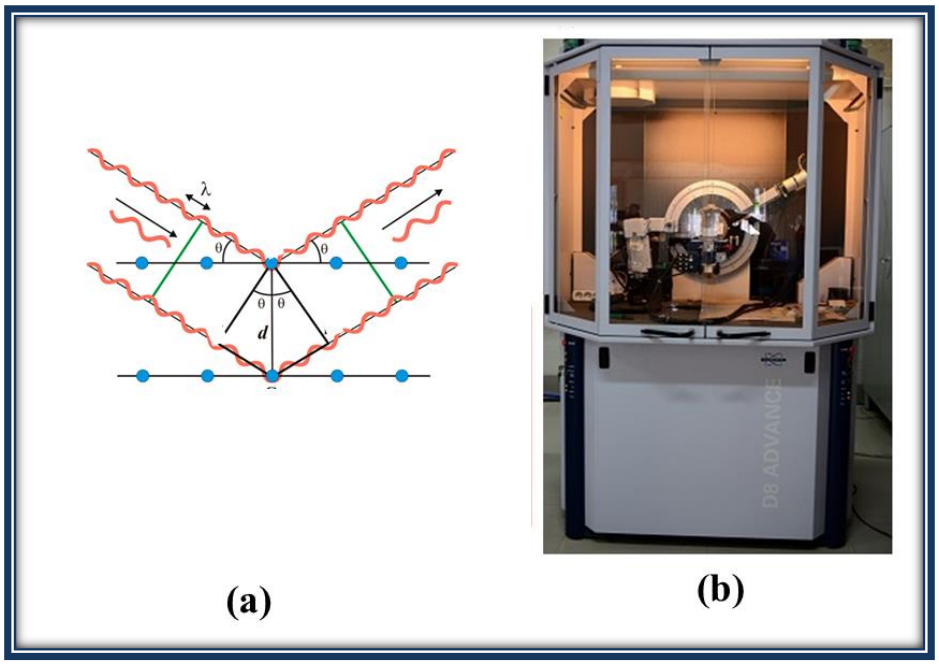

***Figure:2.3** XRD instrument (Bruker 8D advance).*

The Bruker 8D advance system X-ray diffractometer provided the XRD patterns for the produced glass and nanoparticles, as seen in Fig. 2.3. The diffractometer has CuKα (λ~1.54 Å) The X-ray source needed an electric supply with a voltage of 40 kV and a current of 20 mA. An X-ray tube, which can produce radiation with a certain wavelength depending on the cathode metal, a sold slit, a rotating sample holder, and a moving X-ray detector are all parts of an X-ray diffractometer. Powder materials or thin film were placed on the sample holder, which is in the direction of an incident X-ray source with a fixed wavelength, in order to record the XRD data. At the same time, θ and d fluctuate. The constructive interference developed at a specific angle and was detected by the X-ray detector. Computer software handled and connected all of these XRD components. Many crystalline structural factors, including unit cell parameters, lattice constant, crystallite size, stress/strain present in the crystalline sample, etc., can be evaluated using the diffraction patterns.

2.2.3. Fourier-transform infrared spectroscopy (FT-IR)

FT-IR is one technique for obtaining an infrared radiation pattern of emission or absorption by either organic or inorganic materials. Spectral data was gathered using an FT-IR sensor across a wide electromagnetic range. The sum of the electronic, rotational, and symmetric/asymmetric vibrational energy levels is the total internal energy. Active ions and electromagnetic sources have been studied using this spectroscopic approach. Molecular vibrations are primarily associated with electromagnetic waves in the infrared (IR) region. By absorbing IR radiation, molecules are driven to higher vibration states. IR spectroscopy is therefore an effective method for determining a sample's structure.

The basis for the FT-IR apparatus's operation is Michelson's interferometer technique. [76]. The interferometer consists of two mirrors that span the beam splitter and are aligned

perpendicular to each other. The result of the interfering of the reflecting beams from the two mirrors is the output beam, which causes one mirror to move a certain distance whereas the other stays stationary. The Fourier transform method is used to acquire the material's infrared spectrum after the beam passes through the sample and creates an interferogram. How FT-IR spectra were obtained from spectrum two FT-IR spectrometers (Perkin Elmer) is shown in the Figure. 2.4.

Figure: 2.4 *spectrum two FT-IR spectrometers (Perkin Elmer)*

2.2.4. Raman

The most effective analytical technique for observing scattered light and figuring out a material's vibrational energy behaviour is Raman spectroscopy. Both FI-IR and Raman spectroscopy provide structural information due to the rotational and vibrational modes of the chemical system. when the photon emitted from the laser source affects objects in the infrared to near-UV wavelengths. The three situations listed below can be observed once photons and matter interact. The first scenario is that the energy of the emitted and absorbed photons is the same, which is known as Rayleigh scattering. A Stokes shift may have occurred in photons emitted as vibrational energy, according to the second theory. The third is an anti-stokes line,

which indicates that the released photons have been charged. The Raman spectra's last two choices are similarly spaced from the Rayleigh line [77].

Important information on the vibrational modes of the samples is provided by these energy shifts. Since both Raman and FT-IR spectroscopy offer in-depth information on a material's structural properties, they are complementary to one another. However, the main difference between them is the kind of chemical change that these performances induce: a Raman transition may occur when the polarizability of the molecule changes during a vibration transition, implying a positional shift in the molecule's electron cloud, whereas an IR observable transition requires a change in the dipole moment during vibration [76].

As shown in Figure, Raman spectra were captured in the current study utilizing Enspectr R-532 Raman spectroscopy 2.5.

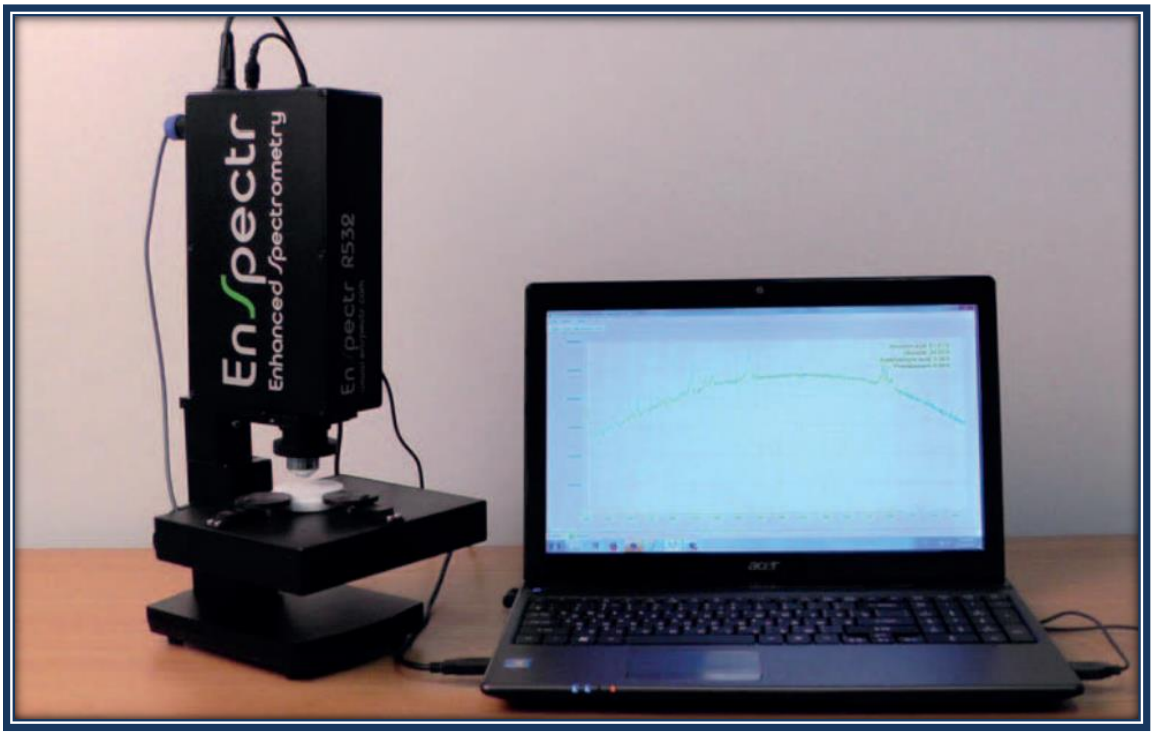

Figure:2.5 *Enspectr R-532 Raman spectroscopy.*

2.2.5. Scanning Electron Microscope (SEM)

Examining the material morphology (particle sizes and shapes), surface imperfections, metallographic details, and surface topology of micro or nanomaterials is best done with a scanning electron microscope (SEM). Exploration of the elemental conformations in bulk or nanomaterial samples is another use for this equipment. The SEM is a very useful electron microscope that uses a high-energy beam of electrons that are ejected or scattered from the specimen to raster scan images of the specimen samples. The only difference is that the electrons are produced by field emission instead of thermionic emission. The generated electrons interact with the specimen's atoms to produce secondary electrons or signals that provide information on the sample's composition, surface shape, electrical conductivity, and micro/nano size [78].

Figure:2.6 *TM3000 Tabletop microscope.*

The field emission gun in a SEM serves as a detector for backscattered electrons, a cathode, an anode, scanning coils, a sample stage, and a secondary electron. Each of these

configurations was managed by specialized software on a highly configured computer system. Cold emission is the term for the release of electrons into a vacuum from a metallic conductor's surface when a strong electric field is present. The reason for this is that an electron's wave function does not vanish. The likelihood that the electron will be discovered outside the barrier is therefore finite.

With a strong electrical field potential gradient, a stream of high-energy electrons was produced by a field emission gun and accelerated in a vacuum. In order to create a finely directed electron beam that strikes the target, electronic lenses deflect and concentrate the original electron beam. As a result, in every region of the samples, secondary, backscattered, radiation, and transmitted electrons are released. The surface structure of the item is related to the secondary electrons' angle and velocity. Numerous different detectors capture X-rays, secondary electrons, and backscattered electrons, producing an electronic signal. To create the final image that can be viewed on a computer screen and stored for further examination, this electronic signal is amplified multiple times. Using a TM3000 Tabletop microscope (as illustrated in Fig. 2.6) and a mics F+ x-stream-2 Oxford equipment equipped with an electron gun source at 15 kV accelerating voltage, the morphological and elemental mapping experiments were carried out by recording SEM and EDAX. Spreading the synthesized nanoparticle on a carbon-coated tape produced the powder sample.

2.2.6. UV-Visible Spectrometer

The UV-Vis Spectrophotometry is a quantitative tool that can quantify the amount of visible or ultraviolet light that a liquid, solid, or thin-film material absorbs or transmits in relation to the reference sample. The foundation of spectroscopy is the interaction of light and matter. A spectrum is created as a result of the excitation and de-excitation that occur when matter

transmits or absorbs light. The Beer-Lambert law states that a monochromatic light beam has an effect on a sample solution that contains a fundamental and engrosses the radiation. Once this is established, the absorbance of a sample solution is directly proportional to both the path length and the concentration of the absorbing ingredient in the solution. The concentration of the absorber in a solution can therefore be controlled using UV/Vis spectroscopy for a fixed route length. When attention was paid to the absorbance variations from the reference solution or samples [79].

Figure:2.7 *UV–vis spectrophotometer (Jasco V770).*

Using a PerkinElmer dual-beam spectrophotometer (model lambda 750), as shown in Figure 2.7, the UV–vis absorption spectroscopy was measured. The UV-visible spectrophotometer may consist of a light source, monochromators, a reference or sample, a detector, an amplifier, and recording equipment. With a range of UV to visible radiation, tungsten and deuterium lamps are the most often utilized light sources. Typically, monochromators consist of prisms and slits that can scatter the main light source and emit two monochromatic radiation beams that are the same wavelength as the reference cell and the sample. We exposed the reference solution and the sample solution to these two monochromatic radiation beams. Both the reference sample cell and the sample cell can send beams to the two-photocell kind of detector. Since photocells produce relatively weak signals, the amplifier can amplify them repeatedly

and produce distinct, recordable signals. With the right software, computers may serve as recording devices, saving all the data and displaying the spectrum that has been captured.

2.2.7. Photoluminescence Spectrofluorophotometer

Any light-sensitive substance, such as powder, liquid, glass, or thin-film samples, can have its photoexcitation and emission measured using a contact-free, multifunctional, non-destructive photoluminescence (PL) spectrofluorometer. A solid or liquid sample is typically struck by a light beam, which absorbs it, excites it, and then releases the radiative emission—preferably in the visible region—along with certain non-radiative relaxations after a predetermined amount of time [80,81]. Physical phenomena known as photoluminescence (PL) occur when materials are excited by different sources and emit light. Both spectrally and temporally, this emitted light may be composed and examined. In semiconductor materials, the radiative transition occurs between the valence and conduction bands, and the actual energy difference is known as the bandgap. The energy of the light that is released is related to the energy level difference between the two-electron states that are involved in the transition from the excited state to the equilibrium state.

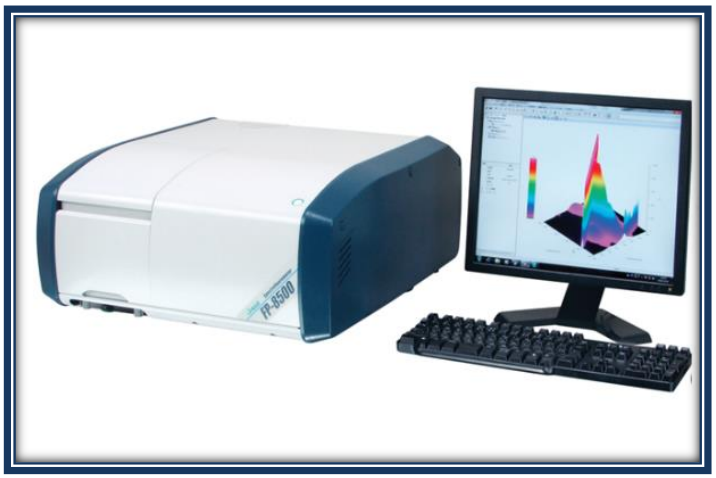

Figure:2.8 *Spectrofluorometer, (Jasco, 8300FP)*

The majority of PL measurement setups understand a particular wavelength of light produced by a Xenon lamp that is directed toward the sample using a monochromator. The sample absorbed the specific radiation, which then became excited and released light. The sample's light is captured by lenses, scattered by a second monochromator, and then picked up by a photodetector. The convertor transforms the electrical signal produced by the photodetector into a digital signal, which is then processed by computer software. The intensity of the PL light that is emitted as a function of its wavelength is used to depict the spectrum.

The produced samples' PL excitation and emission spectra are being recorded using a spectrofluorometer (Jasco, 8300FP), as shown in Figure 2.8. A 300 W Xenon excitation source lamp and two monochromators at each excitation and emission side were included in the PL configuration [82].

2.2.8. Time-Resolved Photoluminescence (TRPL)

The conventional spectrophotometer has been improved upon by TRPL. A rapid photodetector records the emission of a sample as a function of time following excitation while a pulse light source is employed for excitation. Energy transmission from one component to another in mixed composites or samples, the identification of spectrum emissions with distinct emissive states, and the recording of material quality are all possible applications for this technology. Photoluminescent characteristics' inherent recorded lifetime can reveal information about the dynamics of the species' excited states [83,84]. One of the best options for researching decay time or lifetime—the term for the fast/slow electrical deactivation processes that produce photon emission—is TRPL. This lifetime may be affected by interactions with other molecules and the molecular environment. As a result, lifetime variations can reveal details about the local

chemical environment or reveal patterns of reactions. Depending on the materials or flaws in the samples, emission durations varied from picoseconds to milliseconds or seconds.

The pulsed light source (pulsed laser, LEDs, or flash lamp), a monochromator or optical filters, a single-photon sensitive detector, and recording devices such computers with the right software are the key elements of TRPL.

Figure:2.9 *Edinberg FLS 1000 TRPL spectroscopy instrument.*

One popular method for describing the TRPL decay curves is Time-Correlated Single Photon Counting (TCSPC). As shown in Figure 2.9, the Edinberg FLS 1000 TRPL spectroscopic instrument is used to record the decay times curves. The apparatus is equipped with a photomultiplier tube detector and a delta diode laser pulse source. The least square fitting approach was used to analyze all of the decay curves that were recorded [82].

2.2.9. Temperature Dependent Emission Studies

The term "temperature-dependent emission studies" describes research that looks at how a material's or system's emission characteristics change with temperature. The underlying physical or chemical processes taking place within the material or system can be better understood by researchers by examining the temperature dependency of emission properties. Designing sensors, comprehending

energy transfer mechanisms, maximizing device performance, and investigating basic light-matter interaction phenomena all depend on this knowledge.

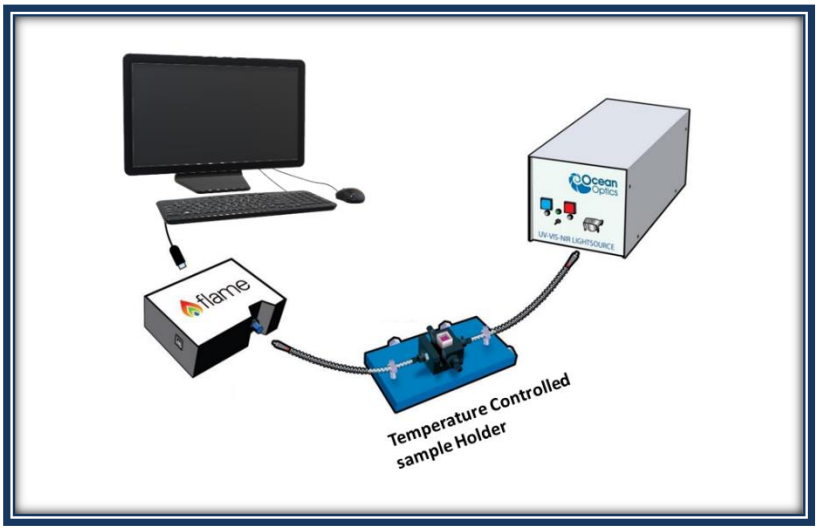

Figure: 2.10 *Schematic representation of Temperature-dependent PL spectrofluorophotometer.*

The TDPL spectrofluorophotometer key parts are the monochromator, temperature-controlled sample holder, photodetector, light source (Xenon lamp or laser), and computers running specialized software, as shown in Fig 2.7. A light source that generates light in the 200–800 nm range is a xenon lamp. The monochromator can choose the preferred wavelength of light to be used for excitation after the emitted beam of light passes through it. The chosen wavelength is incident through optical fibre onto the temperature-controlled sample holder. When a luminescent sample is excited by a specific wavelength, it generates light that may be detected by a photodetector after passing through another optical fibre. Ultimately, the discovered spectrum was captured by a computer for subsequent analysis. In the present study, the Ocean Optics FLAME-S-XR1-ES spectrofluorophotometer is used to record the TDPL characteristics of the produced phosphors.

Elevated temperatures can either enhance or reduce the emission intensity of luminous materials under specific excitation wavelength sources in TDPL data. One of the key aspects of phosphor's suitability for a wide range of photonic applications is the impact of temperature on the photoluminescence characteristics of phosphor materials. Phosphors are typically utilized in lighting devices that need great thermal stability because the UV/blue LED chips produce temperatures between 120 and 150 °C while they are working. Additionally, the phosphor's thermal quenching properties can be employed as a temperature sensor.

26

Chapter 3

Down-shifting Photoluminescence Studies of Thermally Stable Dy^{3+} ions Doped Borosilicate Glasses for Optoelectronic Device Applications

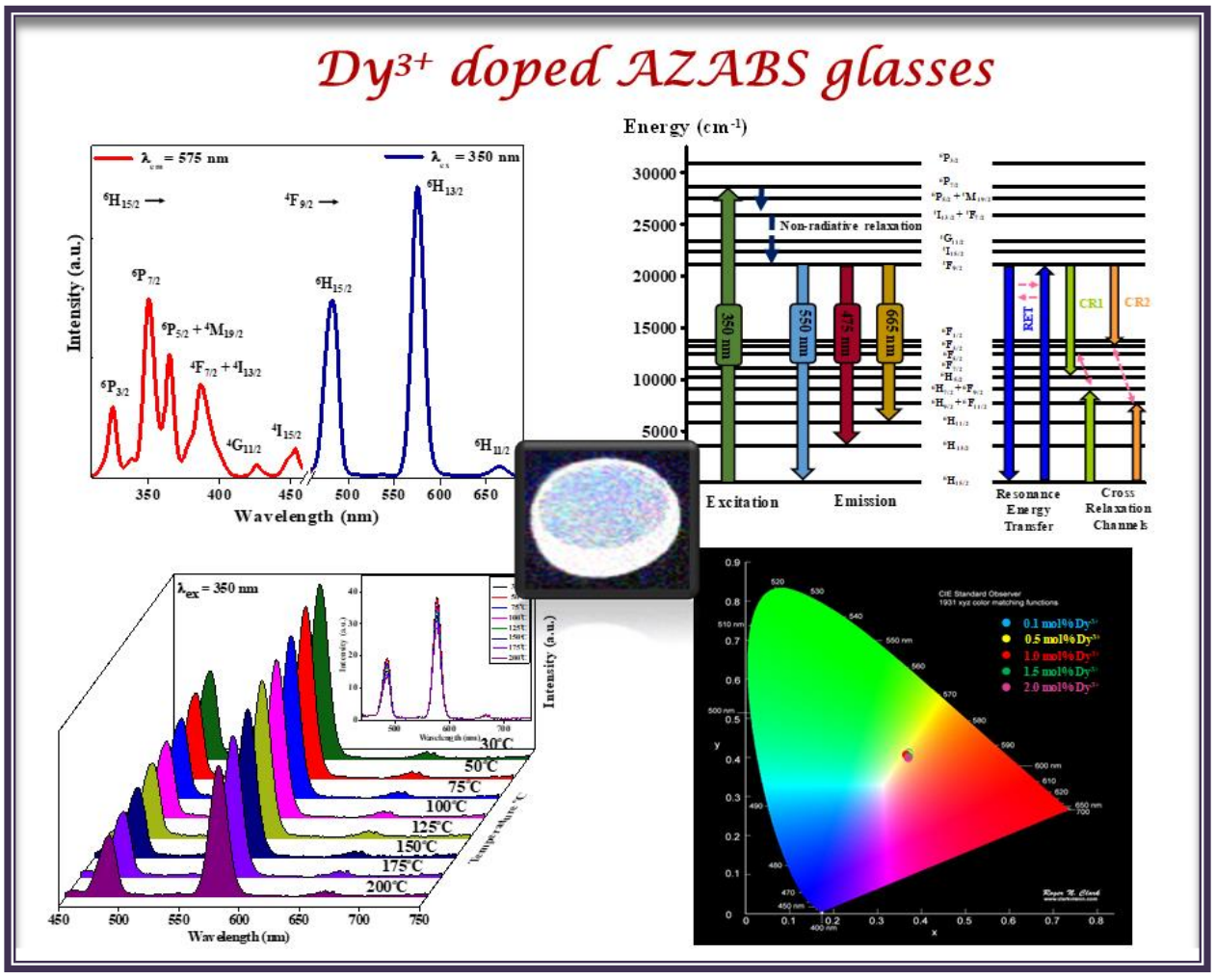

Part of this work has been published in Journal of Materials Science: Materials in Electronic, 33 (2022) 4782–4793 (Impact Factor = 2.8)

In this research work, Dy^{3+} doped Alkali Zinc Alumino Borosilicate (AZABS) glasses have been prepared via melt quenching technique. A series of AZABS glasses of varying concentrations of dysprosium (Dy^{3+}) (0.1 mol% -2.5 mol%) was prepared. It was found that under UV excitation, 0.5 mol% Dy^{3+} doped glass exhibited maximum luminescence intensity. Subsequent photoluminescence studies like emission/excitation spectra, temperature dependent photoluminescence and decay kinetics were also performed. Dexter theory was applied to study the energy transfer mechanism between the dopant ions in the glass matrix. Positive and encouraging results from all the photoluminescence studies for Dy^{3+} doped AZABS glasses confirm that these as-prepared glasses can be used as prospective materials in optoelectronic device applications such as solid-state lighting (SSL) and w-LEDs.

3.1. Introduction

In the fields of photovoltaic devices, lasers, displays, photodynamic treatments, drug delivery, and more, it is well known that materials doped with RE ions have attracted a great deal of interest from researchers worldwide [85–93]. w-LEDs and SSL applications have been the focus of the most extensive research on RE-doped materials. The energy needs of humanity have surpassed our capacity to rejuvenate. Mother Earth is under extreme strain as a result, which will have detrimental effects on our future generations and create numerous major environmental risks. Therefore, in order to leave a cleaner and greener planet for future generations, it is imperative that we develop such environmentally friendly technologies that help lessen the ecological impact of human advancements. The SSL devices have shown the way forward in this area. These devices have proven environmental friendliness and have demonstrated that they can help reduce carbon emissions by around 28 million metric tons annually [94]. Developments in SSL technologies have paved the way for research in w-LEDs

that are far superior to conventional lighting sources like incandescent lamps and tube lights. This is due to the fact that w-LEDs have high efficiency, longer life span and above all, consume much less energy [95].

Now the conventional approach to construct a w-LED was to use an amalgamation of YAG:Ce^{3+} phosphor with a blue InGaN LED chip. But the major disadvantage of using this approach is the lack of red component in the emission which leads to a low color rendering index (CRI), low thermal quenching temperature and halo effect [90,91,96]. Another approach is to fabricate the w-LEDs by mixing RGB phosphors that can be excited by UV LED. This phosphor needs to be encapsulated in an epoxy region made up of a polymer material. The luminescence efficiency of the phosphor depends on the thickness of this material and the concentration of the phosphor. But it has been observed that this epoxy region deteriorates under high temperature, high excitation and high energy sources [97]. To counter the aforementioned disadvantages, RE doped glassy systems are being developed. This is due to the fact that there is no epoxy region involved in the manufacturing process. Also, the sheer fact that glasses have a low production cost, simpler manufacturing procedure, homogenous light emission, higher susceptibility to heat and a homogenous light emission makes them more efficient than phosphors for w-LEDs/SSL applications [91,98].

Boric Acid (B_2O_3) is known to be the most proficient glass former as it leads to the formation of glasses with high thermal stability, high transparency, lower melting points and high RE ion solubility[99]. But, the addition of B_2O_3 in the glass matrix leads to high phonon energies of the host lattice, resulting in more non radiative energy losses, thereby leading to loss of luminescence efficiencies [94,100]. Therefore, metal oxides such as SiO_2 are mixed with the borate glasses to lower this high phonon energy of the lattice thereby leading to increase in its

efficiency as a luminescent device [101,102]. Al_2O_3 in the host matrix helps by acting as a good network modifier and imparts excellent chemical and mechanical strength and also leads to emission property enhancement of the glass [100,103]. Na_2O helps in enhancing the glassy nature characterization as it alters the functional group of boron, thereby changing its coordination[104]. ZnO helps ion enhancing the optical and mechanical properties by increasing the thermal stability, chemical durability and reducing the crystallization of the glassy system [104,105]. All the above highlighted characteristic features of the constituent chemicals such as H_3BO_3, SiO_2, Al_2O_3, ZnO and Na_2CO_3 motivated us to prepare a glass system namely alkali zinc alumino borosilicate (AZABS) Glasses to understand its practical utility in optoelectronic device applications.

RE doped glasses have found immense use in luminescence applications due to the fact that RE ions have a 4f configuration, emitting in the visible/NIR region under UV excitation. This has helped RE doped glasses find applications in various optoelectronic, laser, w-LED and SSL applications. Furthermore, RE doped glasses have better thermal and chemical stability, high doping capacity and low manufacturing cost which makes them superior to conventional phosphors [103,106–108]. Dy^{3+} ions have a $4f^9$ configuration and give visible emission between f-f transitions. They are capable of acting as potential single phase white phosphors [106]. Under UV excitation, Dy^{3+} ions give out intense emissions in the blue and yellow region corresponding to $^4F_{9/2} \rightarrow {}^6H_{15/2}$ and $^4F_{9/2} \rightarrow {}^6H_{13/2}$ transitions respectively. White light emission from such glassy materials doped with Dy^{3+} can be tuned by varying the yellow to blue intensity ratio [106].

In this paper, Dy^{3+} doped AZABS Glasses have been prepared. Various morphological and photoluminescence studies have been carried out on the as prepared glass samples. Dexter

Theory has been applied to study the energy transfer mechanisms between the dopant ions in the glass matrix. The conclusive results from these studies assure us that Dy^{3+} doped AZABS glasses can be utilized for optoelectronic device applications such as w-LED and SSL devices.

3.2. Experimental

Quick melt quenching technique was used to synthesis the Dy^{3+} ions doped AZABS glasses with the composition details as given below:

$$35B_2O_3\text{-}20SiO_2\text{-}(15\text{-}x)Al_2O_3\text{-}15ZnO\text{-}15Na_2CO_3\text{-}xDy_2O_3$$

where (x = 0.0, 0.1, 0.5, 1.0, 1.5, 2.0, 2.5 mol%).

Starting powders like H_3BO_3 (99.5%), SiO_2 (99.9%), Al_2O_3 (99.9%), ZnO (99%), Na_2CO_3 (99.9%) and Dy_2O_3 (99.99%) were purchased from Sigma-Aldrich and in total, 8 grams of sample was weighed in stoichiometric ratio. The synthesis process for the preparation of Dy^{3+} ions doped AZABS glasses were mention in chapter 2 in detailed.

3.3. Results and discussion

3.3.1. X-Ray diffraction studies

Fig.3.1. shows the x-ray diffraction spectra of an undoped AZABS glass. It can be easily seen from the diagram that a single broad hump exists in the spectra around 27^0. This broadness actually confirms the amorphous nature of the host material signifying absence of any long-range structural order in the glassy matrix.

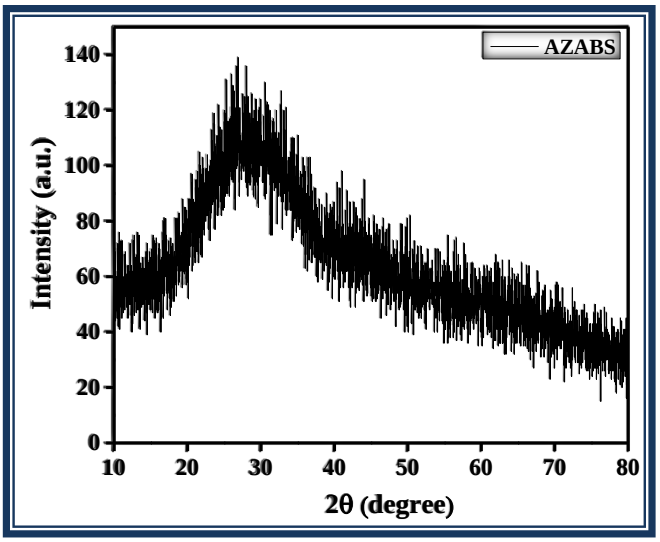

Figure: 3.1. *XRD pattern of an undoped AZABS glass.*

3.3.2. Absorption spectral analysis:

The absorption spectrum of 0.5 mol% Dy^{3+} doped AZABS glass has been provided in Fig.3.2. The spectrum has been recorded in the UV-VIS and NIR region and shows the bands originating from the ground $^6H_{15/2}$ state. As is evident from the graph, lot many bands are present denoting transitions from $^6H_{15/2} \rightarrow {}^7F_{11/2} + {}^6H_{9/2}$, $^6F_{9/2} + {}^6H_{7/2}$, $^6F_{7/2} + {}^6H_{5/2}$, $^6F_{5/2}$, $^6F_{3/2}$, $^4F_{9/2}$, $^4I_{15/2}$, $^4G_{11/2}$, $^4F_{7/2} + {}^4I_{13/2}$, $^6P_{5/2} + {}^4M_{19/2} + {}^4(P, D)_{3/2}$, $^6P_{7/2}$ and $^4M_{17/2} + {}^6P_{3/2}$. These band values match with the ones reported by Carnall et al.[109]. Also, it can be easily seen that bands corresponding to transitions $^6H_{15/2} \rightarrow {}^6P_{5/2} + {}^4M_{19/2} + {}^4(P, D)_{3/2}$ and $^6H_{15/2} \rightarrow {}^4G_{11/2}$ are very weak. This is due to the fact that the host lattice of the glass possesses strong absorption in this region. On the contrary, the transition from $^6H_{15/2} \rightarrow {}^7F_{11/2} + {}^6H_{9/2}$ is highly intense. This is an hypersensitive transition obeying selection rules $|S|=0$, $|L|\leq 2$, $|J|\leq 2$ [94,110,111].

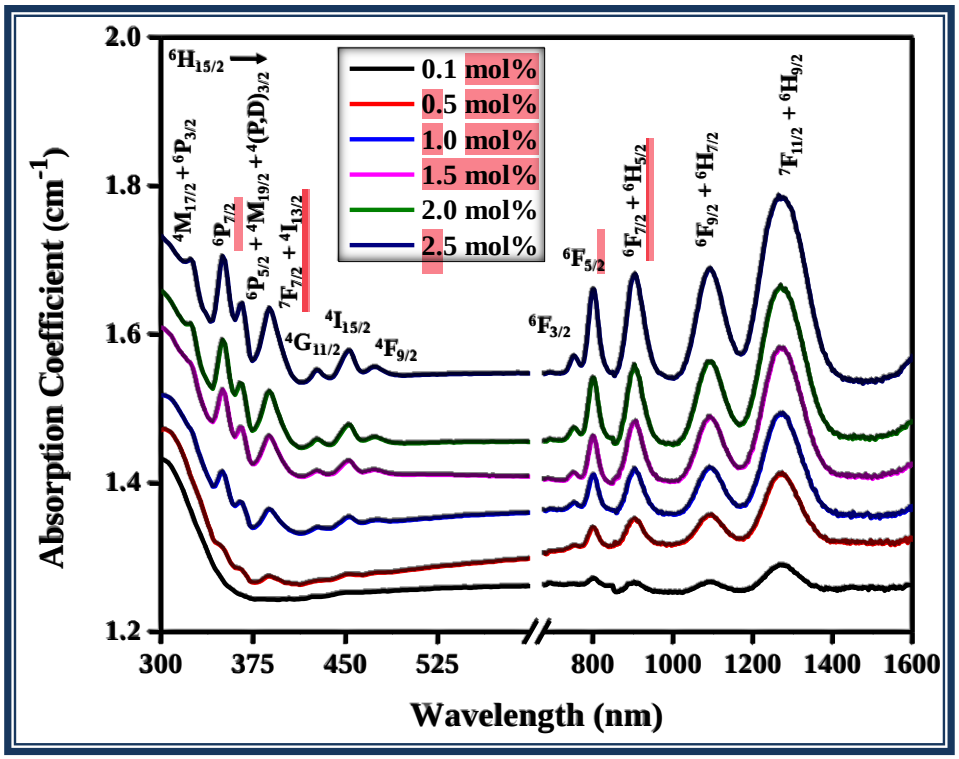

***Figure:3.2**. Absorption of x mol% Dy^{3+} ions (x = 0.1 to 2.5 mol%) doped AZABS glasses.*

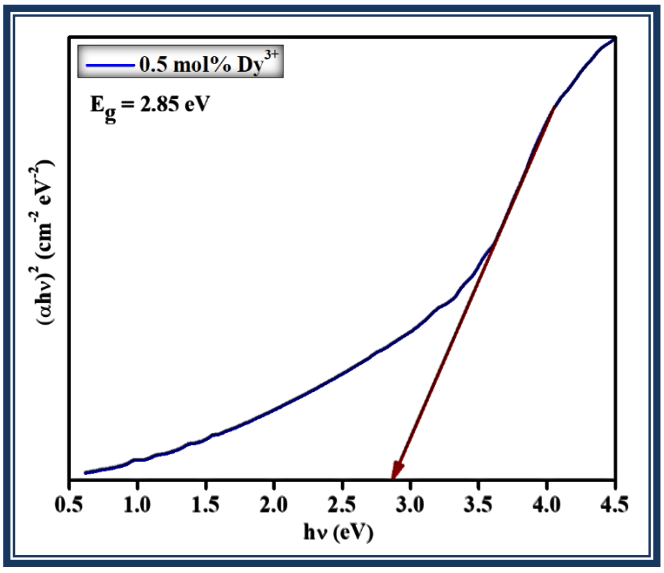

***Figure:3.3.** Tauc Plot for Dy^{3+} 0.5 mol% doped AZABS glass*

Optical bandgap of the Dy^{3+} 0.5 mol% doped AZABS glass was obtained via Tauc plot. The Tauc equation is given as below [112]:

$$\alpha h\nu = C(h\nu - E_g)^n \quad (1)$$

where α is the coefficient of absorption and E_g is the energy band gap, hν is the photon energy, C is energy independent constant and n denotes values specific to various transitions i.e. n=1/2, 2, 1/3 and 3 for direct allowed , indirect allowed, direct forbidden and indirect forbidden transitions [113]. Fig.3.3. shows the Tauc Plot for Dy^{3+} 0.5 mol% doped AZABS glass. The value of direct bandgap obtained from the plot is 2.85 eV.

3.3.3. Photoluminescence (PL) spectral studies:

Optimization of Dy^{3+} doped AZABS glass:

A series of Dy^{3+} doped AZABS (Dy^{3+}= 0.1 mol%, 0.5 mol%, 1 mol%, 1.5 mol%, 2.0 mol% and 2.5 mol%) glasses was prepared to look for the optimum concentration of Dy^{3+} in the glass sample which gives the highest luminescence peak. The emission spectra of this series under 350 nm excitation is given in Fig.3.4. Two sharp bands are seen corresponding to $^7F_{9/2} \rightarrow {}^6H_{15/2}$ (482 nm) and $^7F_{9/2} \rightarrow {}^6H_{13/2}$ (575 nm) transitions, the intensity of which increases till 0.5 mol% concentration of Dy^{3+} and then decreases i.e., concentration quenching occurs after 0.5 mol%. This implies that beyond 0.5 mol%, most of the energy from the host lattice is lost non-radioactively via collisions amongst the dopant ions. So, we have chosen 0.5 mol% Dy^{3+} doped AZABS glasses for our photoluminescence studies purposes. The inset of Fig.3.4 shows the intensity versus concentration graph for the as-prepared glasses.

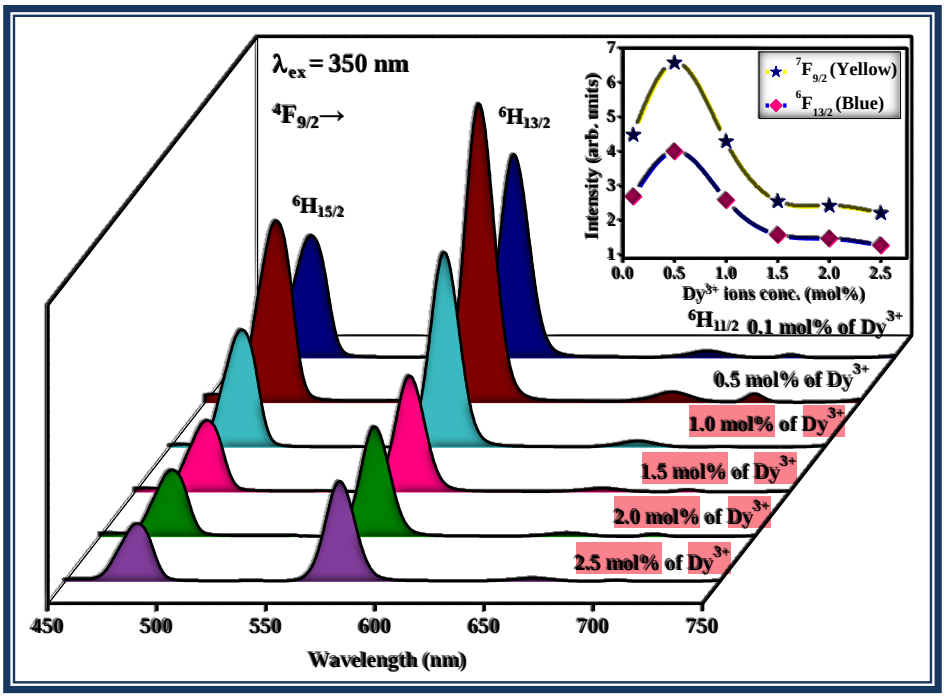

Figure: 3.4*. PL emission spectra of varying Dy^{3+} activator ions concentration (x = 0.1 to 2.5 mol%) doped AZABS glasses at λ_{ex} = 350 nm. The inset diagram shows intensity vs concentration graph.*

PL excitation & emission spectral analysis:

Fig. 3.5. shows the PL excitation spectra of 0.5 mol% Dy^{3+} doped AZABS glass under emission wavelength of 575 nm. Six bands are seen in the spectra corresponding to transitions from $^6H_{15/2} \rightarrow {}^6P_{3/2}$ (325 nm), $^6P_{7/2}$ (350 nm), $^6P_{5/2} + {}^4M_{19/2}$ (365 nm), $^4F_{7/2} + {}^4I_{13/2}$ (385 nm), $^4G_{11/2}$ (425 nm) and $^4I_{15/2}$ (453 nm) [114,115]. Amongst all the excitation transitions, the most prominent one is $^6H_{15/2} \rightarrow {}^6P_{7/2}$ corresponding to 350 nm wavelength. So, this wavelength was chosen to record the emission spectra. The fact that the AZABS glass shows sharp excitation bands from the nUV to blue region proves that these glass samples can be used for w-LEDs applications under UV/nUV excitation.

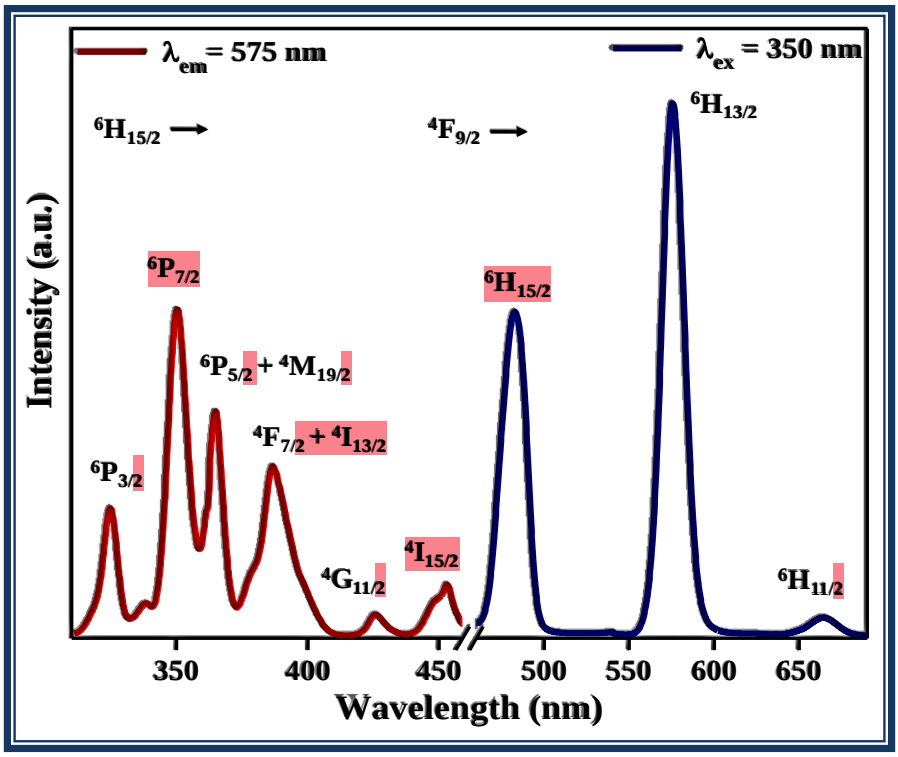

Figure:3. 5. shows the PL excitation spectra of 0.5 mol% Dy^{3+} doped AZABS glass under emission wavelength of 575 nm

The PL emission spectra is given in Fig.3.5. Under 350 nm excitation, three bands are seen in the spectra corresponding to transitions from the energy level $^4F_{9/2}$ to the levels $^6H_{15/2}$, $^6H_{13/2}$ and $^6H_{11/2}$ attributed to the 482 nm, 575 nm and 665 nm wavelength respectively. The intensity of $^4F_{9/2} \rightarrow {}^6H_{13/2}$ is the highest. This transition is an electric dipole in nature and the transition from $^4F_{9/2} \rightarrow {}^6H_{15/2}$ is a magnetic dipole in nature following the selection rules S = 0, L = 2 and J = 2. [94] The Yellow to Blue (Y/B) ratio between this electric dipole transition and magnetic dipole transition for the Dy^{3+} 0.1 to 2.5 mol% doped AZABS glass was calculated to be 1.61 to 1.75. The values of Y/B ratio for all he glasses is greater than unity which is the desired value to obtain white light. Relatively strong yellow peak over blue such as low symmetry sites with no inversion center around the Dy^{3+} ions and high covalence activity between Dy^{3+} ions and

Oxygen ligands. Therefore, the Y/B ratio for Dy^{3+} are used as effective tools to probe the structural nature of the luminescent glass. [116]

The partial energy level diagram showing emission and excitation processes along with cross-relaxation mechanisms is shown in Fig. 3.6. As is evident from the diagram after excitation under 350 nm, the radiative transitions take place from $^4F_{9/2}$ level giving rise to the observed three bands. The self-quenching observed in Fig. 5.4. can be explained via resonant energy transfer mechanism (RET) [117,118]. The possible non radiative, cross-relaxation channels along with RET are given as [94,119]:

19

$$CR1: {}^4F_{9/2} + {}^6H_{15/2} \rightarrow {}^6H_{5/2} + ({}^6H_{7/2}, {}^6F_{9/2})$$

$$CR2: {}^4F_{9/2} + {}^6H_{15/2} \rightarrow {}^6F_{3/2} + ({}^6H_{9/2}, {}^6F_{11/2})$$

$$RET: {}^4F_{9/2} \rightarrow {}^6H_{15/2}$$

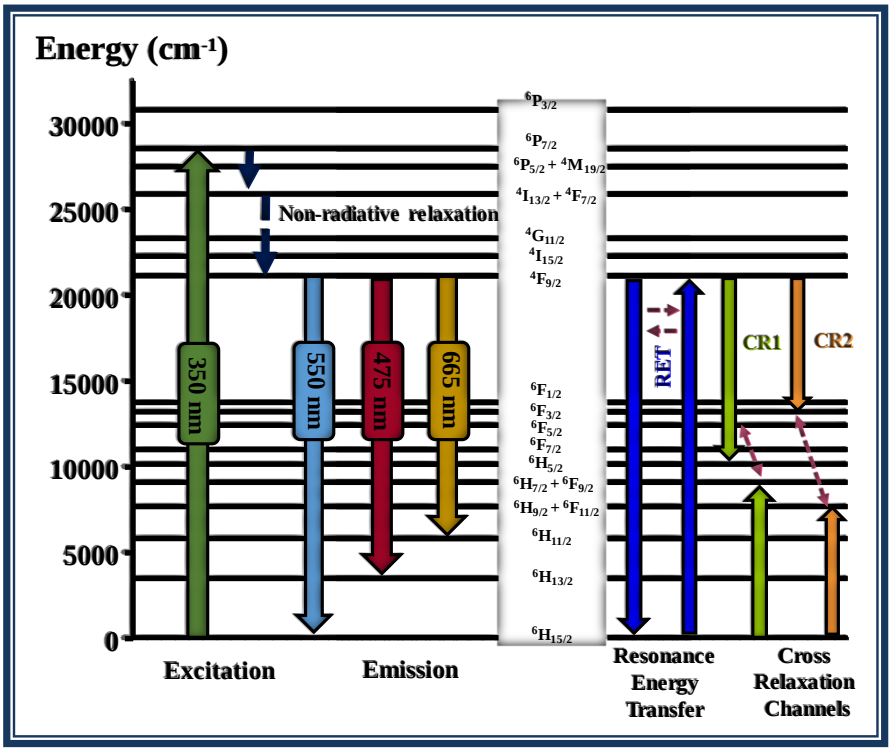

Figure:3.6*. Schematic energy level diagram for Dy^{3+} doped AZABS glasses*

Dexter theory analysis:

To understand the mechanism of energy transfer, Dexter theory was applied to the emission data of prepared doped glasses by using the equation[120]:

$$\log (I/x) = K' - Q\log (x)/3 \quad (2)$$

$$\text{And } K' = \log k - \log \beta \quad (3)$$

Here K' is an independent constant, I is intensity and x is mol% concentration of activator ion. The value of Q determines the type of interaction is responsible for the energy transfer between the neighbouring ions. For Q = 6, dipole - dipole interaction is responsible for energy transfer and for Q = 8 and 10, dipole - quadrupole and quadrupole-quadrupole interaction is responsible respectively. Fig.3.7. shows the plot between log(I/x) and log(x). The value of Q was calculated by using the slope value of the given graph and it came out 5.37, which is close to 6. So, it can be concluded that dipole-dipole interaction was responsible for the energy transfer due to which concentration quenching took place.

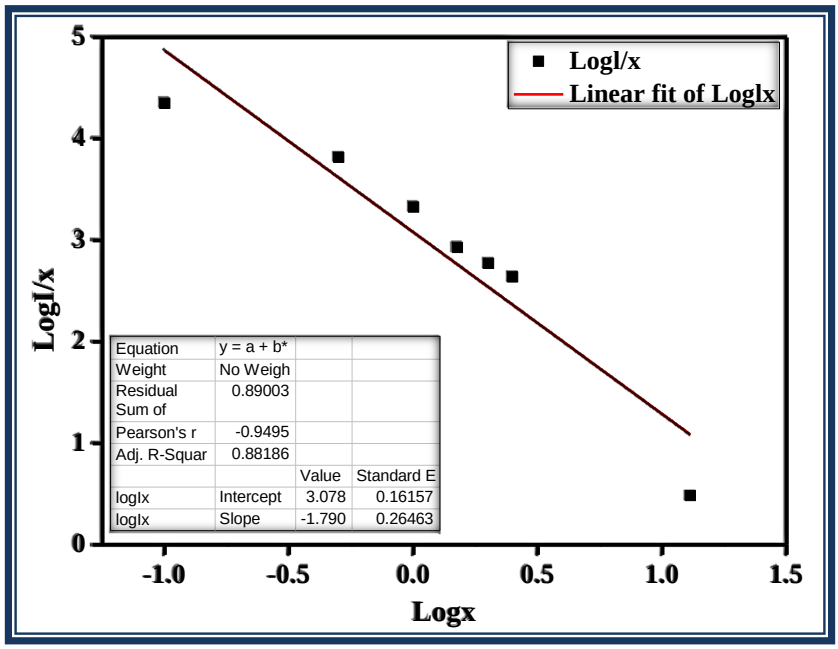

Figure:3.7. *Plot between log(x) vs log(I/x) for Dy^{3+} doped AZABS glasses*

3.3.4. PL Decay spectral analysis:

The PL decay profiles of the AZABS glass samples for 575 nm emission wavelength at 350 nm excitation are given in Fig. 3.8. The PL decay profiles are used to calculate the lifetimes of $^4F_{9/2}$ level. It is evident from the figure that the decay curves show bi-exponential behaviour for all the concentrations of Dy^{3+}. The bi-exponential function signifies that ion-ion interactions are present in the system along with energy transfer giving rise to two components of emission: a slow component and a fast one. There exists a possibility of a different decay for the lanthanide ion. These ions might be at the surface of the glass or within the core of the glassy matrix [121,122]. The experimental lifetimes calculated for the as-prepared doped AZABS glass (x = 0.1 mol% to 2.5 mol%) are 7.87 ms, 6.84 ms, 6.72 ms, 5.57 ms, 5.38 ms and 5.03 ms respectively as shown in Table 3.1. It is seen that the values of the lifetimes decrease with the increase in the concentration of the Dy^{3+} ions. This happens due to the loss of energy via energy transfer between the Dy^{3+} ions themselves. This is also known as quenching. The high lifetime of these glasses indicates that they are well suited for lighting and other such display applications.

Table. 3.1. *CIE chromaticity coordinates (x, y), CCT and average decay time of Dy^{3+} ions doped AZABS glass under 350 nm excitation.*

Sample ID AZABS: *x* mol%Dy^{3+}	CIE (x,y) at λ_{ex} = 350 nm	CCT (K) at λ_{ex} = 350 nm	t_{avg} (ms)
x = 0.1mol%	(0.3759, 0.4098)	4314.72	7.87
x = 0.5 mol%	(0.3776, 0.4117)	4282.46	6.84
x =1.0 mol%	(0.3764, 0.4117)	4310.69	6.72
x = 1.5 mol%	(0.3716, 0.4074)	4409.00	5.57
x = 2.0 mol%	(0.3724, 0.4059)	4383.76	5.38
x = 2.5 mol%	(0.3714, 0.4041)	4399.63	5.03

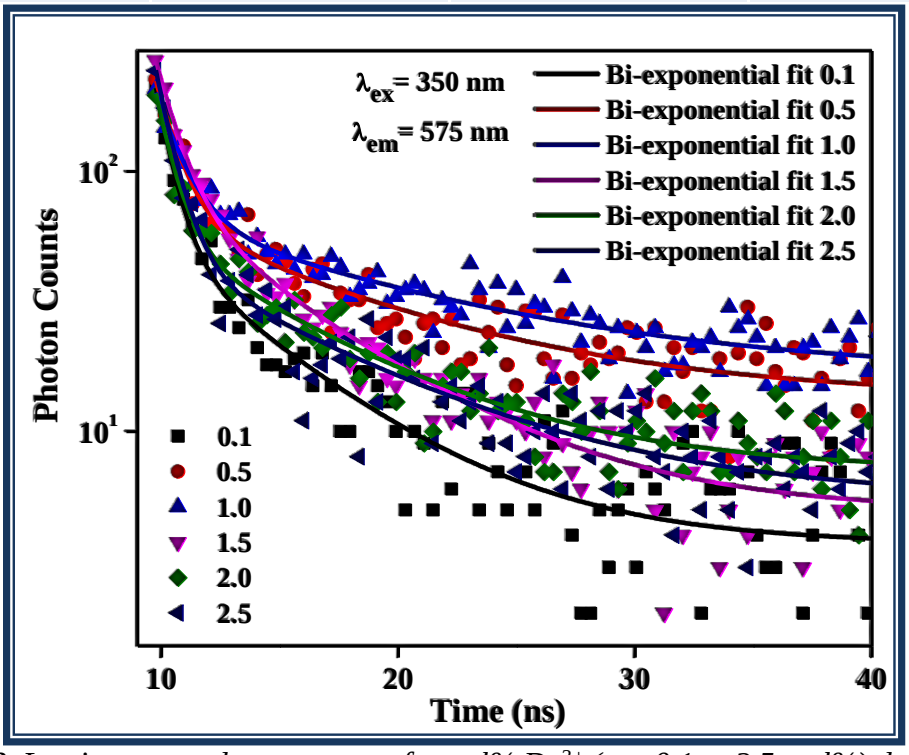

Figure: 3.8. *Luminescence decay curves of x mol% Dy^{3+} (x = 0.1 to 2.5 mol%) doped AZABS glass recorded under 350 nm excitation wavelength.*

3.3.5. Colorimetry analysis:

The PL emission spectra of AZABS glass doped with 0.1 mol% to 2.5 mol% of Dy^{3+} was studied for its photoluminescence properties under 350 nm wavelength excitation. For the recorded spectra, CIE color coordinates were calculated and have been shown in Table 5.1 and Fig.3.9. It is evident from the CIE diagram that these coordinates fall in the white light region of the diagram.

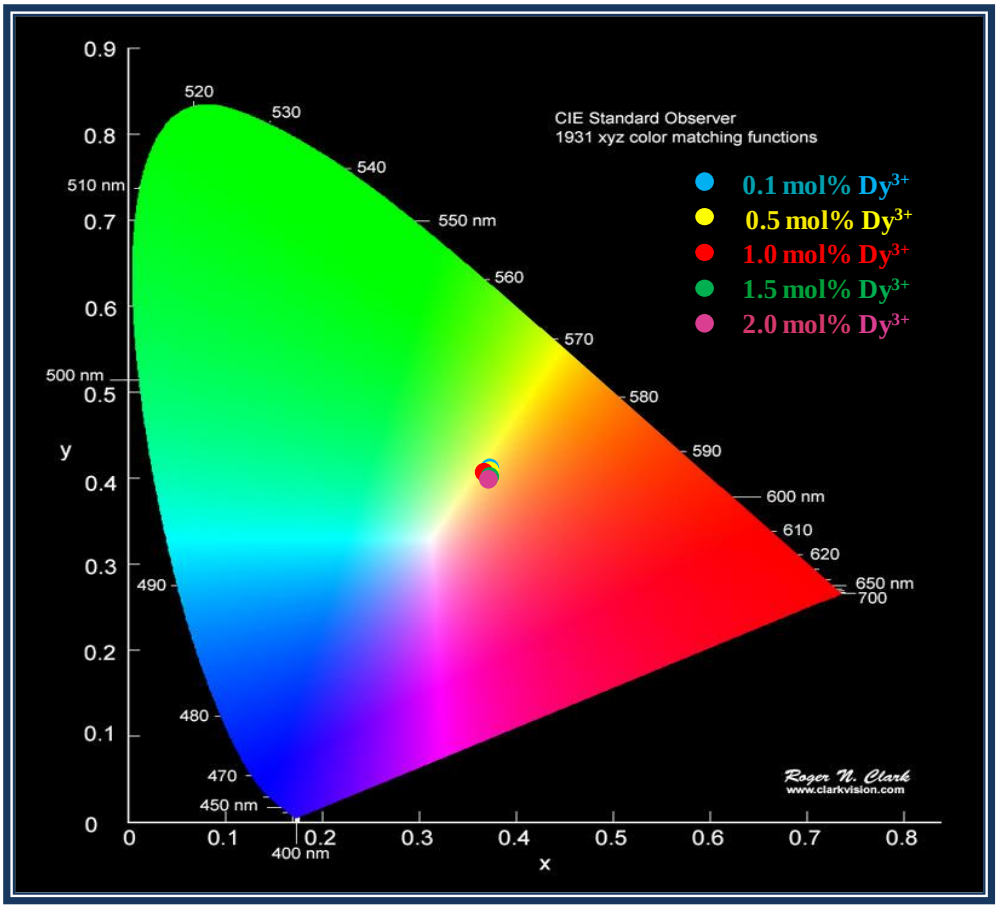

Figure:3.9. *CIE diagram x mol% Dy^{3+} activator ion concentration (x = 0.1 to 2.5 mol%) doped AZABS glasses at λ_{ex} = 350 nm.*

Correlated color temperature (CCT) can further be used to check the luminescence features of the material. It is simply defined as the temperature of a Planckian black body whose color

coordinates closely resemble the standard white light source. CCT expression as given by McCamy is [123]:

$$CCT = -449n^3 + 352n^2 - 6823.2n + 5520.3 \quad (4)$$

Here the value of n is given by $[(x-x_e)/(y-y_e)]$ where $x_e = 0.332$ and $y_e = 0.186$. The CCT values for the doped AZABS glass is given in Table 5.1. It is known that lamps with CCT < 3200 K give warm white light, whereas lamps with CCT > 4000 K give cool white light. The as-prepared glasses have CCT values greater than 4000 K [115]. This fact along with the CIE data proves that Dy^{3+} doped AZABS glasses can indeed be used for w-LED and solid-state lighting applications.

3.3.6. Temperature dependent PL studies:

In applications of solid-state lighting and w-LEDs, where operating temperature can increase beyond 470 K, it is important to know the thermal stability of the material that is to be deployed [124]. The temperature-dependent emission spectra of 0.5 mol% Dy^{3+} doped AZABS glass has been shown in Fig.3.10. The Fig 3.11. shows the tendency of the $^4F_{9/2} \rightarrow {}^6H_{13/2}$ transition to lose intensity with increase in temperature. It is clear from the spectra that the luminescence intensity decreases with the increase in temperature from 30^0C till 200^0C due to the thermal quenching effect. Till 473 K, the intensity reduces to 75% of its value at 298 K.

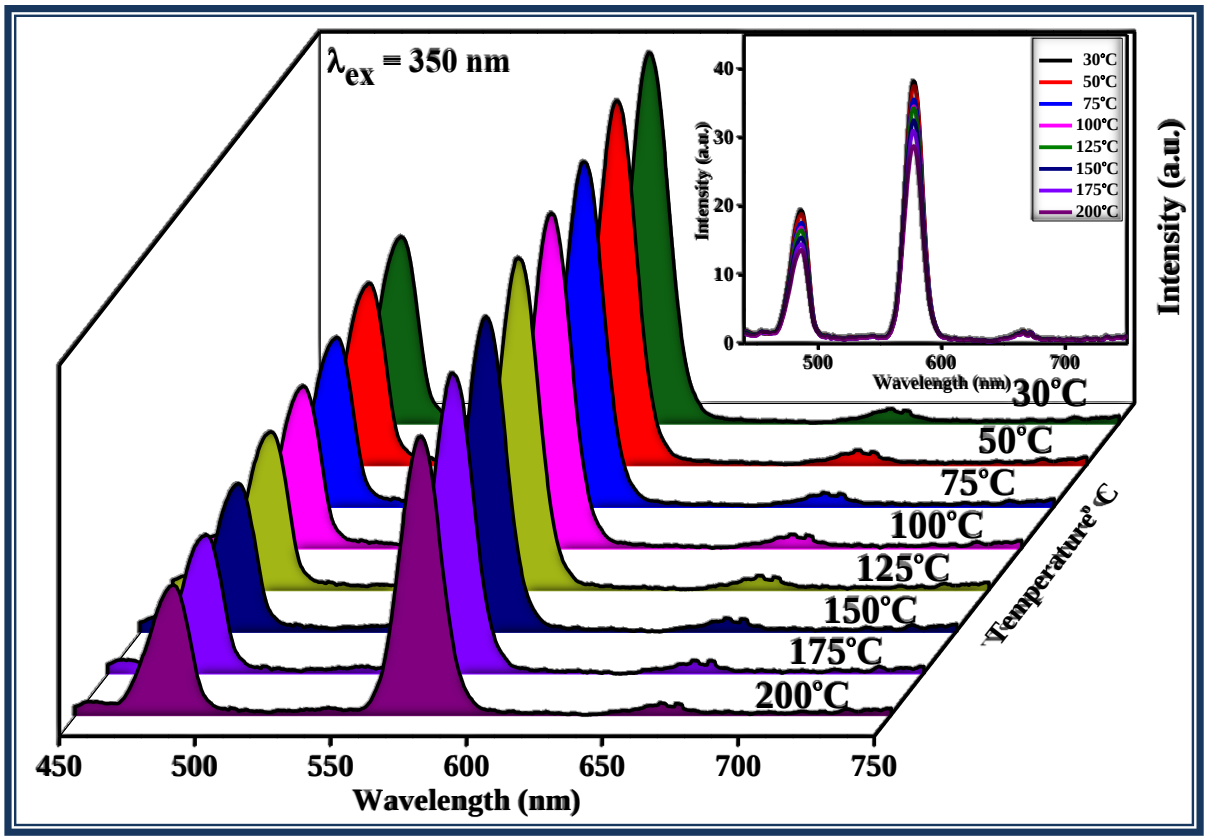

Figure:3.10. *Temperature dependent emission intensity variation of 0.5 mol% Dy^{3+} doped AZABS glass under 350 nm excitation with rise in temperature from RT to 200°C*

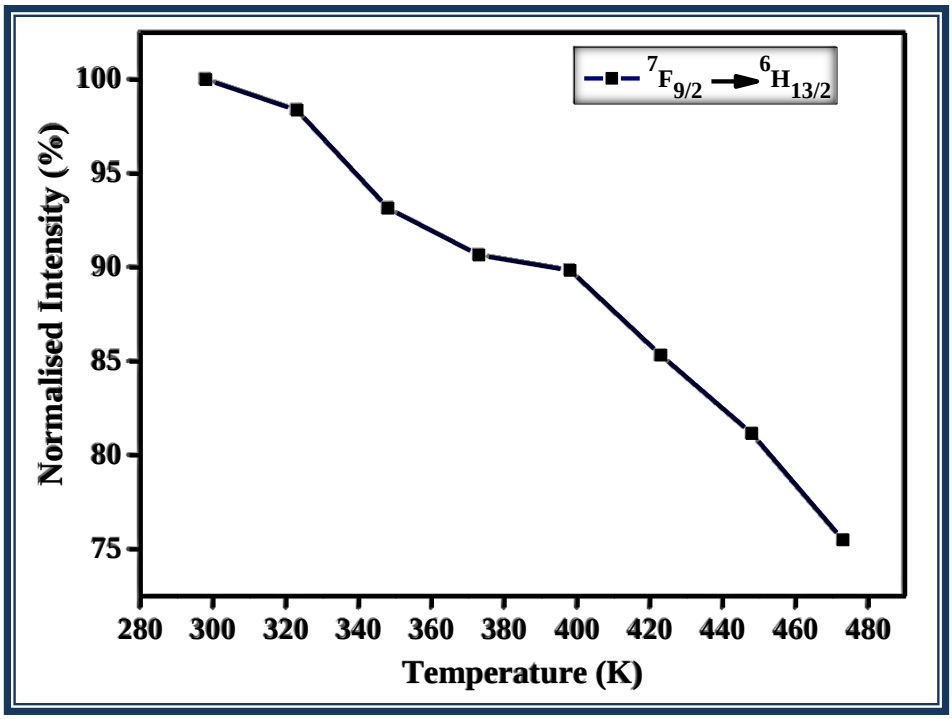

Figure:3.11. *Plot shows the PL intensity with rise in temperature range 298-473 K.*

The thermal quenching effect in luminescence intensity is observed due to phonon interaction in which the excited luminescence centre is thermally activated through a crossing point between the ground and excited states [125]. The activation energy required for thermal quenching can be calculated via Arrhenius Equation [126,127] :

$$I(T) = \frac{Io}{1 + cexp[-\left(\frac{\Delta E}{KT}\right)]} \quad (5)$$

Where I_0 is the initial intensity, I(T) is the intensity at given temperature T, ΔE is the activation energy for thermal quenching and K is the Boltzmann constant (8.629 x 10^{-5} eV). This equation was used to fit the temperature-dependent intensities and the corresponding graph is shown in Fig. 3.12. The activation energy was found out to be 0.226 eV, which is higher than similar reported materials [124–126]. This proves that Dy^{3+} doped AZABS glass shows excellent thermal stability and is suitable for various lighting and w-LEDs applications.

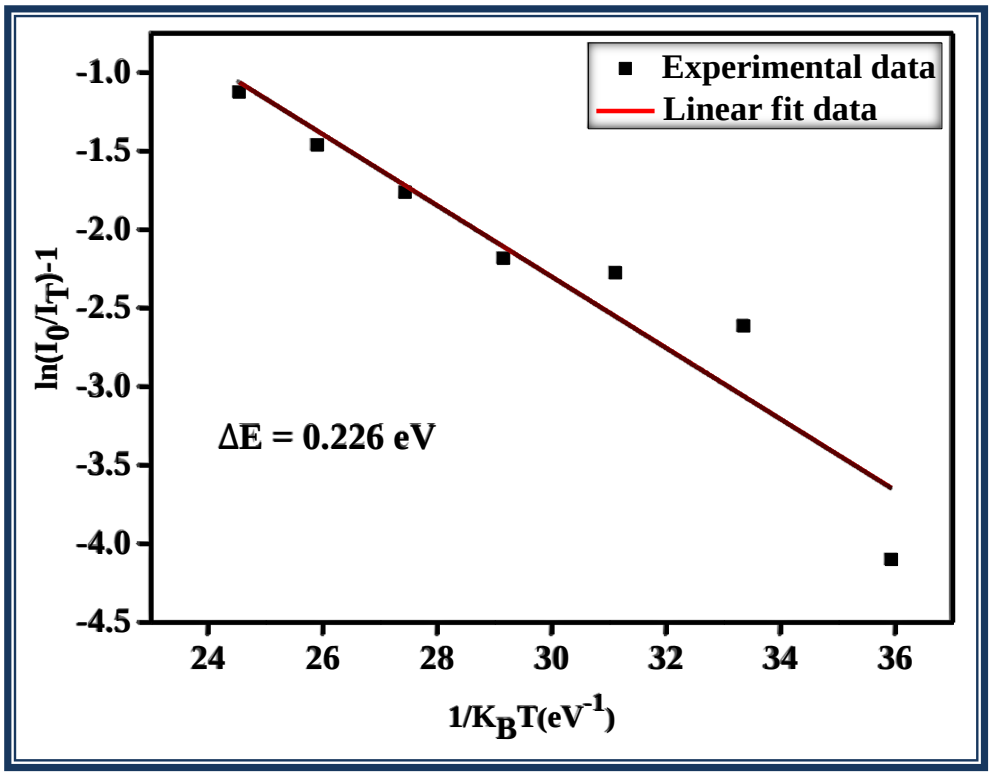

Figure:3.12. *ln[(I₀/I_T)-1] versus 1/k_BT plot to calculate activation energy of 0.5 mol% Dy^{3+} doped AZABS glass.*

3.4. Conclusions

Dy^{3+} doped AZABS glasses were prepared using the melt quench technique. Various morphological and photoluminescence studies were conducted on the as-prepared glass samples. Under 350 nm excitation, the glass samples show sharp bands related to transitions from the energy level $^4F_{9/2}$ to the levels $^6H_{15/2}$ (482 nm), $^6H_{13/2}$ (575 nm) and $^6H_{11/2}$ (665nm). Dexter theory analysis showed that the energy transfer between the dopant ions was of dipole-dipole nature. Temperature-dependent photoluminescence studies show that these AZABS glass samples have excellent thermal stabilities. Decay kinetics of the as-prepared glass samples indicate high lifetimes. Such sharp luminescence intensities under UV excitation coupled with

high lifetimes, superior thermal stabilities of luminescence intensities and positive results from colorimetric calculations prove that Dy^{3+} doped AZABS glasses are suitable candidates for applications in w-LEDs and solid-state lighting.

Chapter 4

Thermally Stable Sm^{3+} doped AZABS Glasses for Warm White Light Generation and w-LED Applications

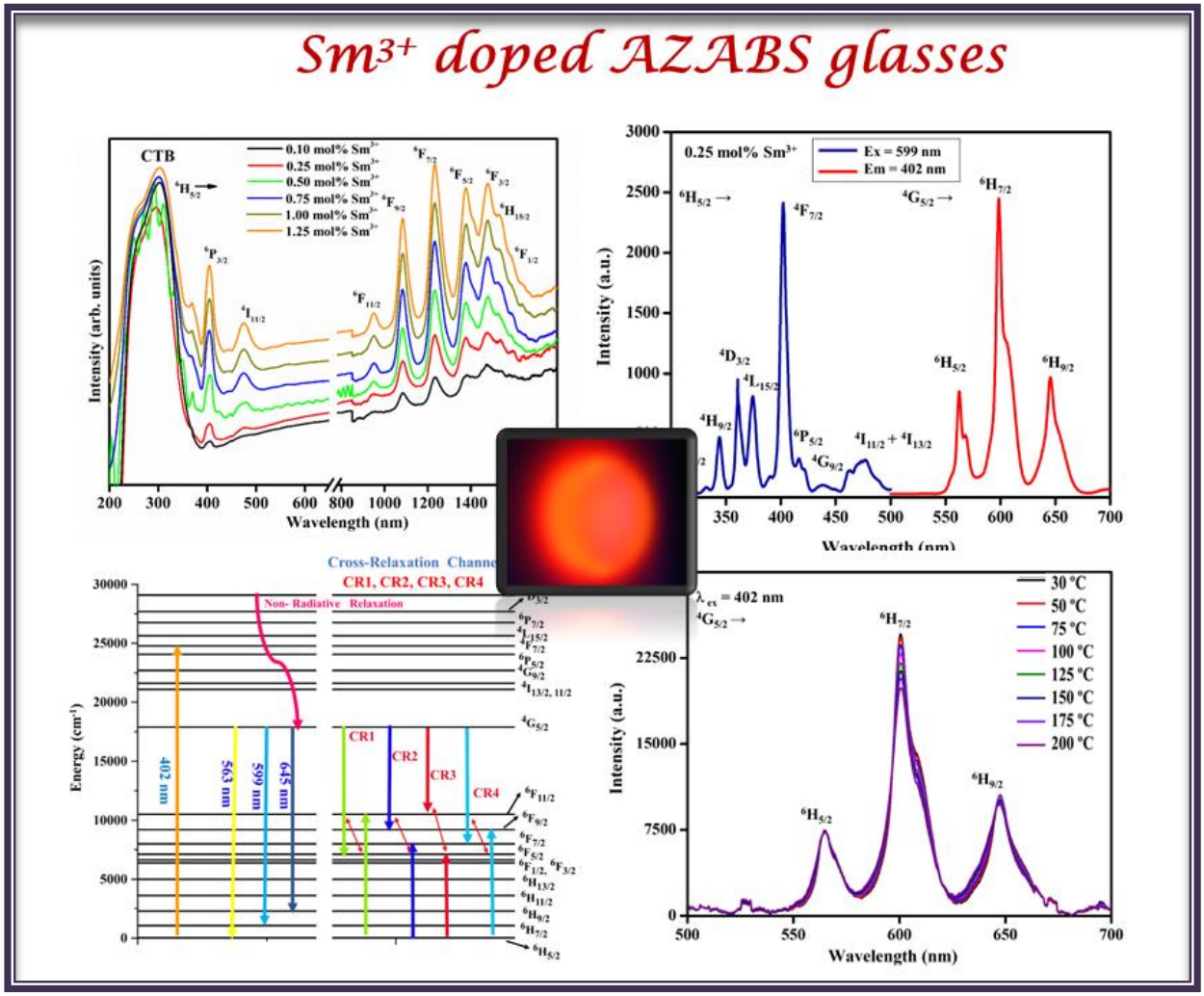

Part of this work has been published in Luminescence 28 (2023), 428-436,

(Impact Factor = 3.2)

Samarium (Sm^{3+}) ions doped AZABS glasses were synthesized via quick melt quench technique. Various spectroscopic studies like optical absorption, photoluminescence (PL) emission, PL excitation, temperature-dependent PL and PL decay kinetics were performed on the as prepared glass system. Under 402 nm excitation, three sharp bands at wavelengths 563, 599 and 645 nm corresponding to transitions $^4G_{5/2} \rightarrow {}^6H_{5/2}$, $^6H_{7/2}$ and $^6H_{9/2}$, respectively can be seen in the PL emission spectra. The 0.25 mol% Sm^{3+} glass has the highest intensity for these emissions. The lanthanide interaction in the glass matrix is dipole-dipole in nature as was proven from Dexter's analysis. The direct bandgap of 0.25 mol% Sm^{3+} doped AZABS glass was calculated to be 2.88 eV. The lifetimes of the as prepared glasses range from 1.93 ms for the lowest concentration of Sm^{3+} to 0.75 ms for the highest. From temperature dependent PL studies, the activation energy for 0.25 mol% Sm^{3+} doped AZABS glass was found to be 0.19 eV which shows high thermal stability of this glass. We propose to utilise these Sm^{3+} doped AZABS glasses for w-LEDs and solid-state lighting (SSL) applications.

4.1. Introduction

Over the past ten years, research on trivalent rare earth (RE) doped materials, such as phosphors, glasses, ceramics, etc., has advanced significantly. Because these materials have so many uses in fields like drug delivery, telecommunications, solar cells, memory devices, white light emitting diodes (w-LEDs), display devices, lasers, fiber amplifications, etc., researchers all over the world have become increasingly interested in and fascinated by them [94,127–133]. It is a well-known fact that research is always application oriented and that application stems out from a problem which needs a sustainable, affordable, efficient yet modern solution. The biggest problem that is being faced today by mankind is excessive consumption of energy to advance our quality of life. Due to this, we have been increasing our carbon footprint since decades which is leading to immense pressure on the environment. Efforts are being drastically

made to replace the conventional sources of energy with more ecologically friendly, less polluting and more efficient materials that can actually help to conserve the environment by reducing our carbon footprint. It is due to this aspiration that SSL has emerged as an active area of research for sustainable materials [134–136].

SSL devices find many uses in varying areas of liquid crystal displays, cellular phone screen illumination, traffic signals, w-LEDs, magneto-optical devices etc.[91,94,110,116]. w-LEDs are one thrust area in the field of SSL technology and a right step in the direction of a cleaner and greener environment. These w-LEDs are more advantageous than the usual sources of light like the incandescent bulbs, tube lights etc. because of their high efficiency, low energy consumption, compact size and long life span[95,137]. There are two ways to fabricate w-LEDs. The first procedure utilizes a yellow solid phosphor YAG:Ce^{3+} which is excited by a blue LED chip of InGaN. The second procedure involves usage of a mix of RGB phosphors excited by a UV light [97,138]. But both these methods have their drawbacks like low color rendering index (CRI), high color correlated temperature (CCT=7750K) and low luminescence efficiency [100,139]. Also, phosphor-based LEDs utilize a polymer-based epoxy block to withhold the phosphor material. The thickness of this polymer material dictates the intensity of luminescence from the LED. But this epoxy region is highly degradable as it is unstable under conditions of high temperature, energy and excitation. Therefore, better alternate materials for fabrication of w-LEDs are required. This is where RE doped glassy systems come into play. No epoxy region is involved in glassy materials. Moreover, glasses have a low production cost, simple manufacturing, homogenous light emission, higher transparency and less susceptibility to heat [95,98,111,140].

Phosphates, silicates, tellurites, borates and borosilicate's as glassy hosts find applications in various fields of photonics due to superior luminescence properties when doped with RE ions [86,97,132,140–145]. Amongst these, borosilicate glasses hold special value as they are known to have high thermal stability, low melting points, high transparency and higher doping capacity of RE ions [146]. But it has been observed that, presence of B_2O_3 in the glass actually reduces the intensity of radiative emissions. This is because addition of B_2O_3 increases the phonon energies of the host lattice thereby increasing non-radiative losses [147]. Hence, certain metal oxides like SiO_2 are mixed in the glasses to help reduce the phonon energies thereby increasing their luminescence efficiencies [116,131,148]. Al_2O_3 is added to the lattice as a network modifier. This results in an increase in the glass stability and luminescence along with higher solubility of RE ions [110,132,149,150]. Addition of ZnO has a dual role (modifier and former) for glass structures and is known to enhance the electrical, magnetic, mechanical and optical properties. ZnO increases the thermal and chemical stability and decreases the possibility of crystallization of glassy system [101,151]. Na_2CO_3 is added to alter the functional groups of boron resulting in the change of their coordination. This helps in the glassy nature enhancement of the lattice [104,148].

As is known, the luminescence properties of RE ions are dependent on 4f-4f transitions which can be tuned specifically for one's requirements by altering the chemical and physical interactions of these ions [152]. Sm^{3+} ions-based materials find usage in many modern-day applications of display devices, SSL and lasers, therapeutic research, optical communications etc.[139,147,153–156]. The Sm^{3+} doped materials give out sharp reddish orange luminescence due to three sharp transitions corresponding to $^4G_{5/2} \rightarrow {}^6H_{5/2}$, $^4G_{5/2} \rightarrow {}^6H_{7/2}$ and $^4G_{5/2} \rightarrow {}^6H_{9/2}$ transitions. By varying the red to orange ratio, white emission from Sm^{3+} doped glassy materials can be tuned for w-LED applications.

In this paper, Sm^{3+} doped Alkali Zinc Alumino Borosilicate (AZABS) glasses have been prepared. Detailed luminescence studies on the glasses were conducted. The energy transfer mechanism between the lanthanide ions was understood by applying the Dexter Theory. The promising results from these studies show that Sm^{3+} doped AZABS glasses can indeed be utilised for w-LED and SSL applications.

4.2. Experimental:

Sm^{3+} ions doped AZABS glasses were prepared via a quick melt quenching technique. The composition details are:

$$35B_2O_3\text{-}20SiO_2\text{-}(15\text{-}x)\ Al_2O_3\text{-}15ZnO\text{-}15Na_2CO_3\text{-}xSm_2O_3$$

where (x = 0.0, 0.10, 0.25, 0.50 0.75, 1.00, 1.25 mol%).

Precursors powders like B_2O_3 (99.5%), SiO_2 (99.9%), Al_2O_3 (99.9%), ZnO (99%), Na_2CO_3 (99.9%) and Sm_2O_3 (99.99%) were purchased from Sigma-Aldrich. A flowchart in Fig.2.1 depicts the aforementioned steps involved in the synthesis procedure in chapter 2.

4.3. Results and Discussion:

Before moving ahead with the discussion on photoluminescence studies, we also recorded the x-ray diffraction data and thermal parameters of the un-doped AZABS glass. The XRD pattern is same as has been reported by us in our earlier work showing a single broad hump signifying the amorphous nature of the prepared glass [148]. Thermal parameters have also been reported by us in our previous work [157]. The numerical values of peak crystallization temperature (Tc), melting temperature (T_m), glass transition temperature (T_g), onset crystallization temperature (T_x) and Hurby's thermal stability parameter (KH) were observed to be same as reported by us earlier. This corroborates the thermal stability of our glass system which can be helpful in various applications.

4.3.1. Absorption spectral analysis:

Fig. 4.1. shows the absorption spectra of all the as prepared doped glasses at room temperature. Various f-f- transitions from ground state $^6H_{5/2}$ to different excited states are visible. Different bands at wavelengths 402, 476, 950, 1083, 1233, 1376, 1475, 1532 and 1601 nm corresponding to transitions from $^6H_{5/2} \rightarrow {}^6P_{3/2}$., $^4I_{11/2}$, $^6F_{11/2}$, $^6F_{9/2}$, $^6F_{7/2}$, $^6F_{5/2}$, $^6F_{3/2}$, $^6H_{15/2}$ and $^6F_{1/2}$ respectively were seen. This can be corroborated by the findings of Carnal et al. [158]. Both electric dipole induced and magnetic dipole induced transitions are observed. The electric dipole induced transitions follow selection rule $\Delta J \leq 6$ whereas the magnetic dipole induced ones follow the rule $\Delta J=0, \pm 1$ [100]. The visible absorption bands appear weak in their intensity as they are spin forbidden or there might be an overlap of different $^{2S+1}L_J$ levels in that region [159]. The bands in the NIR region are sharp with more intensity. This can be attributed to the shielding of 4f electrons due to 5s and 5p electrons These bands are spin allowed [$\Delta S=0$] from the $^6H_{5/2}$ to the ^6H and ^6F states and are assigned as $^6H_{5/2} \rightarrow {}^6F_J$ where J is 1/2, 3/2 5/2, 7/2, 9/2 and 11/2. A charge transfer band (CTB) also exists in the region between 200-300 nm as is evident in the figure.

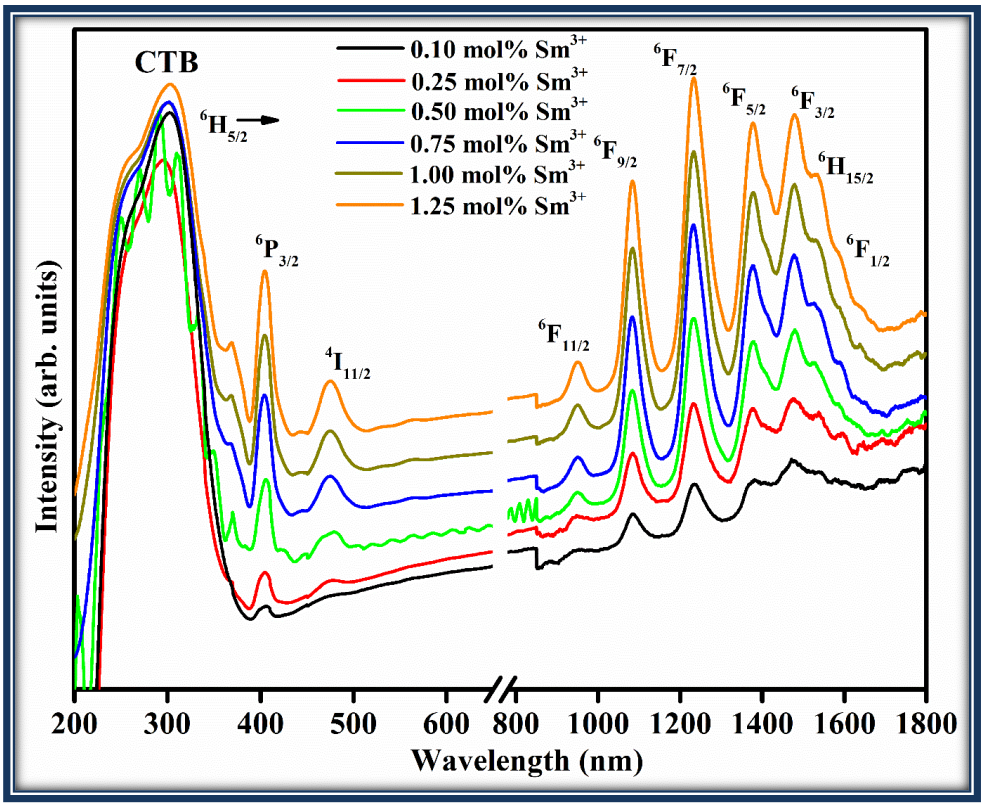

Figure: 4.1 *Absorption spectra of x mol% Sm^{3+} ions (x = 0.10, 0.25, 0.50, 0.75, 1.00 and 1.25 mol%) doped AZABS glasses in UV-VIS-NIR region.*

A Tauc plot for Sm^{3+} 0.25 mol% doped AZABS glass is shown in Fig.3. It was used to calculate the optical bandgap of the as mentioned glass. The Tauc equation is given as [148]:

$$\alpha h\nu = C(h\nu - E_g)^n \qquad (1)$$

where α is the coefficient of absorption and E_g is the energy band gap, hν is the photon energy, C is energy independent constant and n denotes values specific to various transitions i.e., n=1/2, 2, 1/3 and 3 for direct allowed, indirect allowed, direct forbidden and indirect forbidden transitions respectively [90]. The value of direct bandgap as obtained from the Tauc Plot is 2.88 eV as shown in Fig. 4.2.

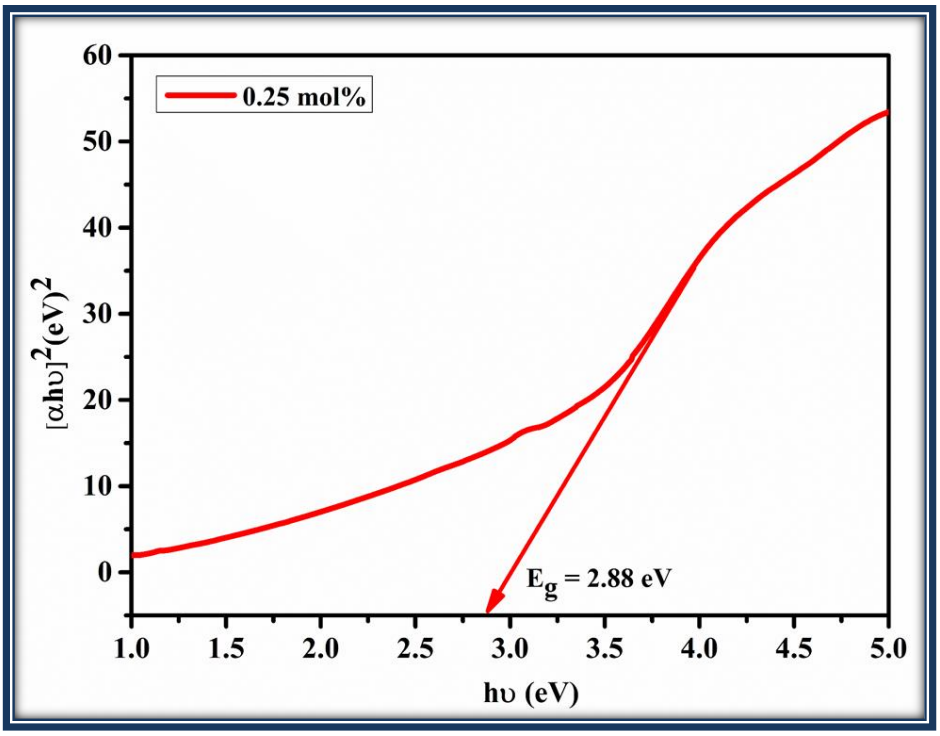

Figure: 4.2 *Tauc Plot for Sm^{3+} 0.25 mol% doped AZABS glass to calculate direct band gap*

4.3.2. Photoluminescence spectral analysis:

Optimization of Sm^{3+} doped AZABS Glasses

In order to determine the optimum concentration of Sm^{3+} in AZABs glass that would give the maximum luminescence under excitation, a series of Sm^{3+} doped AZABS glasses (0.1mol%, 0.25 mol%, 0.5 mol%, 0.75 mol%, 1.0 mol% and 1.25 mol%) was prepared. The photoluminescence emission spectra under 402 nm excitation of the as prepared glasses are shown in Fig. 4.3. The inset shows luminescence intensity vs concentration graph for the glasses. Three sharp bands are present in the spectra at wavelengths 563, 599 and 645 nm corresponding to $^4G_{5/2} \rightarrow {}^6H_{5/2}$, $^6H_{7/2}$ and $^6H_{9/2}$ transitions respectively. The intensity of these bands increases till 0.25 mol% and after that concentration quenching occurs for higher Sm^{3+} doping in the glass. Concentration quenching occurs when there is a non-radiative energy transfer between the activator ions via cross relaxation processes. Increasing the concentration

of activator ions in the lattice decreases the critical distance between them thereby resulting in non-radiative energy transfer. Therefore, we chose 0.25 mol% Sm^{3+} doped AZABS glass for our photoluminescence analysis purposes.

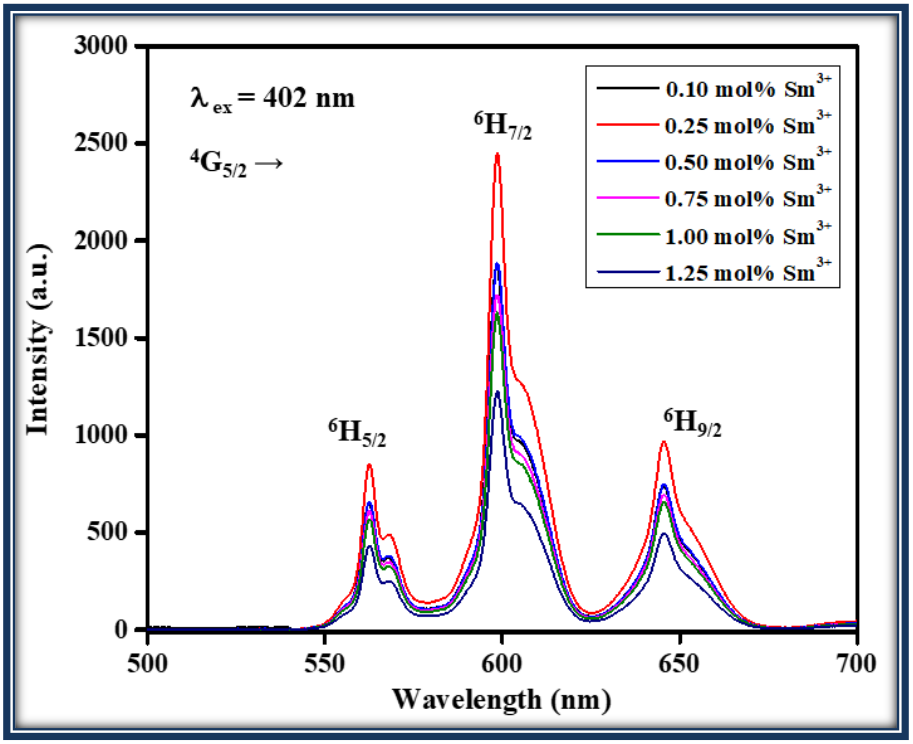

Figure:4.3 *Optimization of Sm^{3+} doped AZABS glasses under λ_{ex} = 402 nm.*

PL excitation & emission spectral analysis:

Fig. 4.4. shows the excitation spectrum of Sm^{3+} 0.25 mol% doped AZABS glass under 599 nm emission wavelength. Eight bands can be seen in the spectra at wavelengths 315, 344,360, 374, 402, 416, 422 and 475 nm corresponding to transitions from $^6H_{5/2} \rightarrow {}^4P_{1/2}$, $^4H_{9/2}$, $^4D_{3/2}$, $^4L_{15/2}$ $^4F_{7/2}$, $^6P_{5/2}$, $^4G_{9/2}$, $^4I_{11/2} + {}^4I_{13/2}$ respectively [147]. The band corresponding to $^6H_{5/2} \rightarrow {}^4F_{7/2}$ is most intense corresponding to 402 nm wavelength. So, this was chosen to be our excitation wavelength in order to record the emission spectra of the sample.

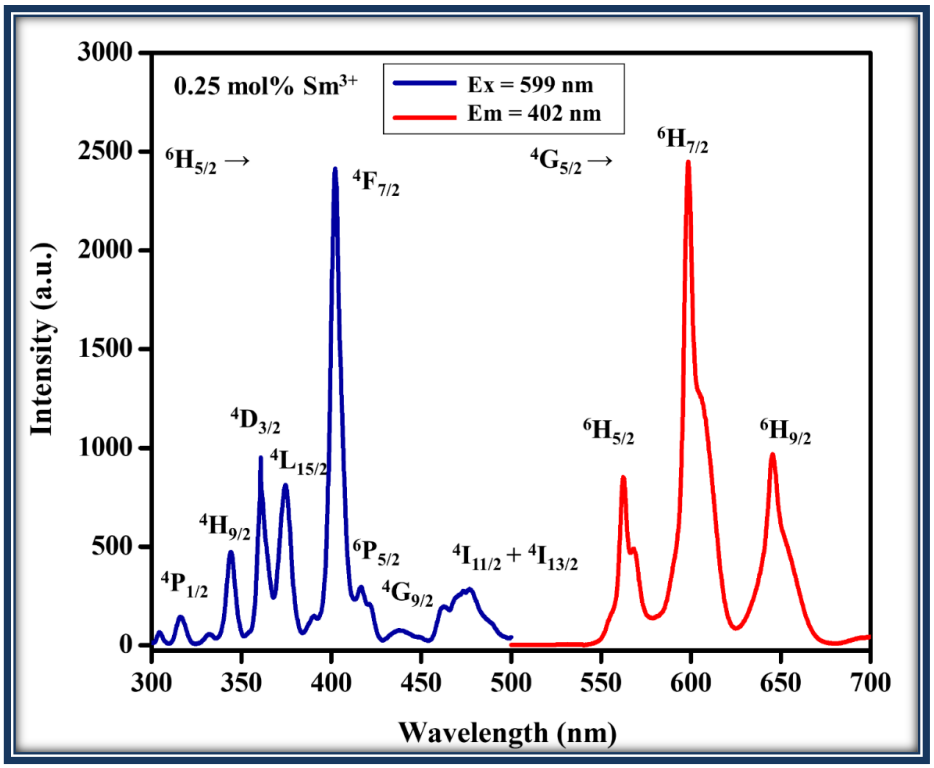

Figure:4.4 *PL excitation and emission spectra of x mol% Sm^{3+} ions (x = 0.10, 0.25, 0.50, 0.75, 1.00 and 1.25 mol%) doped AZABS glasses at λ_{ex} = 402 nm.*

Emission spectrum of Sm^{3+} 0.25 mol% doped AZABS glass at 402 nm excitation is also shown in Fig. 4.5. Three sharp bands at wavelengths 563, 599 and 645 nm corresponding to transitions $^4G_{5/2} \rightarrow {}^6H_{5/2}$, $^6H_{7/2}$ and $^6H_{9/2}$ respectively can be seen in the spectra [131]. The transitions $^6H_{5/2} \rightarrow {}^6F_{9/2}$ and $^6H_{5/2} \rightarrow {}^6F_{7/2}$ as seen in the absorption spectra are hypersensitive in nature. The transition $^4G_{5/2} \rightarrow {}^6H_{9/2}$ is also a hypersensitive transition. Detailed analysis of the absorption and emission spectra of as prepared glass shows that the transition $^6H_{5/2} \rightarrow {}^6F_{7/2}$ is a threefold triplet. This can be due to the fact that $^6H_{5/2}$ might be degenerate in the crystal field due to Sm^{3+} ions getting self-adjusted in the glass network thereby resulting in splitting of the transition [159]. The transition $^4G_{5/2} \rightarrow {}^6H_{7/2}$ in the emission spectra is both electric and

magnetic dipole allowed with selection rule $\Delta J = \pm 1$ whereas the transition $^4G_{5/2} \rightarrow {}^6H_{9/2}$ is purely electric dipole allowed [131].

Asymmetry ratio is defined as the intensity ratio of electric dipole and magnetic dipole transitions. This red to orange ratio ($^4G_{5/2} \rightarrow {}^6H_{9/2}$ / $^4G_{5/2} \rightarrow {}^6H_{7/2}$) is used to determine the degree of asymmetry near the local environment of the lanthanide. The R-O ratios for all the as prepared Sm^{3+} doped AZABS glasses were found to be 0.3972, 0.3949, 0.3958, 0.4029, 0.4039 and 0.4059 for 0.1 mol%, 0.25 mol%, 0.5 mol%,0.75 mol%,1.0 mol% and 1.25 mol% Sm^{3+} doped glasses respectively. High asymmetry ratio for 1.25 mol% Sm^{3+} doped AZABS glass shows more local disorder as compared to other glasses. Since the ratios are less than unity, it shows that Sm^{3+} ions occupy an inverse symmetry site in the glass lattice [159].

The energy transfer mechanism during excitation, emission and cross-relaxation is depicted as a partial energy level diagram in Fig. 4.5 As is evident, all the energy levels above the $^4G_{5/2}$ level are closely spaced. The Sm^{3+} ions are excited to levels above the $^4G_{5/2}$ state but immediately undergo a non-radiative relaxation to the $^4G_{5/2}$ state. Multiphoton relaxation process is prevented due to presence of a large gap between $^4G_{5/2}$ and $^6F_{11/2}$ levels. A summary of possible cross relaxation channels for Sm^{3+} doped AZABS glass is given below:

CR1: $^4G_{5/2}$, $^6H_{5/2} \rightarrow {}^6F_{11/2}$, $^6F_{5/2}$

CR2: $^4G_{5/2}$, $^6H_{5/2} \rightarrow {}^6F_{9/2}$, $^6F_{7/2}$

CR3: $^4G_{5/2}$, $^6H_{5/2} \rightarrow {}^6F_{5/2}$, $^6F_{11/2}$

CR4: $^4G_{5/2}$, $^6H_{5/2} \rightarrow {}^6F_{7/2}$, $^6F_{9/2}$

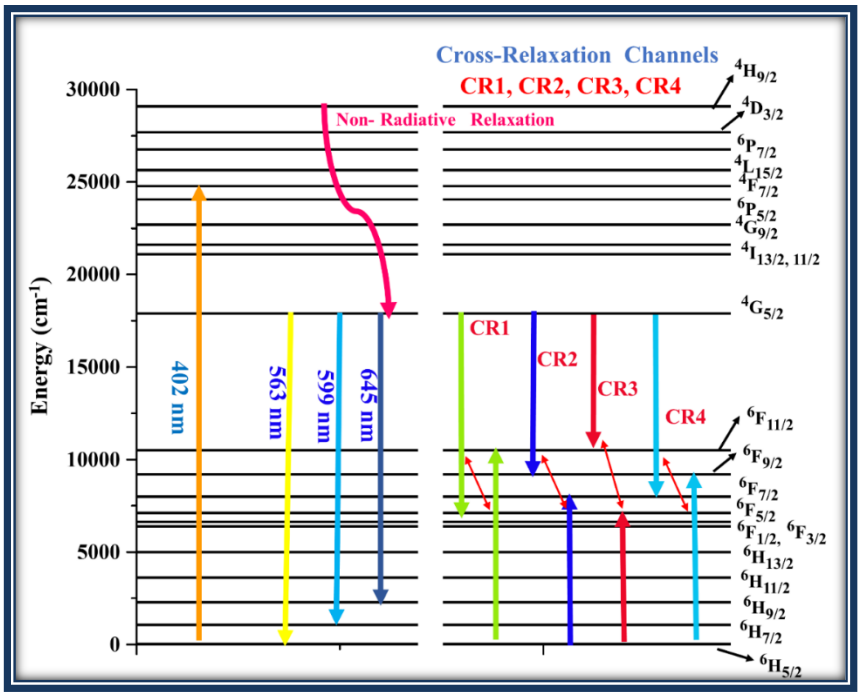

Figure:4.5 *Schematic energy level diagram for Sm^{3+} doped AZABS glasses with excitation, emission and cross- relaxation channels.*

Cross relaxation occurs when the emission and absorption transitions match well with each other. CR3, in this case, is the major energy transfer channel because $^4G_{5/2} \rightarrow {}^6F_{5/2}$ emission band has almost same energy as the $^6H_{5/2} \rightarrow {}^6F_{11/2}$ absorption band [100].

The energy transfer mechanism resulting in concentration quenching is due to cross relaxation (CR) process between the Sm^{3+} ions. These CR processes occur between levels having a small energy difference. A Sm^{3+} in the excited state $^4G_{5/2}$ transfers energy to a Sm^{3+} ion in ground state $^6H_{5/2.}$ This results in the first ion settling in the intermediate $^6F_{5/2}$ state whereas the second ions get excited to the upper $^6F_{11/2}$ state. This is CR1 process and it happens in resonance with the luminescent transition from $^4G_{5/2} \rightarrow {}^6H_{5/2}$. So, these CR processes ultimately lead to non-radiative losses along with the luminescent transitions thereby resulting in the decrease of emission intensities with increasing concentration of Sm^{3+} ions[160].

Dexter's Theory Analysis:

Dexter analysis was conducted to study the mechanism of energy transfer in the glass matrix using the emission spectra data. The equation followed is given by:

$$\log (I/x) = K' - [Q\log (x)]/3 \qquad (2)$$

where K' is given by

$$K' = \log k - \log \beta \qquad (3)$$

Here, K' is some constant, I represent the intensity of luminescence. Also, x is molar concentration of the activator ion in host matrix. Q represents the nature of interaction between neighboring ions for energy transfer. Dipole-dipole interactions, dipole-quadrupole interactions and quadrupole-quadrupole interactions are given by Q=6, 8 and 10 respectively. Fig.6.6. shows the Dexter plot between log (I/x) and log (x). The value of Q was calculated from the slope which came out to be 4.11. This value is near to 6 implying a dipole-dipole interaction between the lanthanide ions and subsequent quenching that was observed during the emission process [161].

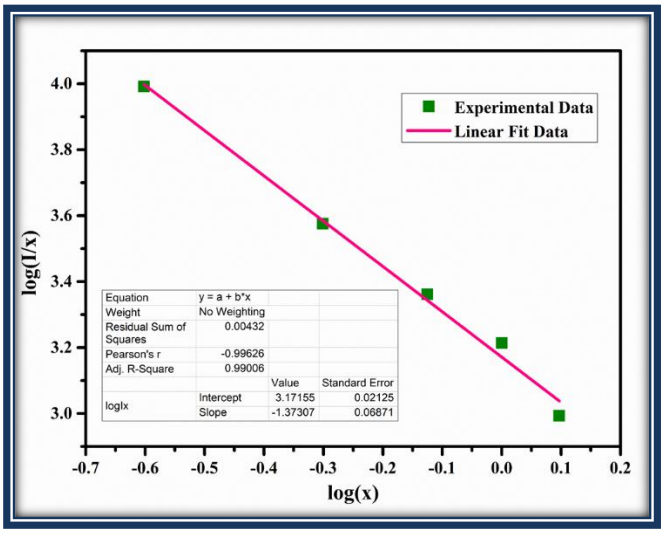

Figure:4.6 *Relationship between log (x) vs log (I/x) for* Sm^{3+} *doped AZABS glasses*

4.3.3. Temperature dependent PL studies:

Since we wish to propose the Sm^{3+} doped AZABS glasses for SSL/w-LEDs applications, it is imperative to determine the thermal stability of the glasses. This is due to the fact that operating temperatures of such optoelectronic devices can go beyond 470K which is high enough to cause operational defects [124]. Fig. 4.7 shows the temperature dependent PL spectra of Sm^{3+} 0.25 mol% doped AZABS glass.

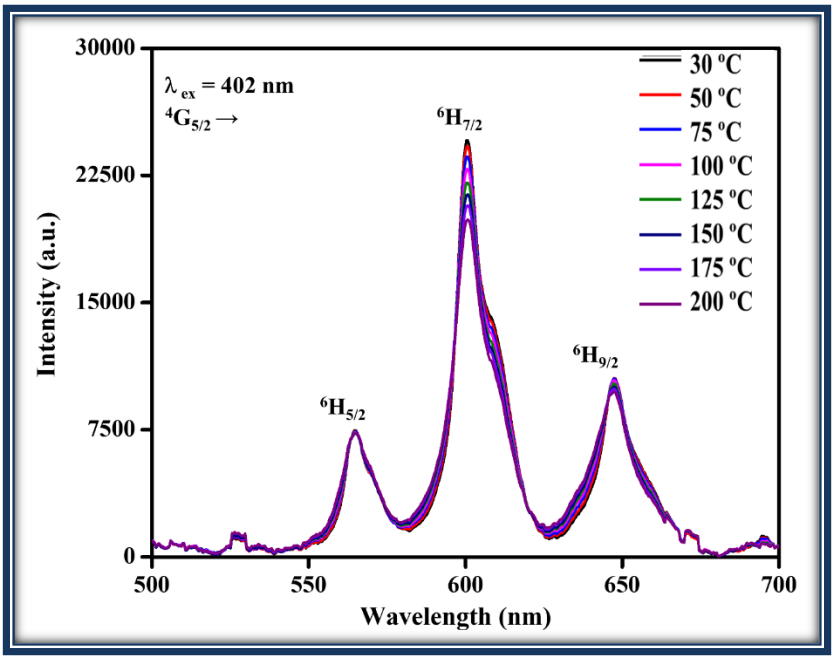

Figure:4.7 *Temperature dependent photoluminescence of 0.25 mol% Sm^{3+} doped AZABS glass 402 nm excitation wavelength.*

The effect of increment of temperature on the intensity of $^4G_{5/2} \rightarrow {}^6F_{7/2}$ transition can be seen in the Fig.4.7. There is a continuous decrease of intensity from 30^0C till 200^0C due to thermal quenching. The intensity decreases to nearly 20% of its value at 200^0C.

The thermal quenching effect observed in the luminescence intensity can be explained via phonon interactions whereby an excited luminescence center gets thermally activated through

a crossing point between ground and excited states [126]. The activation energy required for thermal quenching can be determined using Arrhenius equation given by [148]:

$$I(T)= \frac{Io}{1+cexp[-(\frac{\Delta E}{KT})]} \quad (4)$$

Here, I_0 is the initial intensity, I(T) is the intensity at given temperature T, ΔE is the activation energy for thermal quenching and K is the Boltzmann constant (8.629 x 10^{-5} eV). A graph was plotted showing variation of intensity of $^4G_{5/2} \rightarrow {}^6F_{7/2}$ with temperature using the Arrehnius equation and is shown in Fig. 4.8. The activation energy comes out to be 0.19 eV. As compared to other reported materials, this value is high and leads to the conclusion that AZABS glasses can indeed show good thermal stability if deployed for SSL/w-LED applications[125,126]

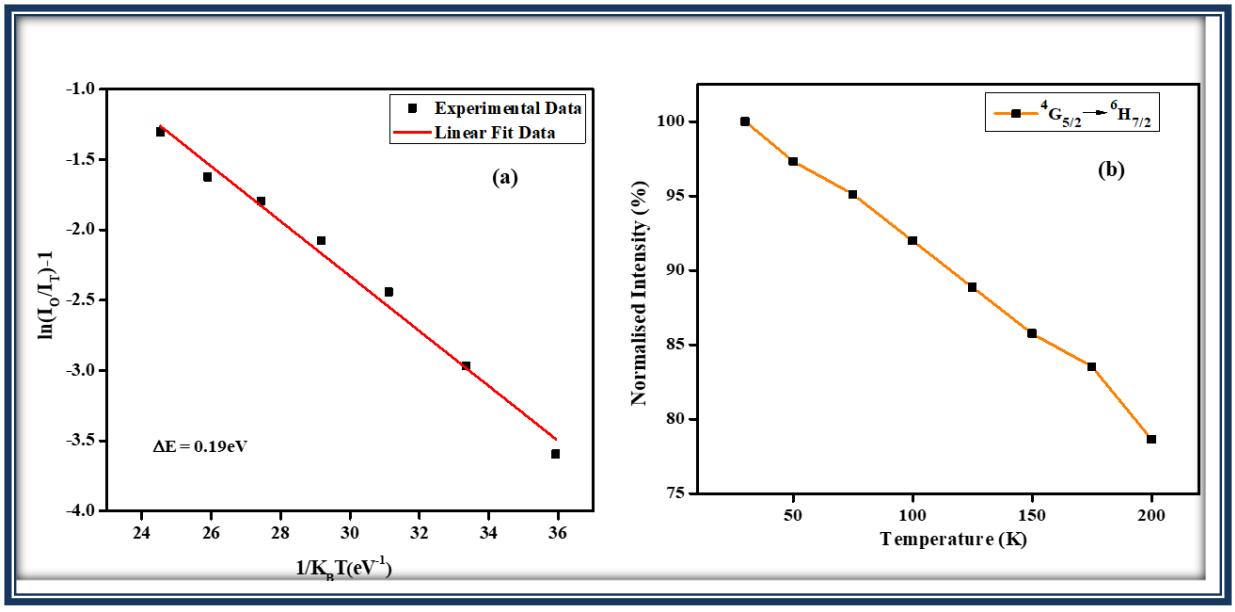

Figure:4.8 *(a)Variation of ln [(I_0/I_T)-1] versus 1/k_BT plot to calculate activation energy of 0.25 mol% Sm^{3+} doped AZABS glass. (b) Plot shows the normalized PL intensity with rise in temperature range 303-473 K.*

4.3.4. Decay kinetics

Fig. 4.9. shows the decay curves of the as prepared Sm^{3+} ions doped AZABS glass under 402 nm excitation for 599 nm emission wavelength. The decay curves show a bi-exponential behaviour given by equation[162]:

$$I = I_0[A_1 \exp(-t/\tau_1) + A_2 \exp(-t/\tau_2)]$$

This presence of a bi-exponential behaviour indicates ion-ion interactions alongside energy transfer.

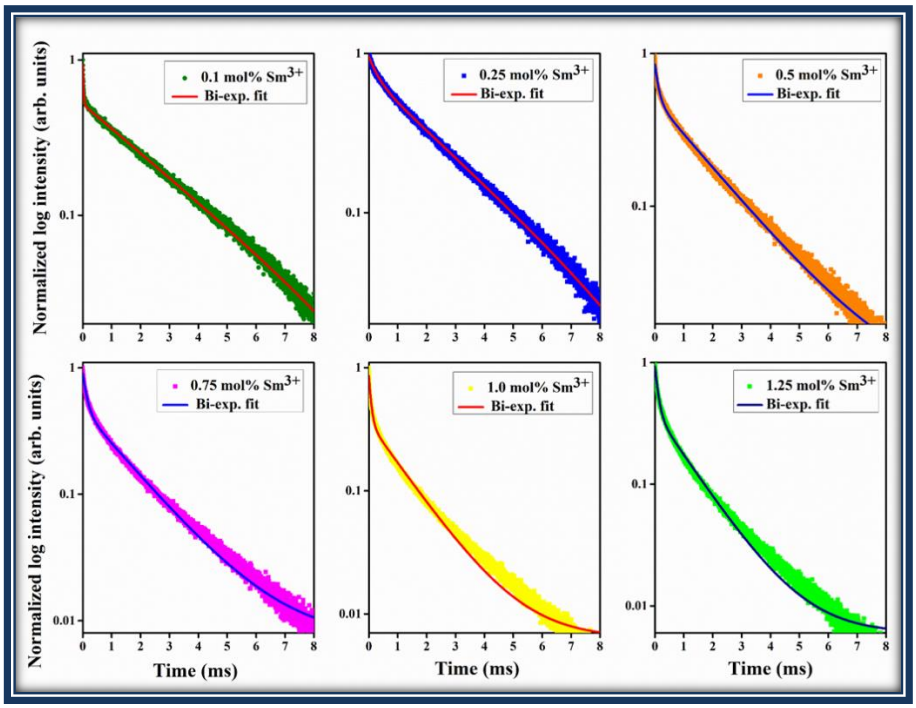

Figure:4.9 *Photoluminescence decay curves of x mol% Sm^{3+} (x = 0.10, 0.25, 0.50, 0.75, 1.00 and 1.25 mol%) doped AZABS glass recorded under 402 nm excitation wavelength*

These interactions produce a slow and a fast component of emission. The ions might be at the surface or at the core of the glass lattice [121]. The avg. value of lifetime was calculated by using the relation-

$$\tau = (A_1\tau_1^2 + A_2\tau_2^2) / (A_1\tau_1 + A_2\tau_2)$$

The lifetimes calculated for the Sm^{3+} doped AZABS glasses (x=0.1 mol% to 1.25 mol%) are 1.93 ms, 1.74 ms, 1.28 ms, 1.05 ms, 0.83 ms and 0.75 ms respectively. A continuous decrease in the lifetimes of the as prepared glass samples can be seen with increase in Sm^{3+} concentration. This can be attributed to loss of energy between the Sm^{3+} ions themselves. Since these glasses have high lifetimes, these can be utilised for lighting and display applications [148]

4.3.5. Colorimetry analysis:

CIE color coordinates were calculated from the emission spectra data of all the Sm^{3+} doped AZABS glasses under 402 nm excitation and have been shown in Fig. 4.10 and in Table 4.1. The coordinates fall in the reddish-orange region as can be seen from the diagram. Correlated color temperature (CCT) of any material is defined as temperature of any Planckian body whose color coordinates closely resemble the white light source.

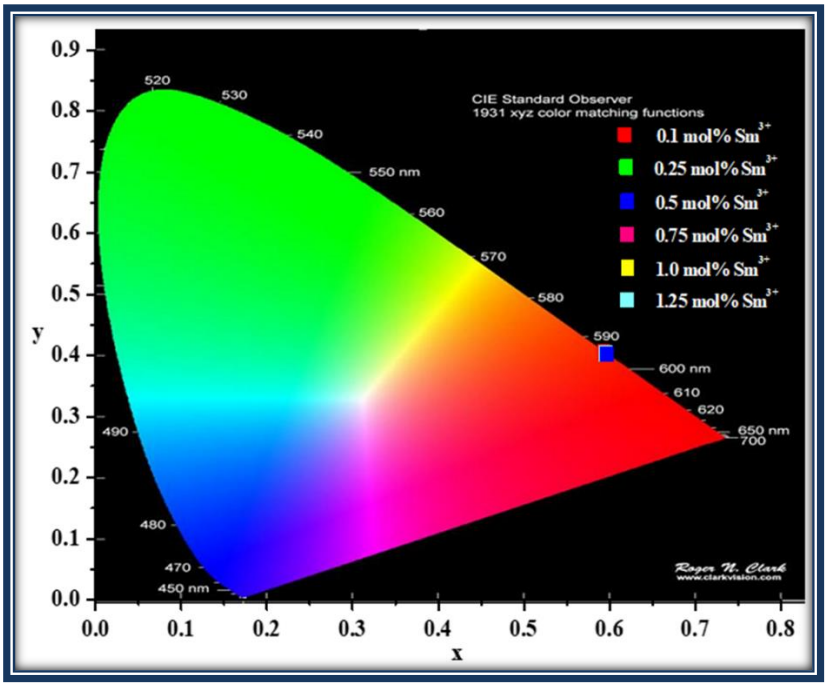

Figure:4.10 *CIE diagram with CIE coordinates of all Sm^{3+} ions doped AZABS glasses under 402 nm excitation wavelength.*

The formula for CCT as postulated by McCamy is[163]:

$$CCT = -449n^3 + 352n^2 - 6823.2n + 5520.3 \quad (5)$$

where the value of n is given by $[(x-x_e)/(y-y_e)]$ where $x_e = 0.332$ and $y_e = 0.186$. Table 1 shows the CCT values of all the doped Sm^{3+} AZABS glasses. For temperatures below 3200K, lamps give warm white light. As is evident from the values, the glasses have CCT values less than 3200K. So these glasses can be used for warm white light generation applications.

Table 4.1 *CIE chromaticity coordinates (x, y), CCT and average decay time of Sm^{3+} ions doped AZABS glass under 402 nm excitation.*

AZABS: *x* mol% (x is Sm^{3+} ion concentration)	**CIE (x,y) at λ_{ex} = 402 nm**	**CCT (K) at λ_{ex} = 402 nm**	**t_{avg} (ms)**
x = 0.10	(0.5932, 0.4051)	1722.54	1.93
x = 0.25	(0.5967, 0.4024)	1720.04	1.74
x =0.50	(0.5963, 0.4026)	1720.12	1.28
x = 0.75	(0.5967, 0.4025)	1720.05	1.05
x = 1.00	(0.5966, 0.4025)	1720.06	0.83
x = 1.25	(0.5951, 0.4037)	1720.72	0.75

4.4. Conclusions:

In this research work, Sm^{3+} doped AZABS glasses have been prepared via quick melt quench technique. To understand the optical and physical characteristics of the as prepared glasses, various characterisations were undertaken. 0.25 mol% Sm^{3+} doped glass showed the highest luminescence intensity under 402 nm excitation and was subsequently chosen for all the optical studies. In the absorption analysis, $^6H_{5/2} \rightarrow {}^6P_{3/2}$, $^4I_{11/2}$, $^6F_{11/2}$, $^6F_{9/2}$, $^6F_{7/2}$, $^6F_{5/2}$, $^6F_{3/2}$, $^6H_{15/2}$ and $^6F_{1/2}$ bands were seen. This data was then utilised to calculate the direct optical band gap of the 0.25 mol% Sm^{3+} doped AZABS glass. The glass shows sharp excitation and emission bands. In the emission spectrum under 402 nm excitation, three bands corresponding to $^4G_{5/2} \rightarrow {}^6H_{5/2}$, $^4G_{5/2} \rightarrow {}^6H_{7/2}$ and $^4G_{5/2} \rightarrow {}^6H_{9/2}$ transitions can be seen. Dexter's analysis of the glass shows that lanthanide interactions are dipole-dipole in nature. These glasses have high thermal

stabilities as could be seen from the high value of activation energy obtained from temperature dependent PL data. On the basis of these results along with the fact that these glasses have high lifetimes for the 599 nm emission, we propose to utilise the Sm^{3+} doped AZABS glasses for SSL and w-LEDs applications.

.

Chapter 5

21

Photoluminescence down-shifting studies of thermally stable Eu^{3+} ions doped Borosilicate Glasses for Visible Red Photonic Device Applications

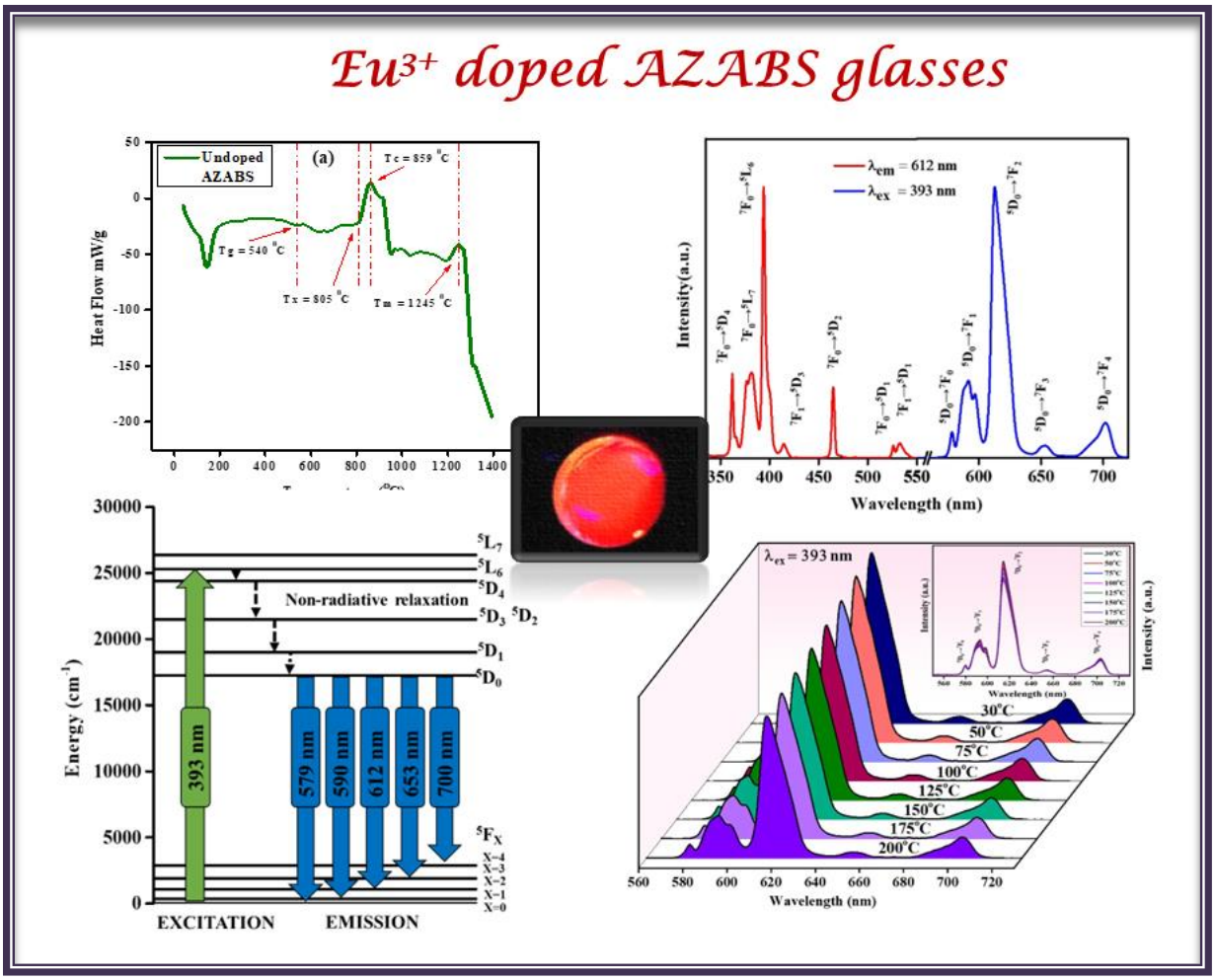

Part of this work has been published in Journal of Non-Crystalline Solids 575 (2022) 121184 (Impact Factor = 3.2)

In this paper we report the synthesis of thermally stable borosilicate glasses doped with europium ions having chemical composition $35B_2O_3.20SiO_2.(15x)Al_2O_3.15ZnO.15Na_2CO_3.xEu_2O_3$ (x = 0.5 to 2.5 mol%) using melt quench process. A broad hump without any sharp peaks observed in the XRD spectrum recorded for an undoped glass confirm its glassy nature. The DSC & TGA has been conducted on an undoped glass to understand thermal stability and aggregate weight loss. The absorption spectral features recorded for the as prepared glasses are used to estimate optical band gap. Under 393 nm sharp excitation, all the glass samples are showing red emission corresponds to $^5D_0 \rightarrow {}^7F_2$ transition (612 nm) and whose intensity continuously increasing with Eu^{3+} ion concentration up to 2.5 mol%. The red to orange color ratio (R/O) estimated from the recorded PL spectral features varies from 3.62 to 3.92 within the variation limits of Eu^{3+} ions from 0.5 to 2.5 mol% indicates relatively low symmetry around Eu^{3+} ions in the as prepared glasses. Relatively higher R/O ratio also reveals that the nature of bonding between Eu^{3+} ions and the surrounding ligands as covalent. Activation energy (0.175 eV) and percentage loss (82%) in PL intensity estimated for 2.5 mol% of Eu^{3+} ions through temperature dependent PL (TDPL) studies reveal the superiority in thermal stability of the as prepared glasses. The PL, TDPL, PL decay studies conducted along with CIE coordinates estimated allows us to contemplate that, the as prepared glasses are quite useful in fabricating thermally stable visible red photonic devices.

5.1. Introduction

The quick growth of technologies like solid-state lighting and other display technologies has led to enormous advancements in the study of luminous materials doped with rare earth (RE) and transition metal (TM) ions [1-6,7]. Glassy materials doped with RE ions are also used in lasers, optoelectronic devices, and civil military applications such nuclear imaging and detection, infrared detectors, and infrared fairings [8-14]. Photo luminescent glass applies these

distinctive properties to photonics, lighting, and photovoltaics by applying down-conversion light from UV to visible or near-infrared (NIR) light and it is suitable for display devices, smart windows, lasers and optical fibers & w-LEDs, among many other applications [7,15,16]. RE doped glasses useful for optoelectronics devices have been fabricated and characterized by many researchers because of their high transparency, low production cost, easy in shaping and relatively high thermal stability [7,17-22]. Quite recently, a good amount of research has been done in fabrication and characterization of RE ions doped glasses as best alternatives for epoxy resin free phosphors in the field of solid-state lighting. Also, RE doped glasses have special feature such as high doping capacity, broad homogeneous bandwidth and good thermal stability when compared with phosphor materials [23]. Apart from this, glasses are getting great attention for its wide applications such as optical devices, optical fiber amplifiers, visible and infrared solid-state lightening devices, digital plasma displays, photovoltaic cell bio-imaging and bio-sensors [23,24]. A glassy material with novel characteristic features such as relatively low phonon energies, high chemical & thermal stability, good RE ion solubility and high transparency suits the aforementioned applications [85]. The band widths of emission transitions and thereby the luminescence efficacy of a doped RE ion in a host matrix depends on the inherent structure of the host and ligand field environment also. Therefore, it is very much important to choose an apt host with relatively less phonon energies for the purpose of obtaining maximum possible luminescent efficiency [88,89]. It is evident from the literature that, B_2O_3 is one of the best glass formers with its remarkable good features such as good thermal stability, low melting point and high solubility of RE ions [14]. Apart from having the aforementioned good features, pure borate host has got self-restraint because of its relatively high phonon energies (1300 cm^{-1}) [25-26]. It is well known that, a host glass with relatively high phonon energy is not suitable for luminescence applications as most of the input excitation

energy gets wasted inside the host because of its high phonon energy [26]. This results in possessing relatively less quantum efficiency which is detrimental for a host matrix to act as a good luminescent material. Normally, metal oxides such as SiO_2 or Al_2O_3 are mixed with borate glass to lower its redundant high phonon energies and to convert it into a good luminescent material best suited for various optoelectronic device applications [26]. Structure of a glass depends on two factors i.e., network former and network modifier. A glass former also known as network formers consists of oxide such as SiO_2, and B_2O_3, which are indispensable in the formation of the glass [27]. Network modifiers added to a network glass former modifies the internal structure of the host and creates a holistic environment around the doped RE ions and facilitates them to possess relatively good luminescence efficiency [28]. Borosilicate glasses can be effectively used for luminescent applications by doping them with RE ions for applications in diversified fields ranging from pharmaceutical industry to nuclear waste immobilization in addition to their regular usage in photonic devices [27, 29]. Controlled heat treatment of these glasses helps in curating various properties such as chemical and physical stability and crystal nucleation strength. The presence of BO_3 triangles in a borosilicate glass and their amalgamation with SiO_2 play an important role in the formation of silicate groups. Addition of Na_2O as a flux to a borosilicate glass can reduce the dispensation temperature and helps in changing the properties of the glass [29,30]. Aluminum oxide (Al_2O_3) is added to a borosilicate glass to increase the physical properties and chemical stability of the host glass [30].The AlO_4 structural units present in Al_2O_3 crosslinks with borate and silicate chains present in a borosilicate host glass and builds the glass more resistive to the attacks of alkali metals[19,31,32].Addition of zinc oxide (ZnO) to a borosilicate glass can increases its glass forming composition range along with other noble features such as low glass transition temperature and high chemical stability. Apart from this, the glasses with ZnO are non-toxic,

non-hygroscopic and are used vigorously for the development of optoelectronic devices [19-21,25]. Among the lanthanides (Ln^{3+}) ions, europium (Eu^{3+}) ions gained much attention due to its unique optical properties such as high brightness and high chemical stability. And among all the RE ions, Eu^{3+} ion is well-known spectroscopic agent for intense red color through down-conversion process in wide variety of materials such as glasses, phosphorus, nanophosphors and organic-inorganic hybrid materials [33]. Europium is the best choice for visible red emission in a host glass, as it possesses simple energy level scheme and site selective nature of intensities between ^7F_J and $^5D_0$ energy levels. Especially this property of europium doped in a host matrix finds many diversified usages for it in the field of photonics [19,34]. In the backdrop of aforementioned various scientific patronages offered by the chemical species such as H_3BO_3, SiO_2, Al_2O_3, ZnO and Na_2CO_3 in the present work we have fabricated a good glassy system (using melt quench method) by name alkali zinc alumino borosilicate (AZABS) glass doped with different concentration of europium ions and characterized them spectroscopically to have an insight into their suitability for w-LEDs (as a red component) and other related SSL device applications.

5.2. Experimental

Quick melt quenching technique was used to synthesis the Eu^{3+} ions doped AZABS glasses with the composition details as given below:

$35B_2O_3$-$20SiO_2$-$(15-x)Al_2O_3$-$15ZnO$-$15Na_2CO_3$-xEu_2O_3 (x = 0.0, 0.5, 1.0, 1.5, 2.0, 2.5 mol%). Starting powders like H_3BO_3 (99.5%), SiO_2 (99.9%), Al_2O_3 (99.9%), ZnO (99%), Na_2CO_3 (99.9%) and Eu_2O_3 (99.99%) were purchased from sigma -aldrich and in total 8 grams of sample weighed in stoichiometric ratio. The detailed synthesis process was discussed in chapter 2.

5.3. Result and Discussion

5.3.1. X-ray Diffraction analysis:

Fig. 5.1 shows the undoped XRD of AZABS glass in the spectral range of $10^{o} \leq \theta \leq 80^{o}$. The broadened peaks around 26.7, 41.8 and 62.5 degrees indicate the amorphous nature of the as prepared glass. The broadness of XRD pattern confirms the absence of any long-range structural order in the as-obtained glass.

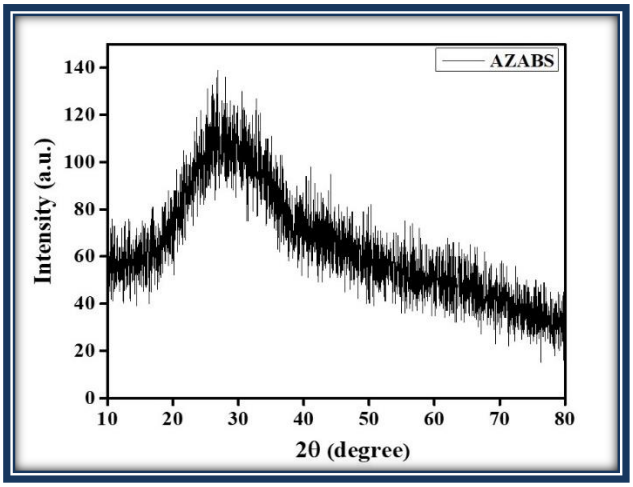

Figure: *5.1 XRD pattern of an undoped AZABS glass.*

5.3.2. Thermal Analysis

DSC of an undoped AZABS glass sample has been recorded in the temperature range from 40 to 1390°C with a heating rate of 10°C/min, and is shown in Fig. 5.2(a). The value of peak crystallization temperature (T_c), melting temperature (T_m), glass transition temperature (T_g), and onset crystallization temperature (T_x) are found to be 540°C, 805°C, 859°C, and 1245°C respectively. The thermal stability of a glass can be calculated by using the following relation [35-38]:

$$\Delta T = T_x - T_g$$

The higher value of ΔT favors the glass formation via restricting the crystallization process and therefore higher value of ΔT also indicates relatively better thermal stability of the glass [36]. In the present work, the values of ΔT was found to be 265°C which is relatively higher than the corresponding values of lead alumino borate (27°C) [37], lead zinc phosphate (120°C) [38], and Zinc Fluoro-borate tellurite (153°C) glasses [36]. In literature, it is reported that glass with ΔT value greater than 100°C is said to be thermally more stable and, therefore and are aptly suitable for fabrication of optoelectronic devices.

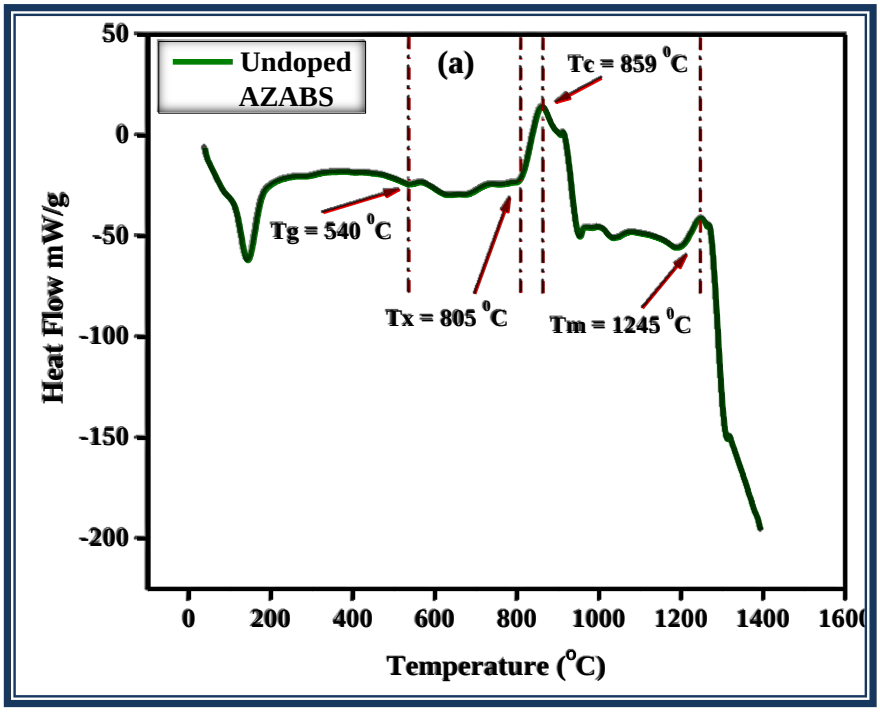

Figure:5.2 *(a) DSC and (b) TGA of an undoped AZABS glass.*

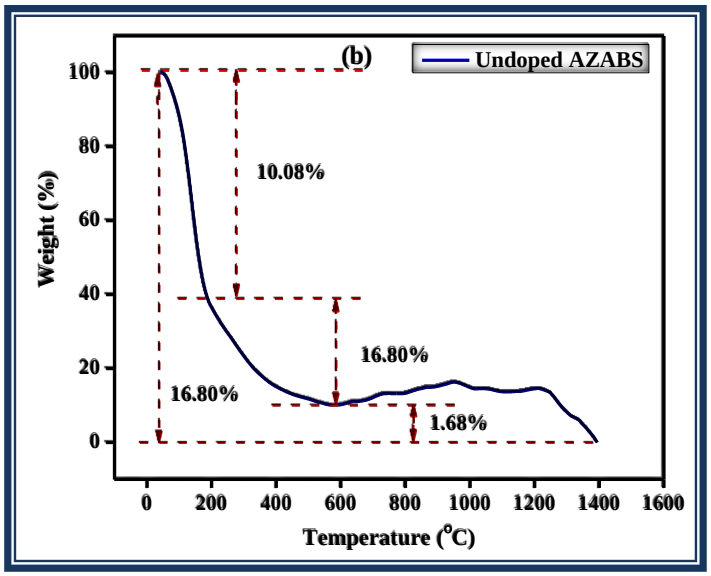

Figure:5.2 *(b) TGA of an undoped AZABS glass.*

Hurby's parameter is another critical parameter that determines the thermal stability of the glass. The Hurby's parameter can be calculated by using the following equation [38]:

$$K_H = (T_x - T_g)/(T_m - T_x)$$

Where K_H is Hurby's parameter of the glass. Relatively higher the value of Hurby's parameter (≥0.1), the better will be the thermal stability of the glass [37]. In the present work, the value of the K_H evaluated for an undoped AZABS glass was found to be 0.602, which confirms that the as prepared glass is thermally more stable. Saad et al. in their work, defined the thermal stability of a glass using the following equations [39],

$$S = (T_C - T_x)(T_x - T_g)/T_g$$

In the above equation, the term (Tc - Tx) carries the information about crystallization rate. Relatively low value of (Tc - Tx) indicates the higher the rate of crystallization. The calculated value of S for the present undoped glass is 26.5. Based upon the results obtained from the ΔT,

K_H, and S it is conspicuous that the undoped AZABS glass sample has good thermally stability and is suitable for light-emitting applications [38].

The TGA curve of the undoped AZABS glass sample is shown in Fig. 5.2(b); the aggregate weight loss is observed in the temperature range from 40 to 1390°C is 16.80%. The weight loss of an undoped sample with temperature occurs in three stages [40]. The first stage is noticed at 40 to 192°C due to evaporation of the absorbed water from the sample's surface. The second stage of weight loss occurs from 192 to 580°C due to the loss of the chemisorbed water, solvents, and organic groups available within the sample. The third stage, which is between 580 to 1390°C, is due to presence of combustibles in the sample [36,40]. The total loss in the sample is 16.80%, and the remaining mass is 83.2%. Hence, it is clear from Fig. 4.2 (b) that the as prepared glass sample is thermally more stable with less loss in mass at high temperatures.

5.3.3. Raman Spectroscopy analysis:

15 The Raman Spectrum is very significant tool for identifying the presence of different functional groups involved in a glassy matrix. Raman spectra of undoped glass have been recorded in the spectral range of 400 – 2000 cm^{-1} as shown in Fig. 5.3. The peak positions and corresponding assignment to Raman vibrational modes pertaining as prepared undoped glass series are listed in Table 5.1. The spectrum represents one dominant band corresponding to 789 cm^{-1}, is characteristic of Si-O-Si vibration, ZnO_4 tetrahedra and symmetric breathing vibrations of six-member rings with one or two BO_3 triangle replaced by BO_4 tetrahedral [15,41,42]. The band at 900 cm^{-1} indicates the presence of pyroborate groups [42].

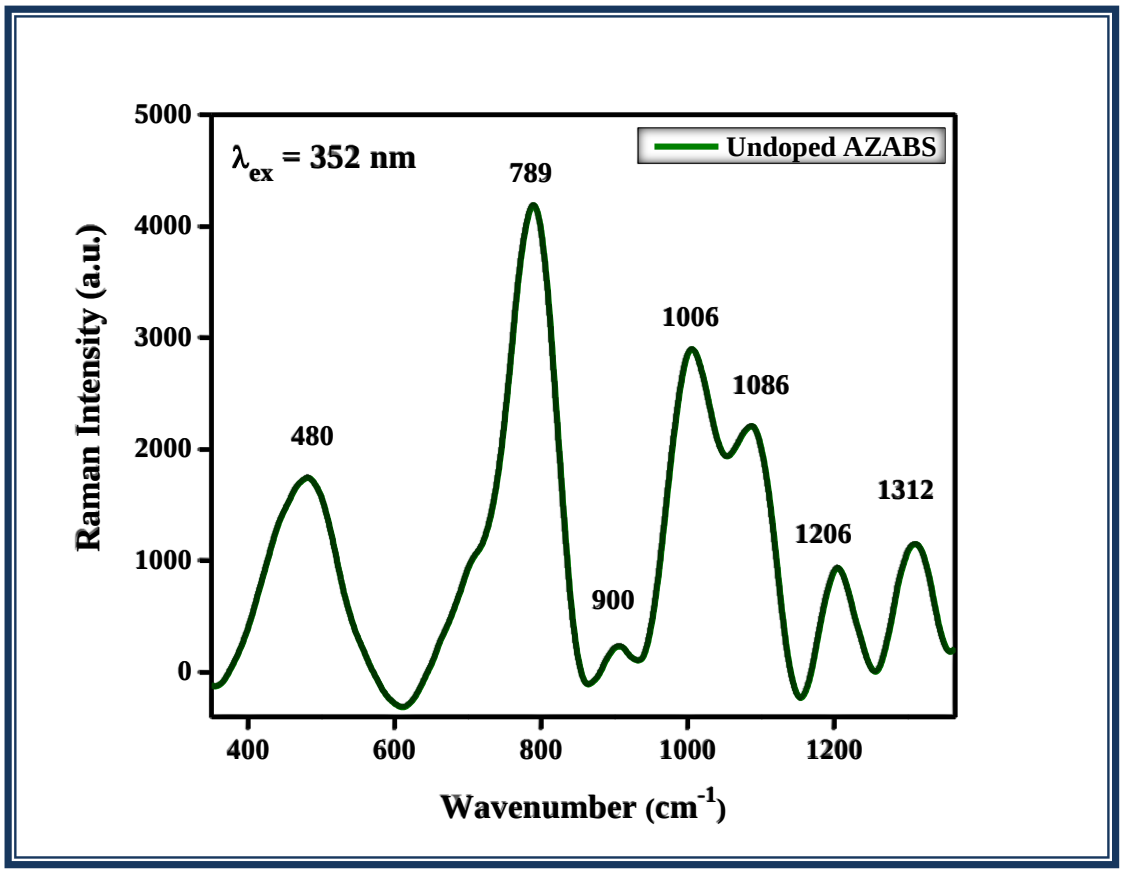

Figure: 5.3 *Raman spectrum for undoped AZABS glass at room temperature.*

The peak observed at 1006 cm^{-1} indicate the availability of the vibration of S-O, B-O-B, B-O-Si and Si-O-Si bending. The rocking or bending vibration as well as di-borate groups is also found in glass network at 480 cm^{-1} [42]. The peak observed at 1086 cm^{-1} ascribed to di borate group while 1206 cm^{-1} to pyro-borate group [15]. Raman Spectra studies on SiO_2-Na_2O have shown a band at 1086, 1206 and 1312 cm^{-1} also attributed to the Si-O stretching vibrational mode of the SiO_4 tetrahedra [43].

Table 5.1 *Assignment of Raman peaks for an undoped AZABS glass.*

Wavenumber (cm^{-1})	Raman assignments	Reference
480	Bending or rocking vibrations of the B-O-Si linkages, B-O-B, B-O-Si and Si-O-Si as well as isolated diborate groups	42
789	Boroxol rings, ZnO_4 tetrahedra and symmetric breathing vibration of six membered rings one BO_4 tetrahedron	42
900	Pyroborate groups or/and symmetric breathing vibrations of boroxol rings.	42
1006	Stretching vibration of Si-O, and due to the presence of BO_4 units	42
1086	SiO_4 asymmetric stretching vibration or/and Pyroborate groups	42
1206	S-O asymmetric stretching vibrations of SiO_4 tetrahedron.	42
1312	Asymmetric stretching vibrations of Si-O-Si.	42

This spectrum suggests a connection from a Si-O-Al due to the addition of Al_2O_3 in the SiO_2-Al_2O_3 glass [44,45]. The peak at 789 cm^{-1} represent the maximum vibrational energy of the glass therefore it could be its phonon energy.

5.3.4. Absorption spectral analysis:

Absorption spectra of AZABS glass doped with Eu^{3+} ions were recorded in UV -Visible region in the range from 350 to 550 nm and is presented in Fig. 5.4. The spectra show various peaks at 361 nm, 379 nm, 396 nm, 415 nm, 466 nm and 533 nm pertaining to $^7F_0 \rightarrow {}^5G_3$, $^5G_4$, $^7F_0 \rightarrow {}^5L_6$, $^7F_1 \rightarrow {}^5L_6$, $^7F_0 \rightarrow {}^5D_2$ $^7F_1 \rightarrow {}^5D_1$ respectively. Assignment of absorption bands has been done based on the data reported in literature by Dieke [46] and Carnall et al [47]. The absorptions bands are because of the 4f-4f transitions of Eu^{3+} ions that took place from the lower ground state ($^7F_0$) and the higher excited state ($^7F_1$). Bands arising from ^7F_J to ^5D_J are

weak as compared to others transitions due to spin forbidden but partially allowed because of the J mixing by the crystal-field. The $^7F_0 \rightarrow {}^5L_6$ transition in the visible region is much stronger than any other transition. On substitution of rare earth ions (with increase in the concentration of Eu^{3+} ions) there is no shifting observed in band positions except some variation in their intensities.

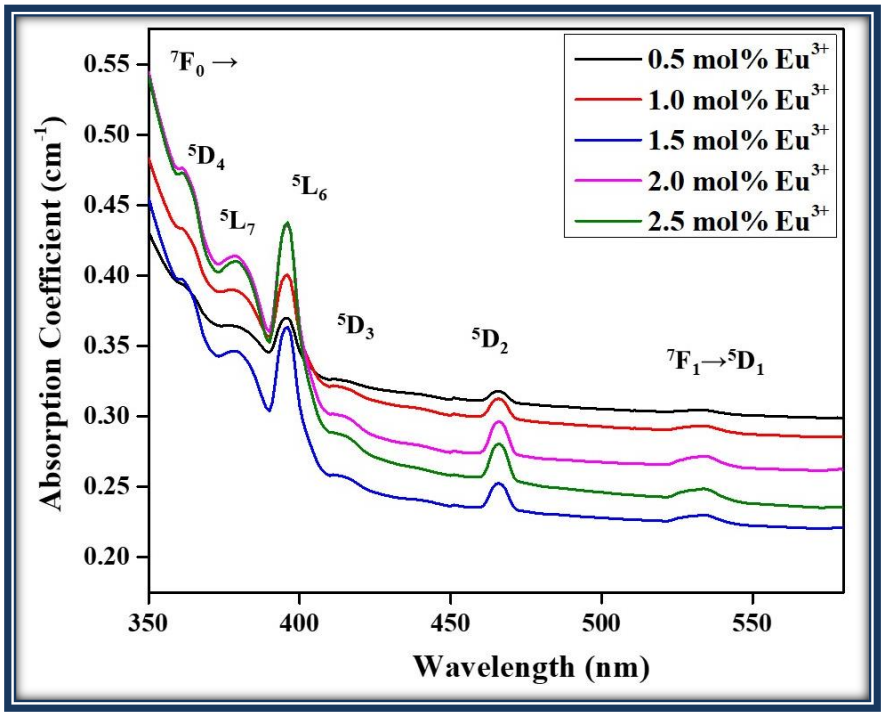

Figure: 5.4 *Absorption of x mol% Eu^{3+} ions (x = 0.5 to 2.5 mol%) doped AZABS glasses.*

By observing the optical edge, the optical band gap for all the glass samples were calculated by drawing graph of Tauc between absorption coefficient (hν) and energy band gap (E_g)

$$\alpha h\nu = C(h\nu - E_g)^n \quad (1)$$

In this equation, C is a constant, hν is the energy of photon, and (n) is the exponent can take values ½ for direct allowed, 2 for indirect allowed transition, 1/3 for indirect forbidden and 3 for direct forbidden transitions. From Fig. 4.5 it is conspicuous that the calculated bandgap

values of AZABS: *x mol%* Eu^{3+} glasses (x = 0.5-2.5 mol%) were found to be in the range from 2.97 to 3.06 eV. With the increase in dopant ion concentration in the host lattice, there will be a slight expansion in the unit cell, which tends to narrow the conduction and valance band causing broadening in the band [48].

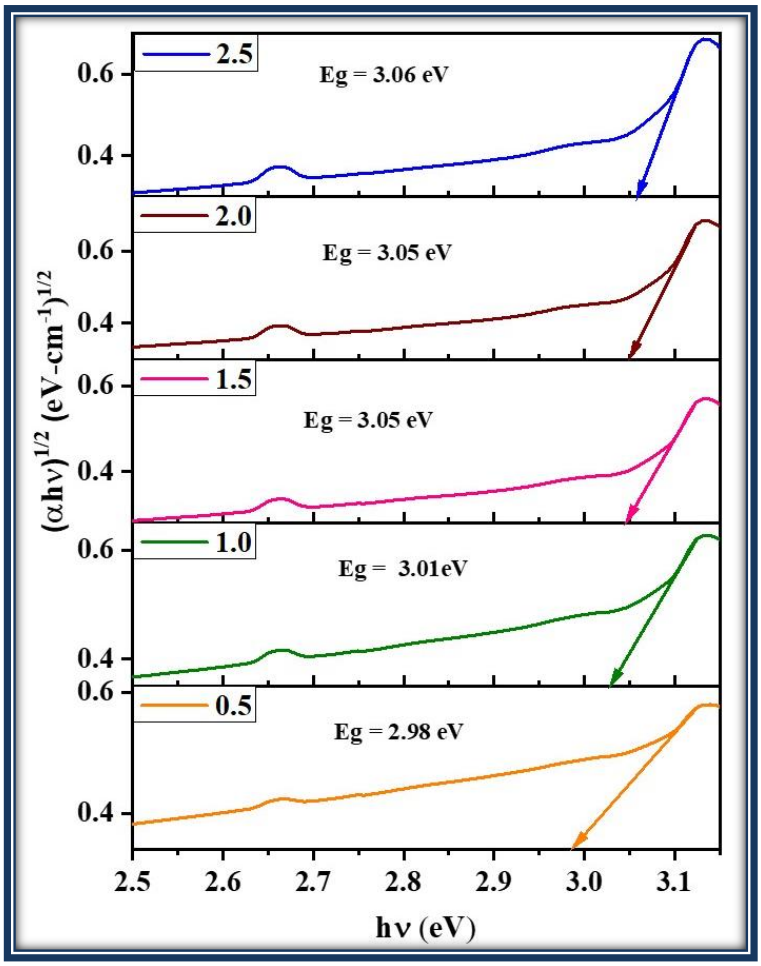

Figure: 5.5 *Tauc plot for direct optical band gap for* Eu^{3+} *ions doped AZABS glasses.*

5.3.5. PL excitation and PL emission spectral studies:

The PL excitation spectrum recorded under 612 nm emission wavelength and PL emission spectrum recorded under 393 nm excitation wavelength for 2.5 mol% Eu^{3+} ions doped AZABS glass was shown in Fig. 5.6. The PL excitation and PL emission spectra observed for the remaining AZABS glasses are quite similar in their band positions with slight variation in their

intensities and hence not shown in Fig. 5.6. The excitation spectra show several peaks pertaining to $^7F_0 \rightarrow {}^5D_4$ (362 nm), $^7F_0 \rightarrow {}^5L_7$ (383 nm), $^7F_0 \rightarrow {}^5L_6$ (393 nm), and $^7F_1 \rightarrow {}^5D_3$ (416 nm), $^7F_0 \rightarrow {}^5D_2$ (465 nm), $^7F_0 \rightarrow {}^5D_1$ (524 nm), $^7F_1 \rightarrow {}^5D_1$ (534 nm) transitions of Eu^{3+} ions.

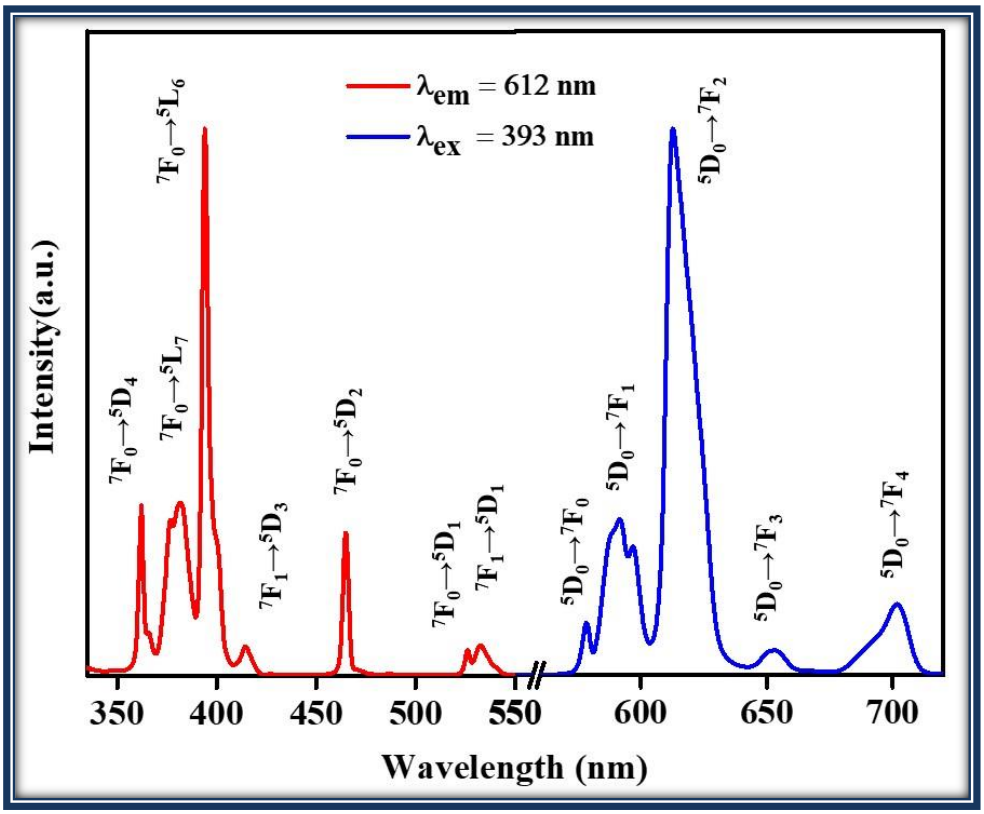

Figure: 5.6 *PL Excitation and PL emission spectrum of 2.5 mol% Eu^{3+} ion doped AZABS glasses recorded at λ_{em} = 612 nm and λ_{ex} = 393 nm.*

Among various excitations peaks, $^7F_0 \rightarrow {}^5L_6$ transition peak observed at 393 nm is relatively more intense than the other excitation bands. The peak position of this transition is considered as an excitation wavelength to read the emission spectra of the as prepared glasses. When excited at 393 nm, various emission band were observed at 579 nm, 590 nm, 612 nm, 653 nm and 700 nm that pertaining to the $^5D_0 \rightarrow {}^7F_0$, $^5D_0 \rightarrow {}^7F_1$, $^5D_0 \rightarrow {}^7F_2$, $^5D_0 \rightarrow {}^7F_3$ and $^5D_0 \rightarrow {}^7F_4$ transitions respectively. Fig. 5.7 shows the PL emission spectra of AZABS doped with *x*mol% Eu^{3+} (x = 0.5, 1.0, 1.5, 2.0, 2.5 mol%) recorded under 393 nm excitation wavelength. On

substitution of rare earth ion (with increase in the concentration of Eu^{3+} ions) there is no shifting observed in emission band positions except some variation in their intensities. As the Eu^{3+} ion concentration increases, the emission peak's intensity also increases with no quenching observed in these glasses up to 2.5 mol%. It is well known that, orange emission transition ($^5D_0 \rightarrow {}^7F_1$) observed at 590 nm and red emission transition ($^5D_0 \rightarrow {}^7F_2$) observed at 612 nm correspond to the known magnetic and electric dipole transitions respectively. The location of Eu^{3+} ions at the sites without any inversion symmetry clearly indicates the fact that, the electric dipole transition dominated the magnetic one suggesting the occupancy of Eu^{3+} ions at sites without any inversion symmetry [49,50].

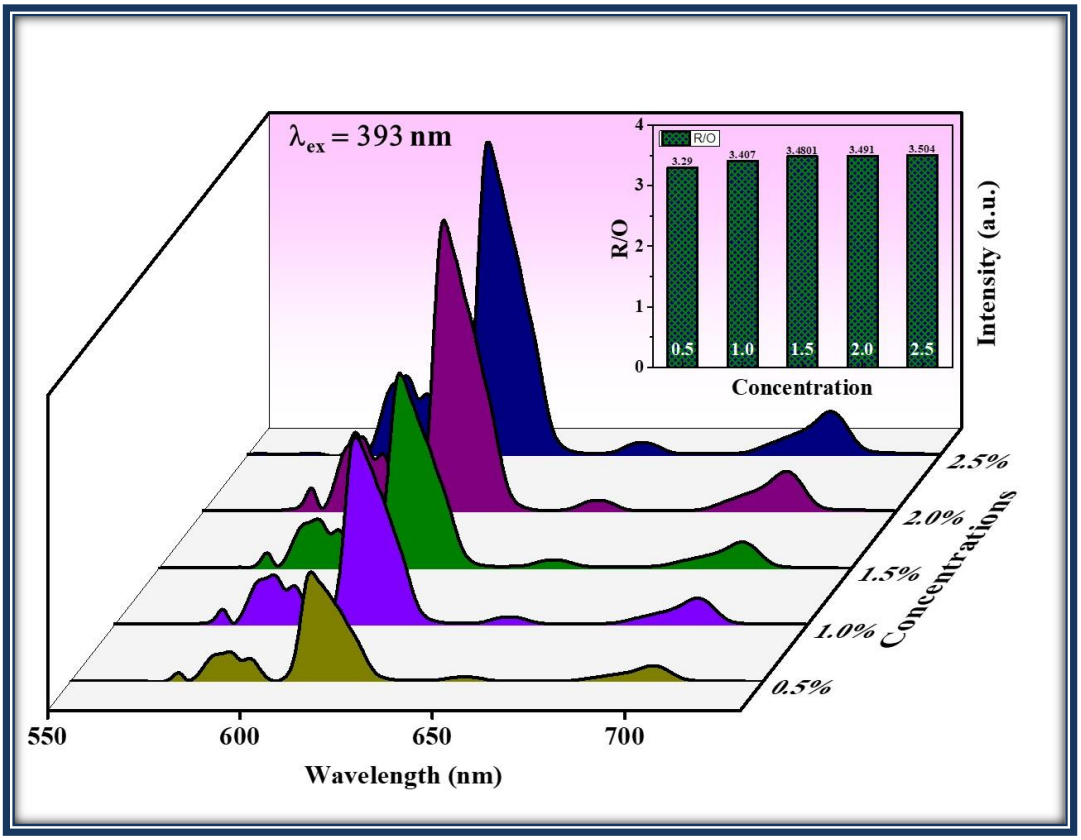

Figure: 5.7. *PL emission spectra of varying Eu^{3+} activator ions concentration (x = 0.5 to 2.5 mol%) doped AZABS glasses at λ_{ex} = 393 nm. The inset bar diagram shows R/O ratio.*

The red/orange ratio (R/O) between the hypersensitive transition to that of invariant transition (I_{613}/I_{590}) shows the asymmetric ratio, which describes the extent of distortion from the

inversion symmetry of Eu^{3+} ions in the matrix. The R/O ratio found in the range from 3.62 to 3.92 as the mol% of Eu^{3+} ions change from 0.5 to 2.5 indicates the presence of Eu^{3+} ions at low symmetrical sites. The higher values of R/O ratio represent direct proportionality with the covalency of bonds between Eu^{3+} and O^{2-} ions. Within the Eu^{3+} ions dopant range (0.5 to 2.5 mol%) the AZABS glass containing 2.5 mol% of Eu^{3+} ions possess higher covalency among all the as prepared AZABS glasses. The insert of Fig. 7 shows the R/O ratio of the as prepared glasses. Hence, it is concluded that, AZABS glasses can be effectively used for photonic devices designated for visible red emission. Schematic energy level diagram is represented in Fig.5.8 which is based PL excitation and PL down-conversion spectra of the as prepared Eu^{3+} doped AZABS glasses. The Eu ions excited to the higher energy levels immediately returns to lower energy levels through non-radiative decay process to $^5D_0$ meta-stable state. Subsequently, the Eu ions return to the ^5F_x (x=4,3,2,1,0) lower levels through radiative decay process. The vertically up/down solid lines show the excitation/radiative emissions respectively, whereas non-radiative (NR) emission transitions are shown by dashed arrows. The NR radiations might be occurring because of resonant energy transfer (RET) or cross-relaxation (CR) [49,50].

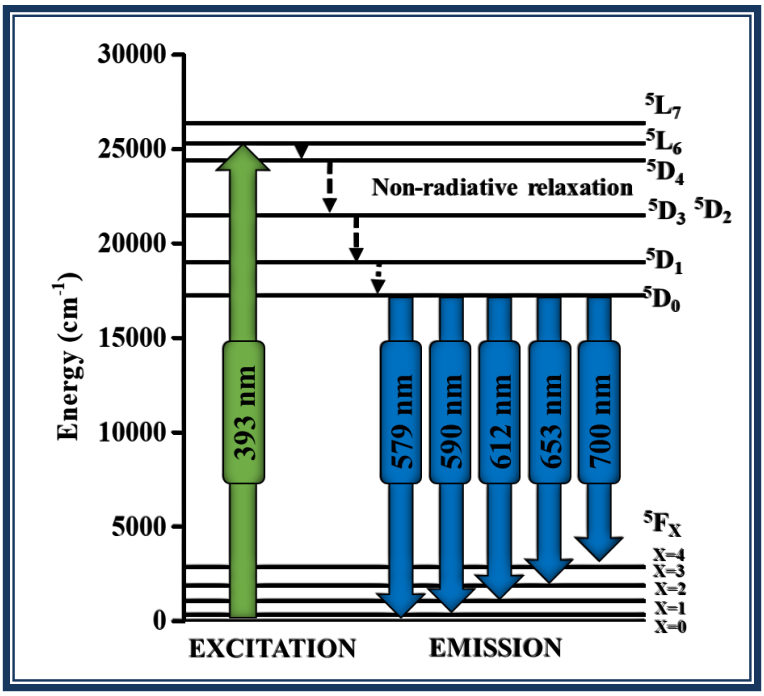

Figure: 5.8 *Schematic energy level diagram for Eu^{3+} ion.*

5.3.6. Emission spectral analysis using Judd-Ofelt (J-O) theory:

The J-O intensity parameters (Ω_λ) provides the information about the type of bonding that exist between the doped rare earth ions and its local structure/surrounding ligands [51]. It is customary to apply J-O theory to the absorption spectral features to understand the bonding nature as well as radiative properties of the doped rare earth ions in a host matrix. However, for Eu^{3+} ions doped materials, the applicability of J-O theory to the absorption spectral features will face certain difficulties because of high intensity values observed for certain transitions observed from ground state ($^7F_0$ and $^7F_1$) to higher energy states ($^5D_1$, $^5D_2$ and $^5L_6$). As the energy difference between $^7F_0$ ground state to $^7F_1$ state is very minimum (approximately equal to 265 cm^{-1}), application of J-O theory to the absorption spectral features needs thermal correction. To circumvent this difficulty, the J-O intensity parameters are evaluated utilizing the emission spectral information [52]. In case of Eu^{3+} ions, the transition from $^5D_0$ to $^7F_1$ originates from magnetic dipole allowed transitions while $^5D_0$ to ^7F_J (J = 2, 4 and 6) transition

arises from allowed electric dipole transitions. It is well known that, magnetic dipole allowed transitions are independent of host while electric dipole allowed transitions depend upon the host matrix [53]. Therefore in the present work, the J-O intensity parameters (Ω_λ where λ = 2, 4 and 6) of Eu^{3+} ions are evaluated by taking the intensity ratio of $^5D_0$ to ^7F_J (where J = 2, 4, 6) transitions [$\int I_J d\vartheta$] to $^5D_0$ o $^7F_1$ transition [$\int I_1 d\vartheta$] by using the below equation [11,53]:

$$\frac{\int I_J d\vartheta}{\int I_1 d\vartheta} = \frac{A_J}{A_1} = \frac{e^2}{S_{md}} \frac{\vartheta_J^3}{\vartheta_1^3} \frac{n(n^2+2)^2}{9n^3} \Omega_\lambda < \Psi_J \| U^\lambda \| \Psi'_{J'} >^2 \quad (2)$$

Where ϑ_1 is the wavenumber (cm^{-1}) corresponding to $^5D_0$ to $^7F_1$ transition and ϑ_J is the wavenumber (cm^{-1}) belongs to $^5D_0$ to ^7F_J transitions (where J = 2, 4, 6), S_{md} is the magnetic dipole line strength of $^5D_0$ to $^7F_1$ transition of the Eu^{3+} ions which is host dependent. In the present work, the value of Ω_6 cannot be evaluated because the transition is missing in the luminescence spectra. The J-O parameters thus evaluated are depicted in Table 4.2. From the data appearing in Table 2 it is conspicuous that, within the concentration range studies, 2.5 mol% Eu^{3+} has highest Ω_2 values than the other glasses indicating relatively high covalency and low symmetry. The resulted J-O parameters have been found similar trend and comparable with earlier reported work such as Oxyfluoroborate [54], ZnAlBiB2.0Eu [19] and SABiBEu15 [55] as depicted in Table 5.2. This information is in consonance with the result of red to orange (R/O) intensity ratios estimated for as prepared glasses.

Table 5.2 Judd-Ofelt parameters ($\Omega_\lambda \times 10^{-20} cm^2$) of Eu^{3+} ions in AZABS glasses along with other reported values.

Glass System	Ω_2	Ω_4	Ω_6	Trend	References
0.5	10.77	2.73	-	$\Omega_2 > \Omega_4$	present work
1.0	10.95	2.74	-	$\Omega_2 > \Omega_4$	present work

1.5	11.14	2.75	-	$\Omega_2 > \Omega_4$	present work
2.0	11.39	2.86	-	$\Omega_2 > \Omega_4$	present work
2.5	11.57	2.80	-	$\Omega_2 > \Omega_4$	present work
ZnAlBiB2.0Eu	2.19	1.49	-	$\Omega_2 > \Omega_4$	19
Oxyfluoroborate	3.45	2.93	-	$\Omega_2 > \Omega_4$	54
SABiBEu15	4.40	1.14	-	$\Omega_2 > \Omega_4$	55

5.3.7. Radiative properties:

The J-O intensity parameters have been utilized to understand the important radiative properties such as radiative transition probability (A_R), luminescence branching ratio (β_R), total transition probability (A_T) and radiative lifetime ($\boldsymbol{\tau_R}$) to observe emission transitions for Eu^{3+} ions doped in the as prepared AZABS glasses [51]. These radiative properties are used to predict the lasing potentiality for the electric dipole transition between the excited and lower lying levels [53,56]. The radiative transition probability (A_R) can be expressed by using the formula between the initial and final stage.

$$A_R = \frac{64\pi^2\lambda o^3}{3h(2J+1)}\left[\frac{n(n^2+2)^2}{9}S_{ED} + n^3 S_{MD}\right] \quad (3)$$

Where, λ_0 is peak wavelength/energy of transition, S_{ED} and S_{MD} are electric and magnetic dipole line strengths respectively other factors have their standard meaning.

The total radiative probability A_T of emission state is obtained by summation of the higher to all lower states,

$$A_T = \sum A \quad (4)$$

The radiative lifetime (τ_R) of excited state is a reciprocal of the total radiative probability and is expressed as:

$$\tau_R = \frac{1}{AT} \quad (5)$$

Another important parameter used to understand the optical potentiality of the as prepared glasses is the luminescence branching ratio β_R is calculated from the expression given below:

$$\beta_R = \frac{A}{A_T} \quad (6)$$

Where A is radiative transition probability of particular emission and A_T total radiative probability. All the above radiative parameters calculated for the as prepared glasses and are listed in Table 4.3. It is conspicuous from Table 5.3 that, the transition $^5D_0$ to $^7F_2$ has highest A_R values and β_R values for $^5D_0 \rightarrow {}^7F_2$ transition for all the as prepared glasses. An emission transition with branching ratio larger than 0.5 could act as a potential laser transition [51]. Accordingly, the β_R value obtained for the $^5D_0 \rightarrow {}^7F_2$ transition with 2.5 mol% Eu^{3+} in the as prepared glass is relatively high (0.803) and is quite suitable to produce lasing action in visible red region [11].

Table 5.3 *Transition probability (A_R (s^{-1})), luminescence branching ratio (β_R), total transition probability (A_T (s^{-1})) and radiative lifetime (τ_R (ms)) for the observed emission transitions of Eu^{3+} ions doped AZABS glasses.*

Transition	A_R	β_R	A_T	τ_R
Glass 0.5				
$^5D_0 \rightarrow {}^7F_1$	21.5	0.152		
$^5D_0 \rightarrow {}^7F_2$	111.57	0.793	140.62	7.11
$^5D_0 \rightarrow {}^7F_4$	7.55	0.053		
Glass 1.0				
$^5D_0 \rightarrow {}^7F_1$	21.1	0.151		

$^5D_0 \rightarrow {}^7F_2$	111.04	0.795	139.53	7.17
$^5D_0 \rightarrow {}^7F_4$	7.39	0.052		
Glass 1.5				
$^5D_0 \rightarrow {}^7F_1$	21.0	0.149		
$^5D_0 \rightarrow {}^7F_2$	111.95	0.797	140.32	7.13
$^5D_0 \rightarrow {}^7F_4$	7.37	0.052		
Glass 2.0				
$^5D_0 \rightarrow {}^7F_1$	20.9	0.146		
$^5D_0 \rightarrow {}^7F_2$	113.86	0.799	142.38	7.02
$^5D_0 \rightarrow {}^7F_4$	7.62	0.053		
Glass 2.5				
$^5D_0 \rightarrow {}^7F_1$	20.8	0.144		
$^5D_0 \rightarrow {}^7F_2$	115.26	0.803	143.48	6.97
$^5D_0 \rightarrow {}^7F_4$	7.42	0.051		

5.3.8. Evaluation of CIE color co-ordinates

To understand the colorimetric performance of AZABS glasses doped with *x* mol% Eu^{3+} ions (*x* = 0.5, 1.0, 1.5, 2.0, 2.5 mol%), the CIE chromaticity coordinates were determined by using emission spectral data (λ_{ex} = 393 nm). The CIE coordinates (x, y) estimated for the as prepared glasses are shown in Table 5.4. The CIE chromaticity coordinates estimated for all the as prepared glasses under 393 nm excitation wavelength are shown in Fig. 4.9. Hence, result indicating that Eu^{3+} doped AZABS glasses are quite suitable for plasma display panels and solid state lightening devices. To understand about the red emission, color purity has been calculated by using formula:

$$Color\ purity = \frac{\sqrt{(x-x_{ee})^2 + (y-y_{ee})^2}}{\sqrt{(x_d-x_{ee})^2 + (y_d-y_{ee})^2}} \quad (7)$$

Where, (*x* and *y*) are the coordinates calculated from the PL spectra of the glass sample, (x_{ee} and y_{ee}) are the coordinates of white point and (x_d and y_d) are the coordinates of the dominant wavelength point. The calculated value of color purity for 2.5 mol% Eu^{3+} is found to be 98.48%

indicating pure red emission which is relatively higher than the other reported values in literature [57]

Table 5.4. *CIE chromaticity coordinates (x, y), and average decay time of x mol% Eu^{3+} doped AZABS glass at 393 nm excitation.*

Sample ID AZABS: *x* mol%Eu^{3+}	CIE (x, y) at λ_{ex} = 393 nm	t_{avg} (ms)
x = 0.5 mol%	(0.6494, 0.3502)	1.98
x =1.0 mol%	(0.6502, 0.3464)	1.93
x =1.5 mol%	(0.6502, 0.3494)	1.82
x =2.0 mol%	(0.6506, 0.3490)	1.78
x =2.5 mol%	(0.6507, 0.3489)	1.70

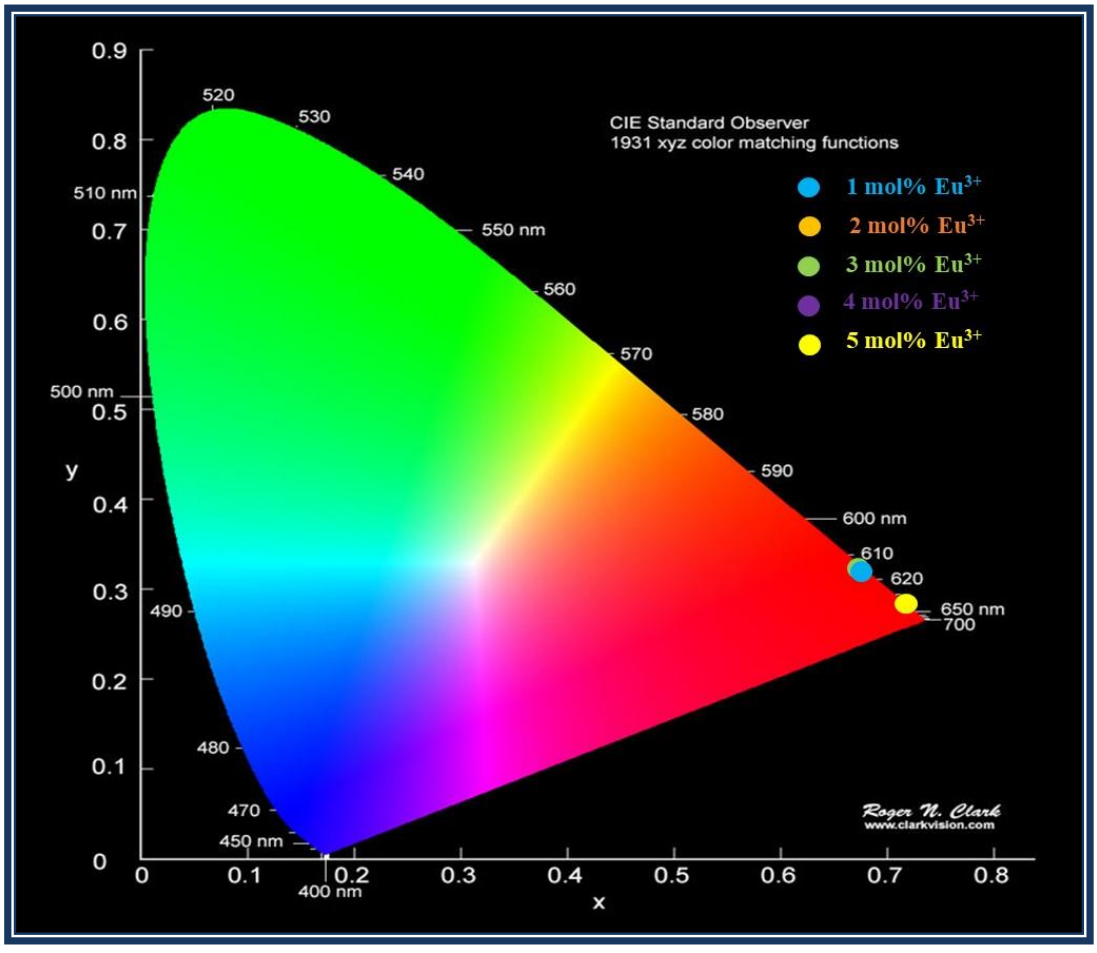

Figure: 5.9 *CIE diagram x mol% Eu^{3+} activator ion concentration (x = 0.5 to 2.5 mol%) doped AZABS glasses at λ_{ex} = 393 nm.*

5.3.9. PL decay analysis:

The PL decay curves observed for red emission (612 nm) shown by *x* mol% Eu^{3+} ions doped AZABS glasses under 393 nm excitation wavelength are shown in Fig. 5.10. It can be seen that all the PL decay curves are well fitted to a double-exponential function. The bi-exponential nature of the decay may be due to the energy transfer from an excited donor ion to an unexcited acceptor ion present in the host matrix and may be explained suitably using the below expression [58]:

$$y=A_1*exp(-x/t_1)+A_2*exp(-x/t_2)+y_0. \quad (8)$$

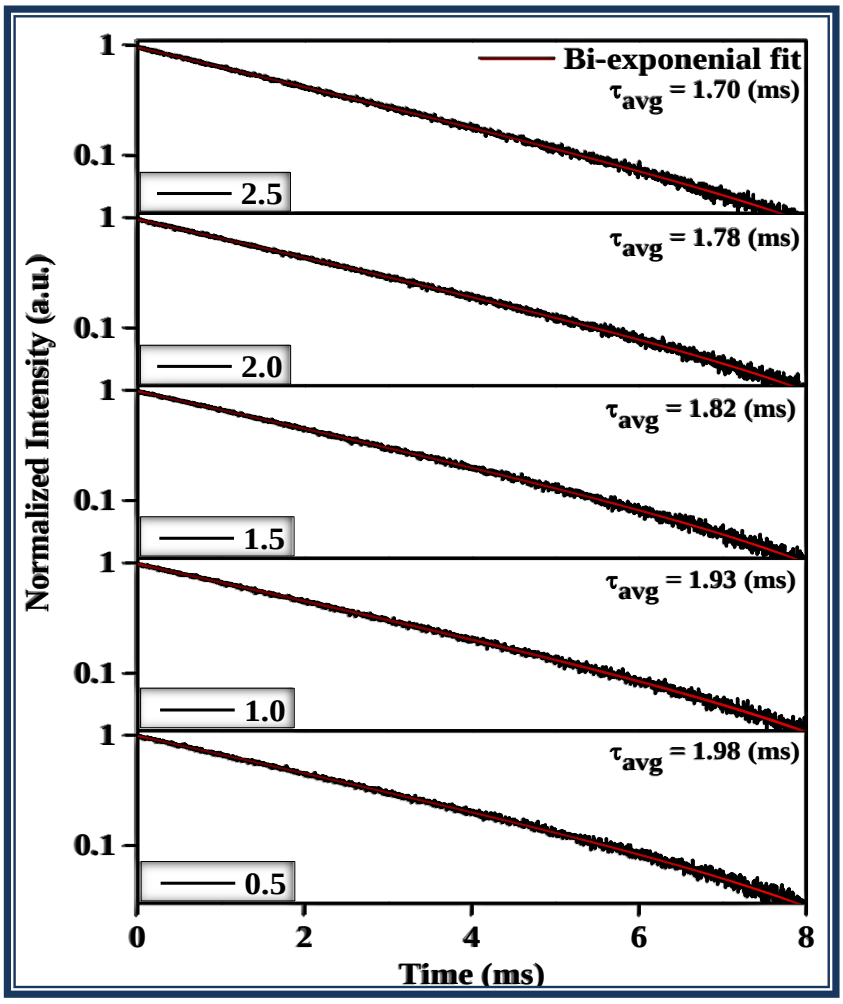

Figure:5.10 *Luminescence decay curves of x mol% Eu^{3+} (x = 0.5 to 2.5 mol%) doped AZABS glass recorded under 393 nm excitation wavelength.*

If there are no interactions present between the doped RE ions, then the decay shown by such materials fits to a single exponential function. However, if there are ion-ion interactions present inside the host lattice, then resulting emission consists of slow and fast decay components. For the lanthanide ions, there are different non-radiative decays which makes the curves well fitted to a double exponential function [59]. The measured decay lifetimes for the as prepared samples are found to be 1.98, 1.93, 1.82, 1.78. 1.70 ms for 0.5, 1.0, 1.5, 2.0, 2.5 mol% Eu^{3+} respectively. It is observed that the measured lifetime values are decreasing with increase in europium ions concentration. This can be attributed mainly to cross relaxation processes between the lanthanide ions. The average lifetime calculated for all the as prepared Eu^{3+} ions doped AZABS glass are depicted in Table 4.

5.3.10. Temperature dependent PL and estimation of activation energy:

To study the thermal quenching behavior, AZABS glass doped with 2.5 mol% of Eu^{3+} ion, the PL emission spectra was recorded under 393 nm excitation by varying the temperature from 30 to 200^{o}C. The PL emission intensity decreases with increase in temperature as shown in Fig. 5.11 for 2.5 mol% of Eu^{3+} ion doped AZABS glass.

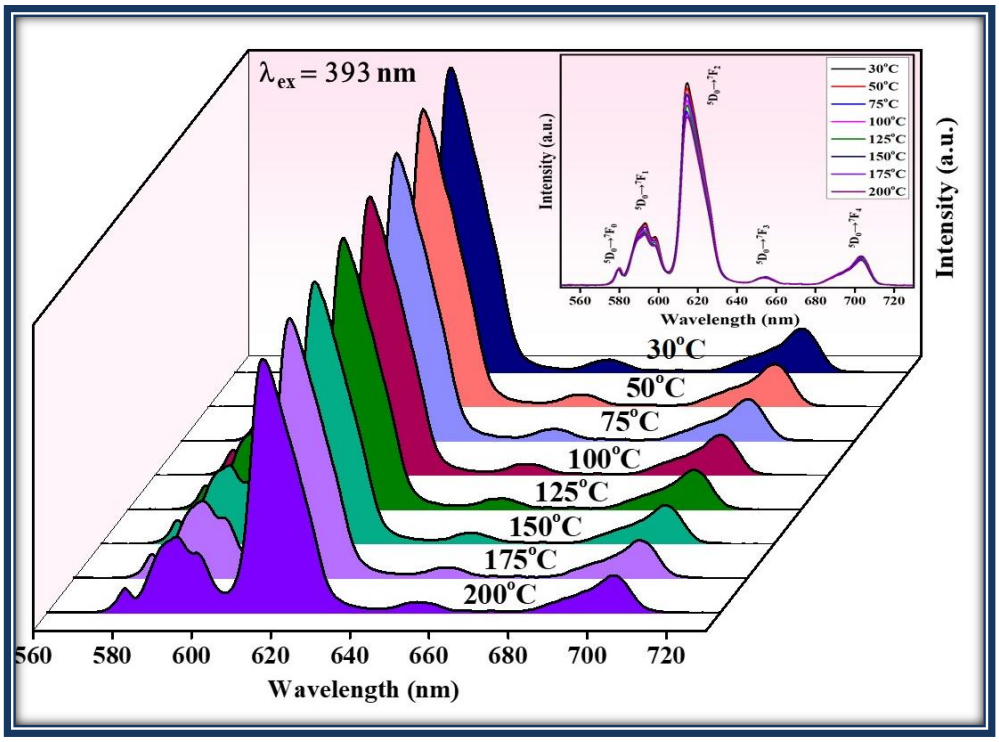

Figure:5.11 *Temperature dependent emission intensity variation of 2.5 mol% Eu^{3+} doped AZABS glass under 393 nm excitation with rise in temperature from RT to 200°C*

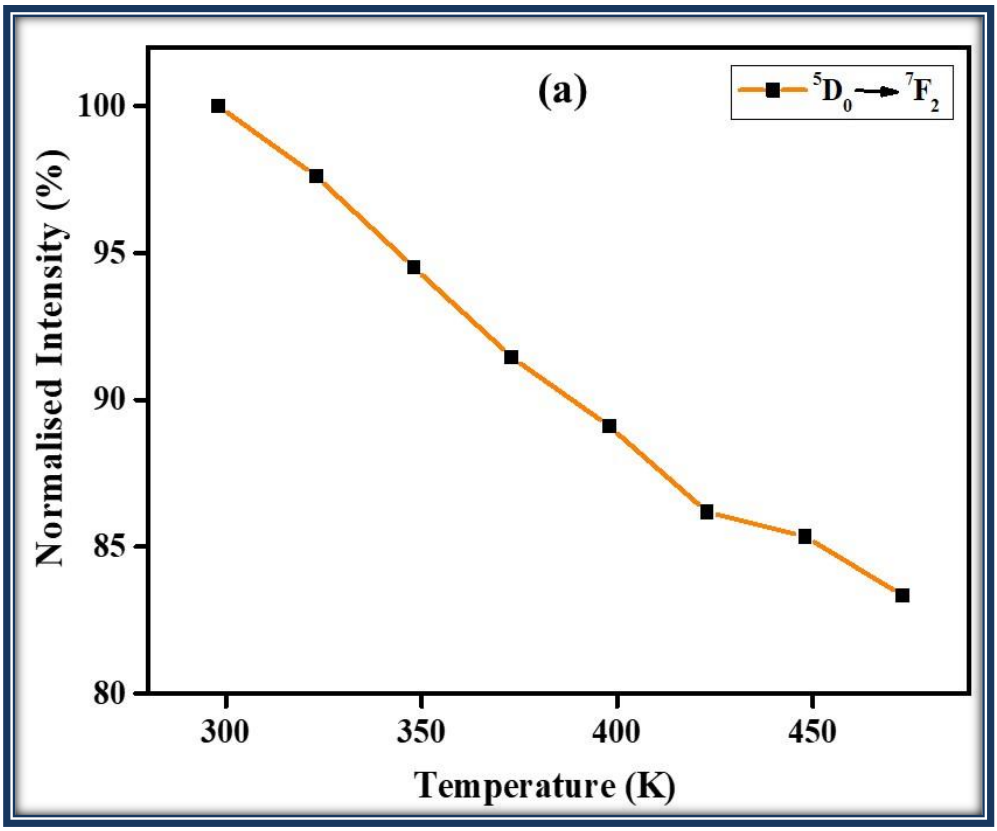

Figure:5.12 *(a) Plot shows the normalized PL intensity with rise in temperature range 298-473K.*

Fig. 5.12 (a) shows plot between normalized intensity of $^5D_0 \rightarrow {}^7F_2$ transition with rise in temperature by considering the respective transition highest emission intensity at 30°C taken as 100%. At 200 °C, emission intensity reduces to 83%, which shows that AZABS glass doped with Eu^{3+} is thermal stable [60]. The retention of PL intensity observed in the present work (83% at 200°C) is relatively better than the red emitting Eu^{3+} activated phosphors reported in literature. [61-62]

Additionally, to examine the thermal properties of glass sample, the activation energy (ΔE) was calculated. The value of ΔE has been calculated from the relation between the temperature and the intensity of emission, with the help of Arrhenius equation [50,63].

$$I_T = \frac{I_o}{1+C\ exp\left(-\frac{\Delta E}{K_B T}\right)} \quad (9)$$

Where I_0 and I_T are the intensity of PL at RT and temperature in kelvin respectively. C is the arbitrary and K_B (8.617×10^{-5}eV/K) is the Boltzmann constant respectively. The slope of linear fitted plot between $\ln((I_0/I_T)-1)$ versus $1/K_BT$ gives the ΔE, as shown in Fig.5. 12 (b). The value of ΔE estimated for AZABS glass doped 2.5 mol% Eu^{3+} ion is 0.175 eV. This suggest that AZABS glass doped 2.5 mol% of Eu^{3+} ions have good temperature stability.

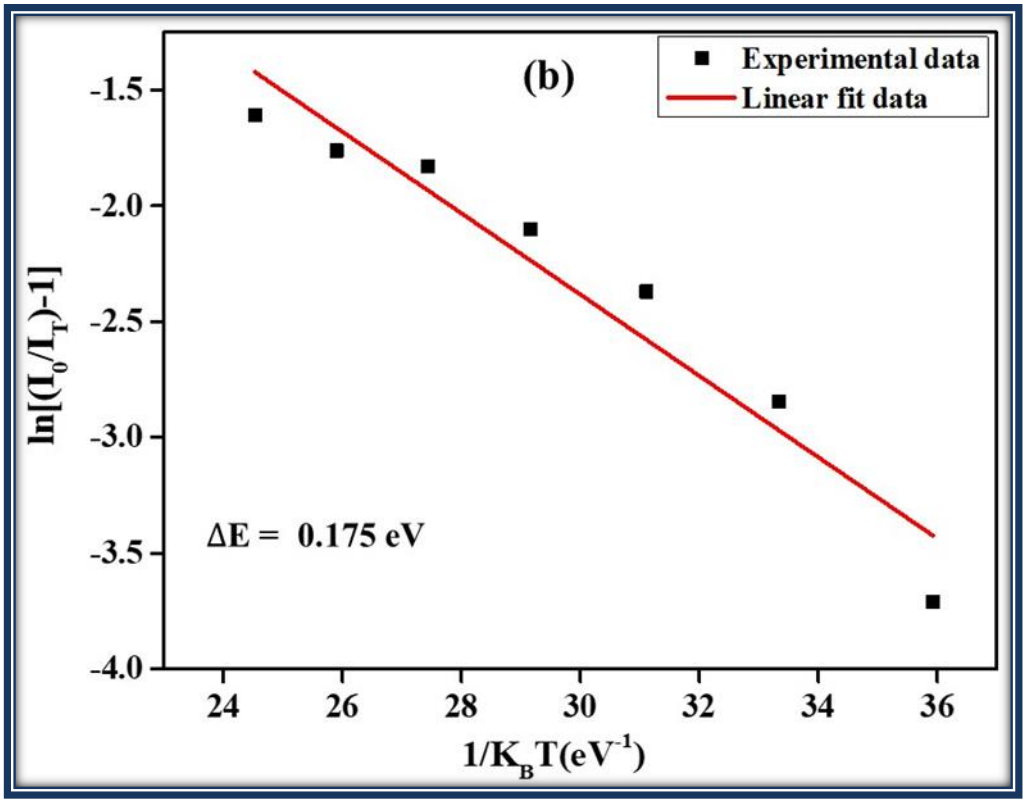

Figure:5.12 *(b) Linear relationship of ln[(I0/IT)-1] versus 1/kBT plot to calculate activation energy of 2.5 mol% Eu3+ doped AZABS glass.*

5.4. Conclusions

AZABS glasses doped with *x mol%* Eu^{3+} ions (*x* = 0.1 to 2.5 mol %) were synthesized via conventional melt quenching technique and investigated using XRD, absorption, PL excitation

& emission, temperature dependent PL and PL decay spectral analysis. Amorphous nature of the as synthesized undoped glass has been confirmed from the XRD spectrum. The DSC and TGA shows the thermal stability and aggregate weight loss of an undoped glass respectively. The total loss of mass observed (16.80%) for and undoped glass indicates its thermal stability at high temperatures. The absorption spectral features recorded for the as prepared glasses are used to estimate optical band gap and found to be in the range from 2.98 to 3.06 eV. The sharp excitation bands observed in the PLE spectra reveals the feasibility of using commercially available UV red LEDs as an excitation source. The R/O ratio observed in the range 3.62 to 3.92 suggests that the Eu^{3+} ions are present at a low symmetry site. Within the Eu^{3+} ions dopant range (0.5 to 2.5 mol%) the AZABS glass containing 2.5 mol% of Eu^{3+} ions possess higher covalency among all the as prepared AZABS glasses. Emission spectral features are subjected to J-O analysis to understand the nature of bonding between the doped RE ions and the surrounding ligands along with the radiative properties of the as prepared glasses. Relatively higher Ω_2 J-O intensity parameter obtained for 2.5 mol% Eu^{3+} in AZABS glass indicates relatively high covalency and low symmetry. This information is in consonance with the result of red to orange (R/O) intensity ratios estimated for as prepared AZABS glasses. The CIE coordinates of all as prepared glasses were located in the red region. The delay profile of the $^5D_0$ level shows bi-exponential nature of all given concentration of europium ions and found that the lifetime of 0.5 mol% Eu^{3+} is 1.98 ms for $^5D_0$ is relatively high. Temperature dependent study conducted on 2.5 mol% of Eu^{3+} doped AZABS glass reveals its thermal stability. All the aforementioned results observed for thermally stable Eu^{3+} doped AZABS glasses finally allows us to contemplate the potentiality of 2.5 mol% Eu^{3+} in AZABS glass for the fabrication of visible photonic devices such as solid-state lightening devices (red component in w-LEDs) and visible red lasers.

Chapter 6

Linear and Nonlinear PL from Thermally Stable $KYF_4:Eu^{3+}$ Cubic Nanocrystals

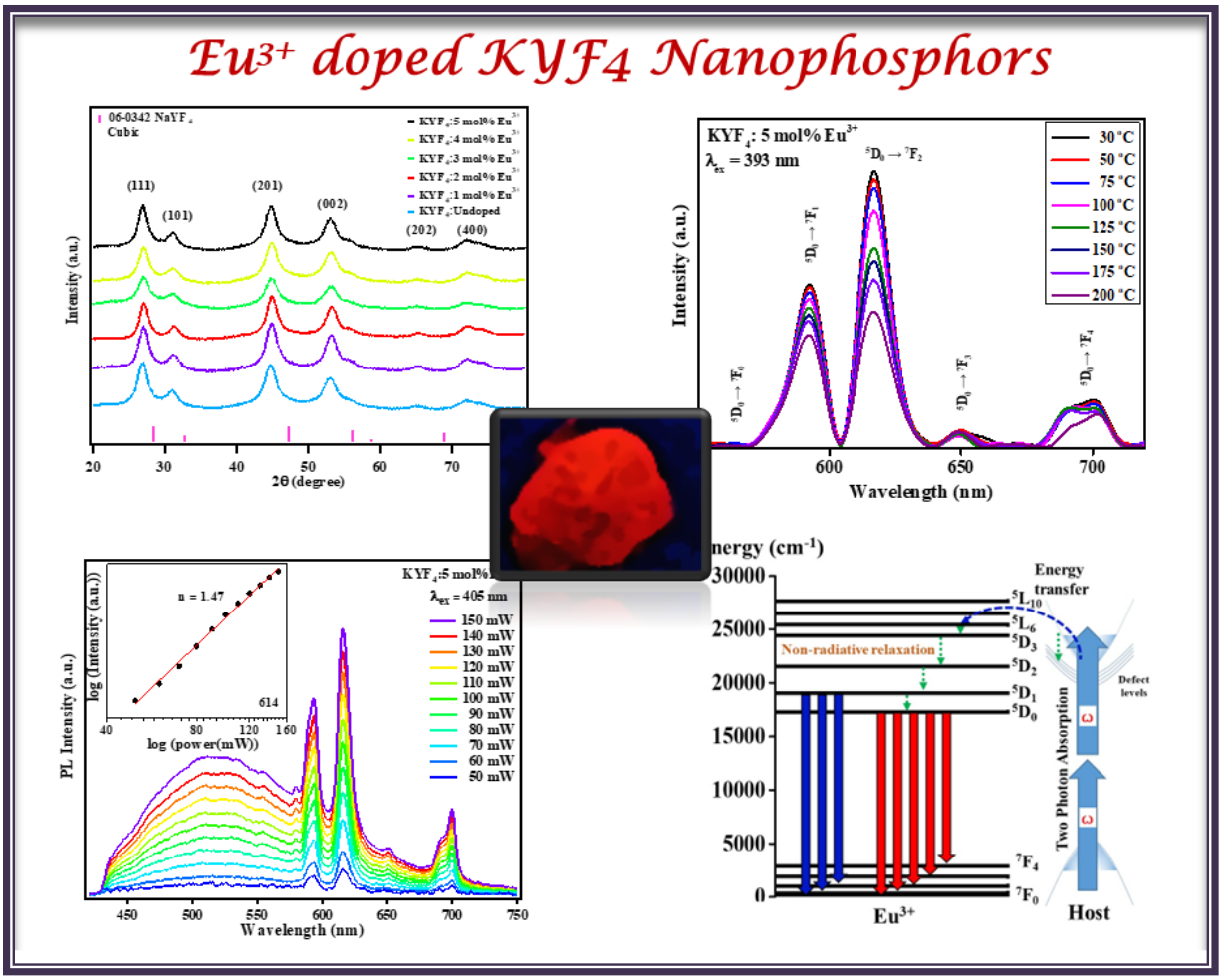

Part of this work has been published in Journal of Alloys and Compounds, 885 (2021), 160893, (Impact Factor = 5.8)

This chapter deals with the synthesis of cubic phase $KYF_4:Eu^{3+}$ nanophosphors via wet chemical route. Morphological studies such as XRD, SEM and EDAX mapping were done to ascertain shape, size and composition of the as prepared nanophosphors. Debye Scherrer formula applied to the XRD spectral features of the as prepared nanophosphors reveals the average size in the range 3 - 4 nm. The JCPDS data analysis for $KYF_4:Eu^{3+}$ nanophosphors confirm cubic structure with lattice constant $a = b = c = 5.448Å$ and $\alpha = \beta = \gamma = 90°$. The SEM image mapping clearly demonstrates the uniform distribution of all the constituent elements such as potassium, yttrium, fluorine and europium. Up-conversion (UC) studies carried out using 800 nm spitfire femtosecond laser produces peaks at 576, 590, 612, 650, 700 nm pertaining to the transitions $^5D_0 \rightarrow {}^7F_j$ (J = 0, 1, 2, 3, 4) respectively. In addition to this, three higher order peaks are also observed at 523 531, 552 nm pertaining to $^5D_1 \rightarrow {}^7F_j$ (J = 0, 1, 2) transitions respectively. Down-shifting (DS) studies under 393 nm and 405 nm excitation were also recorded to understand the utility of the as prepared phosphors for lighting applications. These nanophosphors are capable of emitting visible emission under UV/NIR excitations. The powder dependence studies conducted on UC and DS reveals the excitation process as two photon and single photon respectively. DS temperature dependent PL spectral revels good thermal stability for the as prepared phosphor. The interesting results obtained allows us to contemplate that the as prepared $KYF_4:Eu^{3+}$ nanophosphors are useful for bio-imaging (through UC) as well as lighting applications (through DS).

6.1. Introduction

A nonlinear optical process known as up-conversion (UC) occurs when two or more NIR photons are absorbed, transforming low energy NIR radiation into high energy visible radiation. The UC technique can be used in a variety of sectors, including solid state lasers, 3D displays, white LEDs, solar cells, photodynamic treatment, temperature sensing, optical imaging, and

biological labeling, thanks to this unique wavelength change [164]-[165][166]. Unlike the conventional luminescent probes such as quantum dots (QDs) and organic dyes, nano-sized fluoroprobes i.e., the up-conversion nanoparticles (UCNPs) have multiple absorptions and emission centers. These UCNPs have unique properties such as photo and thermal stability, narrow emission bandwidths (<10nm), large excited lifetimes, superior photostability, low cytotoxicity and large anti-stokes shifts (i.e. up to 500 nm) that differentiates peaks due to emission and NIR excitation. Also, under NIR excitation, relatively high penetration depth in tissues and weak autofluorescence facilitates the usage of UCNPs in medical fields for bio-imaging and target drug delivery applications [167]-[168]. Most of the UC materials uses rare earth (RE) ions as active ions. Most of the trivalent RE ions (Ln^{3+}) in which 14 electrons are filled in the 4f inner shell, presenting a great similarity in electron configurations $4f^n5s^25p^6$ (n=1 - 14). The 4f shell is partially filled and exhibits similar physical, chemical, optical and magnetic properties. These properties are dependent on various things like crystals structure, morphology as well as on chemical composition which are very sensitive to the bonding states of RE ions [169]. The absorption, as well as emission transitions produced by RE ions are very sharp as such transitions are produced between 4f energy levels [170].

Spectral properties of RE doped chlorides, oxides, fluorides and phosphate have been studied extensively to understand their suitability as potential luminescent applications [171]. However, most of the aforementioned systems are sensitive to moisture and thus are not quite suitable for bio labeling except the fluoride compounds with a formula such as $AREF_4$ (A = alkali, RE = rare earth F = Fluoride) [5[172]]. Among $AREF_4$ host lattices, $KREF_4$ (K stands for potassium) especially have attracted much more attention because of the high reflective index and low phonon energy that make them excellent host matrix for both DS as well as UC processes [173][171][174]. The $KREF_4$ exhibits two polymeric forms of crystal structures, namely cubic

and hexagonal phases depending upon the methodology and synthesis conditions [175][176]. Apart from this, relatively less phonon energy, non-hygroscopic nature, ability to convert NIR & UV radiations in to visible (through UC & DS processes), good dissolving nature in solvents and relatively higher chemical stability makes the fluoride based nano crystals as promising host lattices for various luminescent applications when doped with RE [177]-[178].

Trivalent rare-earth (RE^{3+}) doped with luminescent materials have gained so much attention due to their applications in the field of white LEDs as red emitting phosphors, plasma screens and so on [31]. Among all RE ions, Eu^{3+} ions are better known as the activator for intense red color through DS process in a wide variety of materials such as glasses, phosphors, nanophosphors and organic-inorganic hybrid materials [32-36]. In general, the emissions of Eu^{3+} are strongly dependent on the crystal structure of the host and sensitive to the local environment where the rare earth have been situated [37] and found from 550 to 750 nm, pertaining to the transitions of $^5D_1$ and $^5D_0$ states to ^7F_j states (j = 0 to 6). Apart from this, it is also suitable for various applications as it exhibits large stokes shifts (>150 nm). Y. Du et al. reported Eu^{3+} $KREF_4$ nanoparticles via thermal decomposition method [38]. S. Ahmad, S. Das, and their co-workers recently published the optical spectra of Tb^{3+} and Eu^{3+} doped $KLaF_4$ via wet chemical route [179][180]. To date, UC process of Eu doped fluoride nanoparticles remains nearly untouched. Due to a lack of resonant energy level, the energy level structure of the Eu^{3+} does not permit UC emission by directly exciting with NIR radiation [181]. Deeper knowledge of understanding the optical behavior of Eu^{3+}ions in KYF_4 is extremely important for the development of novel luminescent materials suitable for solid state lighting devices as well as nano-labels.

In this paper, we have shown that, $KYF_4:Eu^{3+}$ emits strong UC & DS luminescence through two photons (femtosecond laser irradiation) and single photon absorption process. KYF_4 was synthesized by wet chemical route with different concentrations of *x* mol% Eu^{3+} ions (*x* = 0 - 5%) in cubic phase to study the enhancement of red emission in it [41]. Structural, morphological and photoluminescence studies have been carried out for the crystallinity, phase identification and luminescence efficiency respectively. The intense red emission via dual mode (DS & UC) makes Eu doped KYF_4 nanophosphors as promising host material for bio-imaging and lighting applications [42-44]

6.2. Experimental Section

KYF_4 host lattices were prepared by employing wet chemical route. The complete synthesis process was discussed detail in chapter 2.

6.3. Results and Discussion

6.3.1. Structural and morphological studies of $KYF_4:Eu^{3+}$ nanophosphors.

The phase crystallinity identification of x mol % of Eu^{3+} (*x* = 0 to 5) doped KYF_4 nanophosphors was examined by powder XRD at the room temperature and is shown in Fig.3.1 (a). These nanoparticles having pure cubic phase as the peak position and the intensity matches well with the cubic unit cell with Fm3m space group pertaining to $NaYF_4$ (JCPDS file no.06-0342). It is conspicuous from Fig.1 that, there is a slight shift in diffraction peaks towards the lower angle 2θ (1 - 3º angles) side may be due to the replacement of smaller ionic radii of Na^+ with larger ionic radii of K^+. The sample might be isostructural to that of the cubic phase of KYF_4 [35].

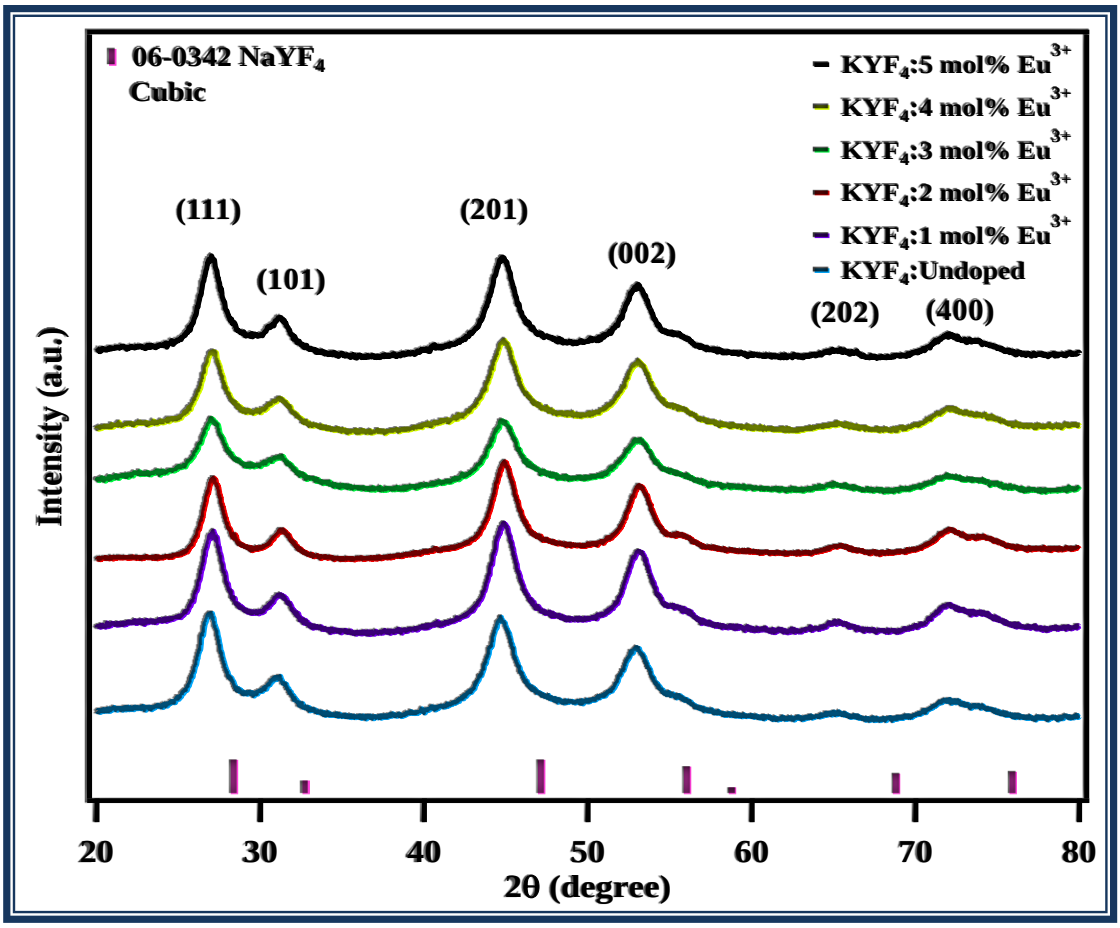

Figure: 6.1(a). *Powder XRD patterns of Eu^{3+} doped cubic KYF_4 (Eu^{3+} = 1, 2, 3, 4 and 5 mol%) nanophosphors.*

The average size of the particles in the as prepared phosphors can be determined using the following Debye Scherrer formula [33]:

$$D = \frac{K\,\lambda}{\beta\,Cos\theta}$$

Where, D is the size of the nanocrystal, K = 0.94 is the shape factor, β is the full width at half maximum (FWHM), $\boldsymbol{\lambda}$ is the wavelength of the XRD and 2θ is the angle at which maximum intensity was observed. The average nanocrystal sizes were estimated to be in the range of 3 - 4 nm. The broadness of XRD peaks is found be invariant with the doping concentration. i.e., XRD peaks' broadening is solely a result of host matrix nano dimensions, which is invariant

with the doping concentration. The JCPDS data of $NaYF_4$ has been used to construct the unit cell structure of KYF_4 as presented in Fig.3.1(b). The cubic structure is having lattice constant $a = b = c = 5.448Å$ and $\alpha = \beta = \gamma = 90°C$.

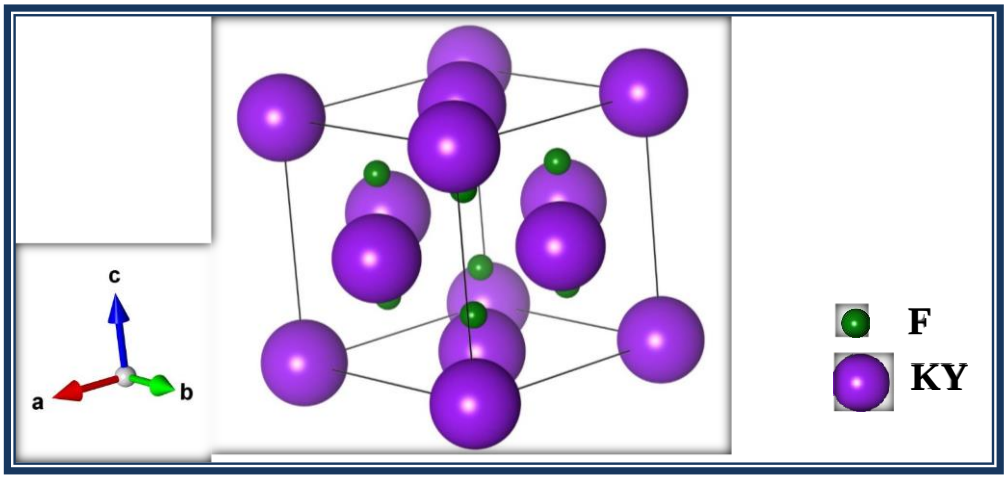

Figure: 6.1(b) *Crystal structure of KYF_4.*

The SEM image of KYF_4 doped with 5 mol% of Eu^{3+} is shown in Fig.3.2 (a). From the elemental mapping results shown in Fig.3.2 (b - f), it was clear that all the elements such as potassium, yttrium, fluorine and europium were uniformly distributed over the particles, which suggest that KYF_4 doped with *x* mol% Eu^{3+} (*x* = 1 - 5%) samples were successfully synthesized.

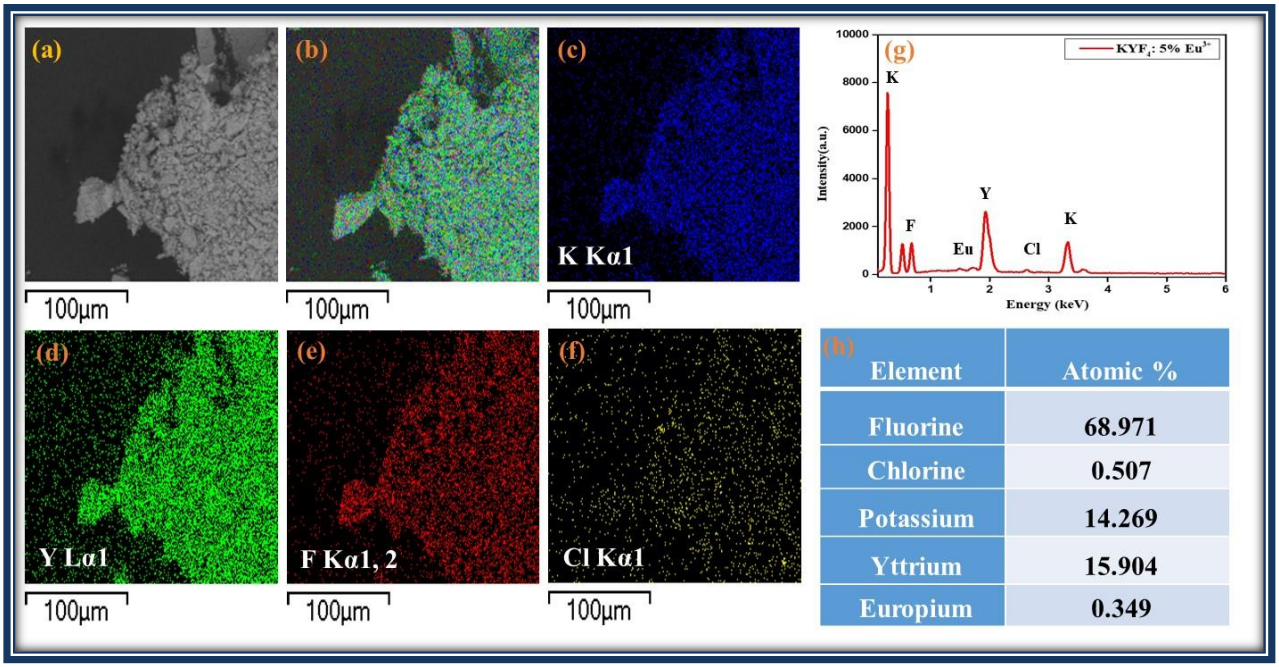

Figure: 6.2. *(a) SEM Image of KYF_4:5 mol% Eu^{3+} and corresponding (b) Mixed elemental Mapping and (c-f) individual of Potassium (K), Yttrium (Y) and Fluorine (F), Europium (Eu) (g) EDAX Spectrum and (h) relative elemental At% from EDAX Spectrum.*

The energy dispersive X-ray analysis (EDAX) spectrum and elemental mappings suggest that all the element that are used during the synthesis are present (Fig. 3.2). Fig. 3.2 (h) also gives relative atomic% of elements present in the nanophosphors. However, the EDAX contains relative information, including many unwanted and native elements such as Carbon, Oxygen etc. Thus, the elemental information is only indicative and cannot be accurately quantified.

6.3.2. Down shifting photoluminescence studies of $KYF_4:Eu^{3+}$ nanophosphors.

The photoluminescence (PL) excitation (under 615 nm emission) and PL emission (under 393 nm excitation) spectra of KYF_4 doped Eu^{3+} ions were shown in Fig.3.3. Under 615 nm emission wavelength, the PL excitation spectrum shows excitation peaks of Eu^{3+} resulting from $^7F_0$ and $^7F_1$ energy levels to different higher energy levels observed at 361, 393, 415, 464, 524 and 534 nm pertaining to $^7F_0 \rightarrow {}^5D_4$, $^5L_6$, $^5D_3$, $^5D_2$, $^5D_1$ and $^7F_1 \rightarrow {}^5D_1$ transtitions of Eu^{3+} ions

respectively. Among various excitation levels, the most intense peak was observed at 393 nm ($^7F_0 \rightarrow {}^5L_6$) and was used as an excitation wavelength (λ_{ex}) to record the PL emission spectra.

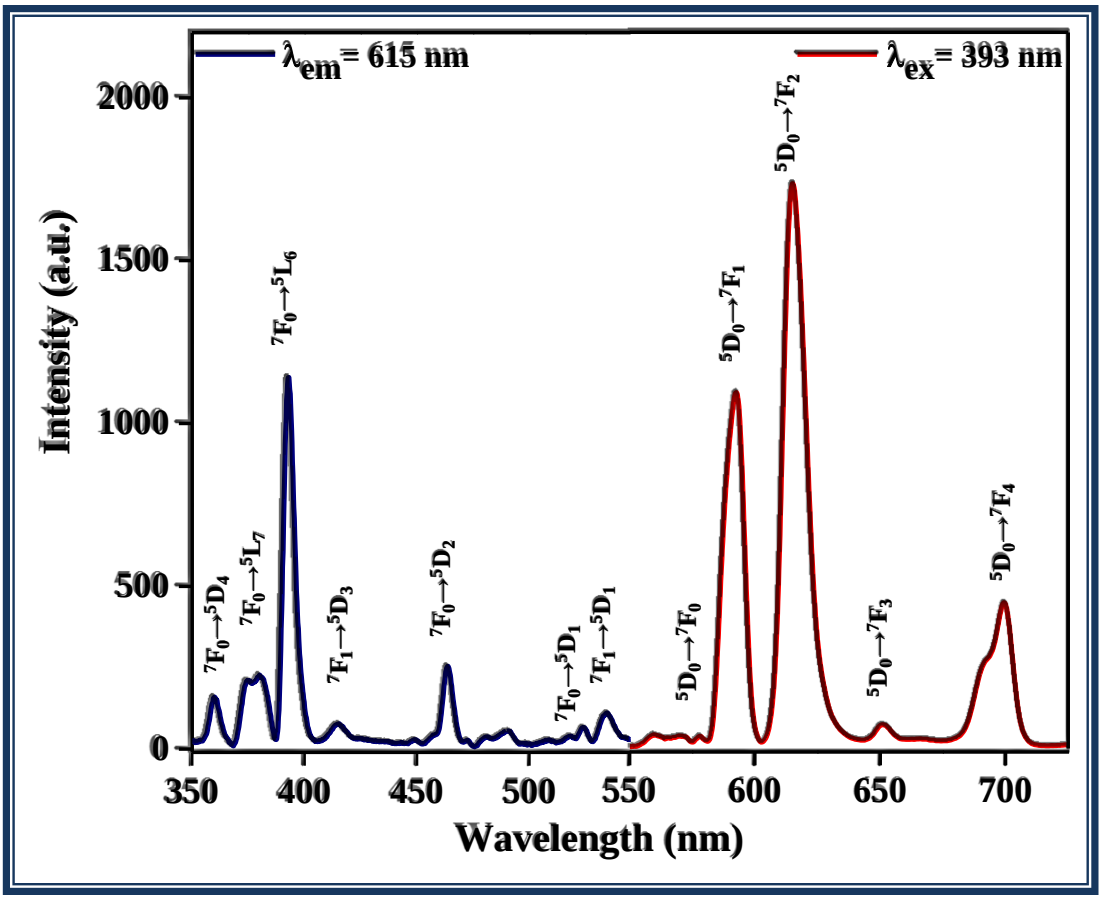

Figure: 6.3 *PL excitation spectra under red emission at λ_{em} = 615 nm ($^5D_0 \rightarrow {}^7F_2$) and PL emission spectra under excitation at λ_{ex} = 393 nm ($^7F_0 \rightarrow {}^5L_6$) for the as prepared KYF_4:5 mol% Eu^{3+}*

When excited at λ_{ex} = 393 nm, four PL emission peaks were observed at 592, 615, 650 and 700 nm pertaining to $^5D_0 \rightarrow {}^7F_1$, $^7F_2$, $^7F_3$ and $^5D_0 \rightarrow {}^7F_4$ transitions respectively [182]-[183]. Among the four emission peaks observed, the one observed at red region of the visible spectrum (615 nm) is relatively very intense. The emission spectra of KYF_4 doped with *x* mol% Eu^{3+} (*x* = 1, 2, 3, 4, 5) recorded under 393 nm excitation is shown in Fig.3.4. The PL spectra shown in Fig. 4 reveals two well-known peaks at 592 and 615 nm pertaining to $^5D_0 \rightarrow {}^7F_1$ (orange) and $^5D_0$

$\rightarrow {}^7F_2$ (red) transitions respectively. The intensity of the peak originated at 592 nm is insensitive to the local environment as it is magnetic dipole (MD) in nature. Another peak observed at 615 nm is electric dipole (ED) transition and is hypersensitive in nature and Eu^{3+} ions occupy inversion symmetry [184]. The ${}^5D_0 \rightarrow {}^7F_0$ is a forbidden transition because of the J = 0 value.

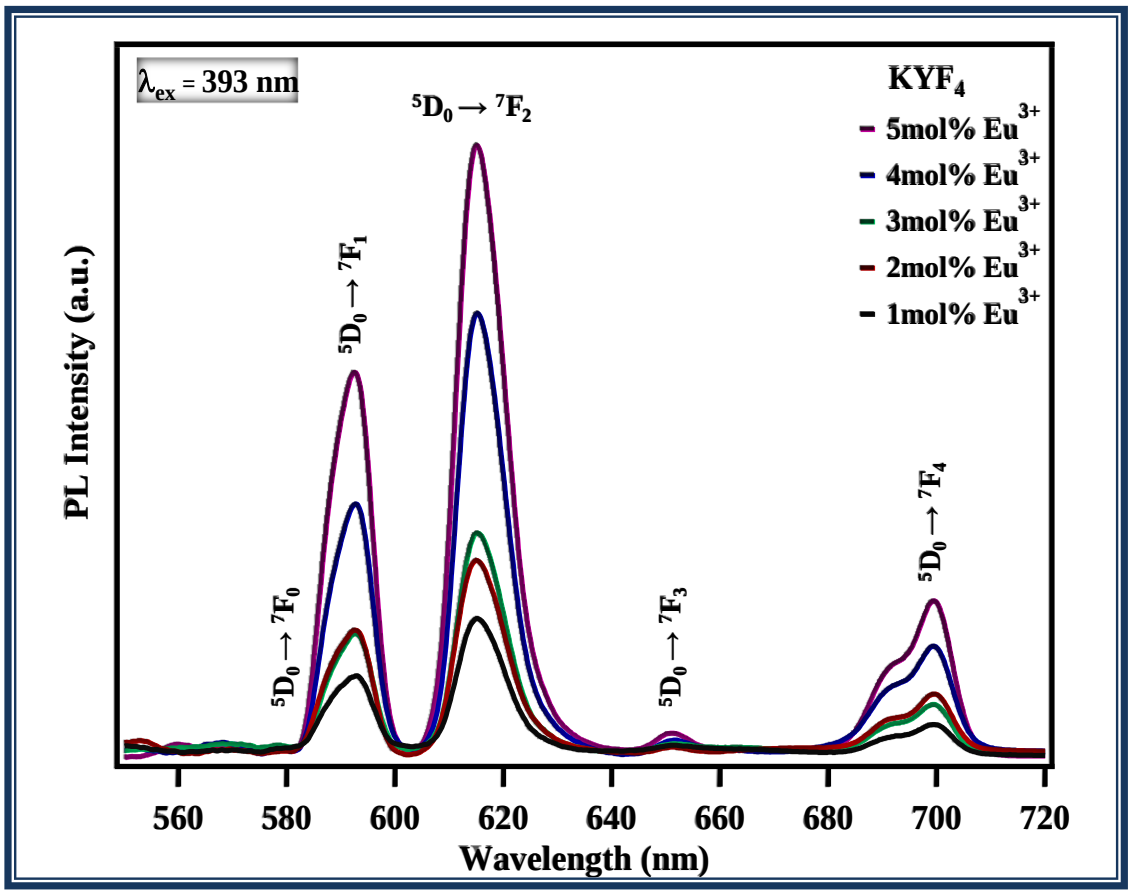

Figure: 3.4(a). *DS PL emission spectra of KYF_4: x mol% Eu^{3+} (x = 0 - 5%) under 393 nm excitation (baseline corrected)*

The intensity of the PL emission peaks shown in Fig. 3.4 (a) are increasing with increase in Eu^{3+} ions concentration continuously. Red to orange (R/O) intensity ratio between the hypersensitive transition (615 nm) to that of invariant transition (592 nm) gives the asymmetric ratio which represents the degree of distortion from the symmetry of inversion pertaining to Eu^{3+} ions in the KYF_4 matrix. Thus, the R/O ratio is generally regarded as a structural probe,

as it gives the information pertaining to bonding nature (ionic or covalent) existing between the doped RE ions and ligands surrounding it [180]7,51]. The R/O ratios for different Eu^{3+} ion concentration is calculated to be 1.5 - 1.8 indicates that Eu^{3+} ions are located in non-symmetric site due to large covalent bonding. The calculated CIE color coordinates of Eu^{3+} doped KYF_4 phosphor under 393 nm excitation lies in red region of the visible spectrum as shown in Fig. 3.4(b).

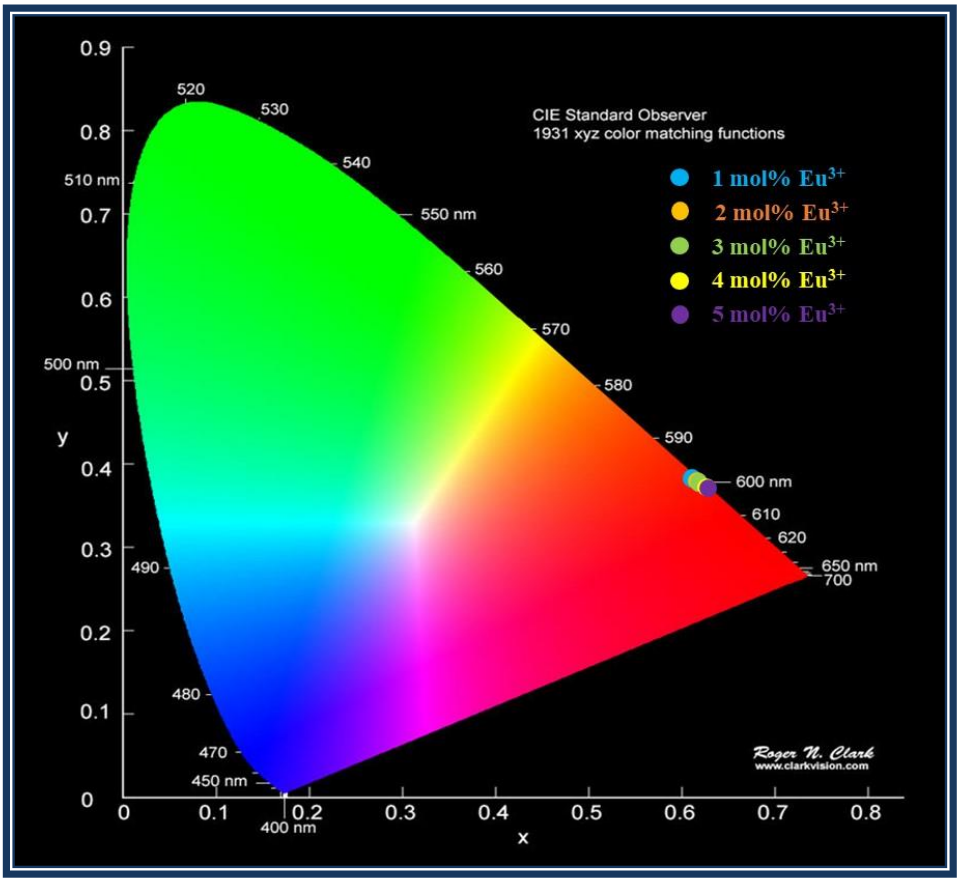

Figure:6.4(b). *CIE diagram of DS KYF_4: x mol% Eu^{3+} (x = 0 - 5%) nanophosphor under 393 nm excitation.*

This clearly demonstrates that the as prepared phosphors can be effectively used as red component sources needed for the fabrication of white LEDs through DS process. The power dependence PL emission spectra recorded for KYF_4:5 mol% Eu^{3+} nanophosphor under 405 nm

diode laser excitation (155 mW) is shown in Fig. 3.5. The PL emission spectra shown in Fig. 3.5 are very similar to the PL emission peaks observed under 393 nm excitation shown in Fig. 3.4 [167],52-[185].

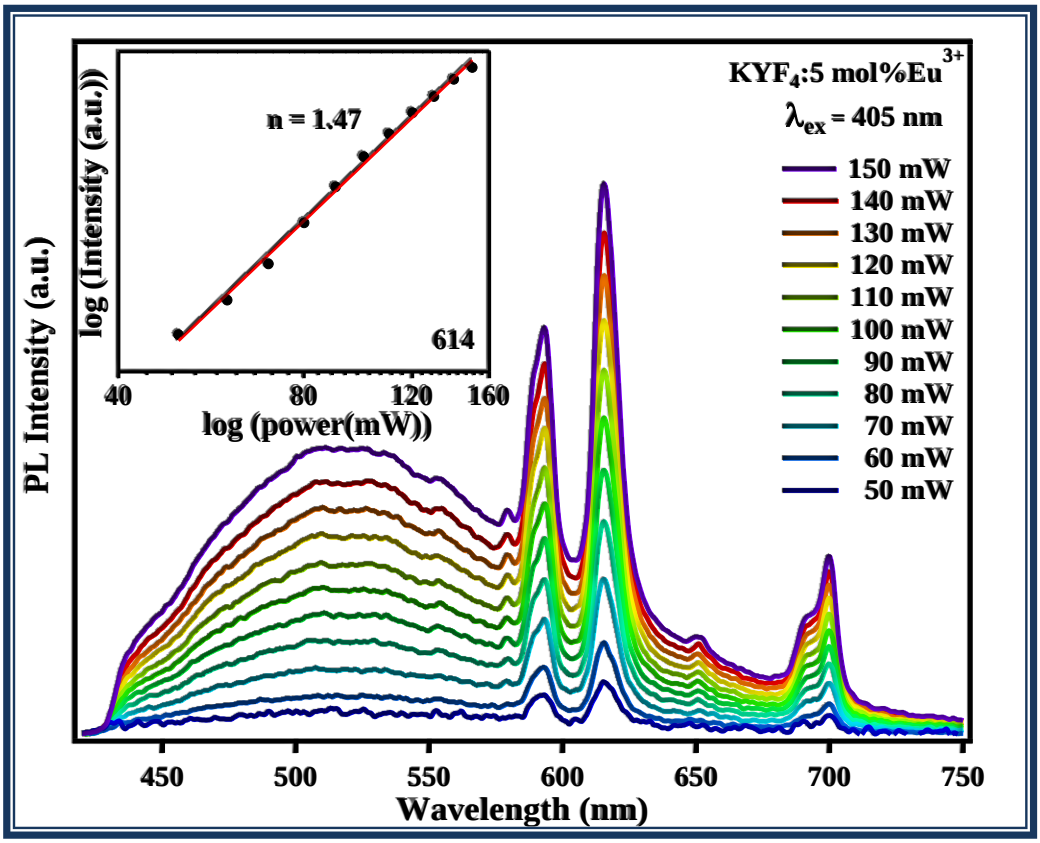

Figure: 6.5. *Power dependence PL emission spectra of KYF4: 5 mol% Eu3+ (under 405 nm diode laser excitation). Inset figure show the log-log intensity vs power graph plotted for red emission at 615 nm.*

It can be seen form the inset of Fig. 3.5 that the value of n ~ 1 suggest that one photon excitation is involved in the DS process of the as prepared phosphors. Fig. 3.6 shows a typical energy level diagram of Eu in KYF_4 in DS process. When electrons are pumped from ground state to a higher level $^7F_0 \rightarrow {}^5L_6$ via single photon DS process (405 nm), the electrons at $^5L_6$ level relax non-radiative to $^5D_3$, $^5D_2$, $^5D_1$ and $^5D_0$ levels and finally radiatively transfers energy to the

ground states ^7F_J (J = 0 - 4). As a result, the characteristic DS luminescence emission of Eu^{3+} occurs as depicted in Fig.3.6.

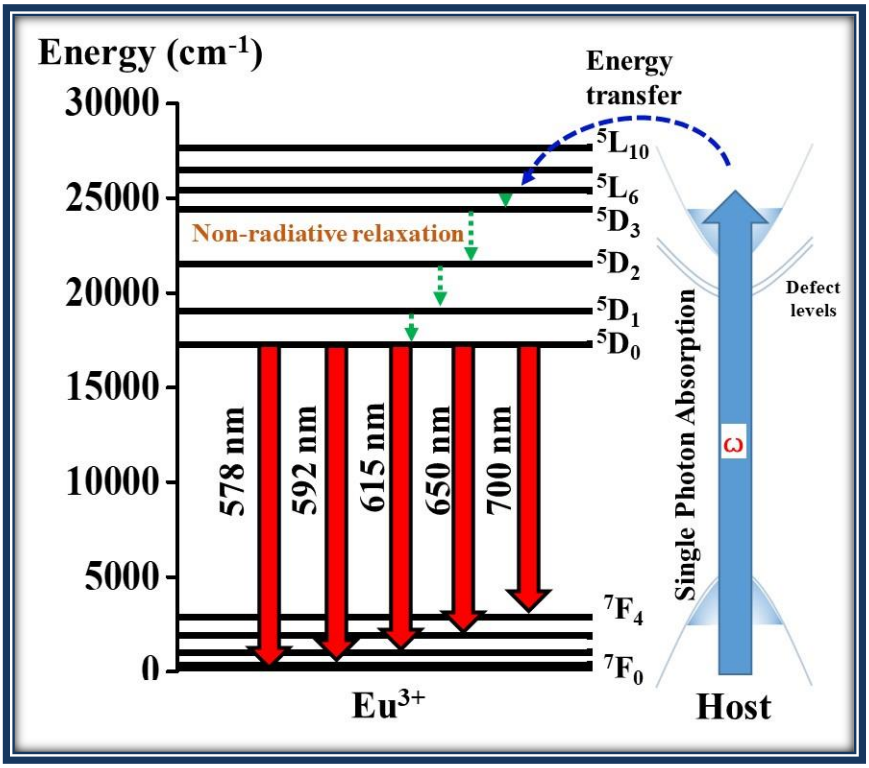

Figure: 6.6. *Schematic energy level diagram and DS mechanism of Eu^{3+} ion in KYF_4 doped with x mol% Eu^{3+} (x = 5) pumped by 405 nm diode laser.*

6.3.3. Temperature dependent DS PL studies of $KYF_4:Eu^{3+}$ nanophosphors

The thermal quenching behavior of KYF_4 doped Eu^{3+} ions was analyzed by recording the DS PL spectra (under 393 nm excitation) at different temperatures starting from ambiance to 200°C and is shown in Fig. 3.7. From this result it is conspicuous that, as synthesized $KYF_4:Eu^{3+}$ nanophosphor is portraying excellent thermal stability. The data pertaining to temperature dependent photoluminescence behavior of a phosphor can be used to estimate its activation energy (ΔE) using the following equation given by Arrhenius [55, 56]:

$$I_T = \frac{I_o}{1 + C\ exp\left(-\frac{\Delta E}{K_B T}\right)}$$

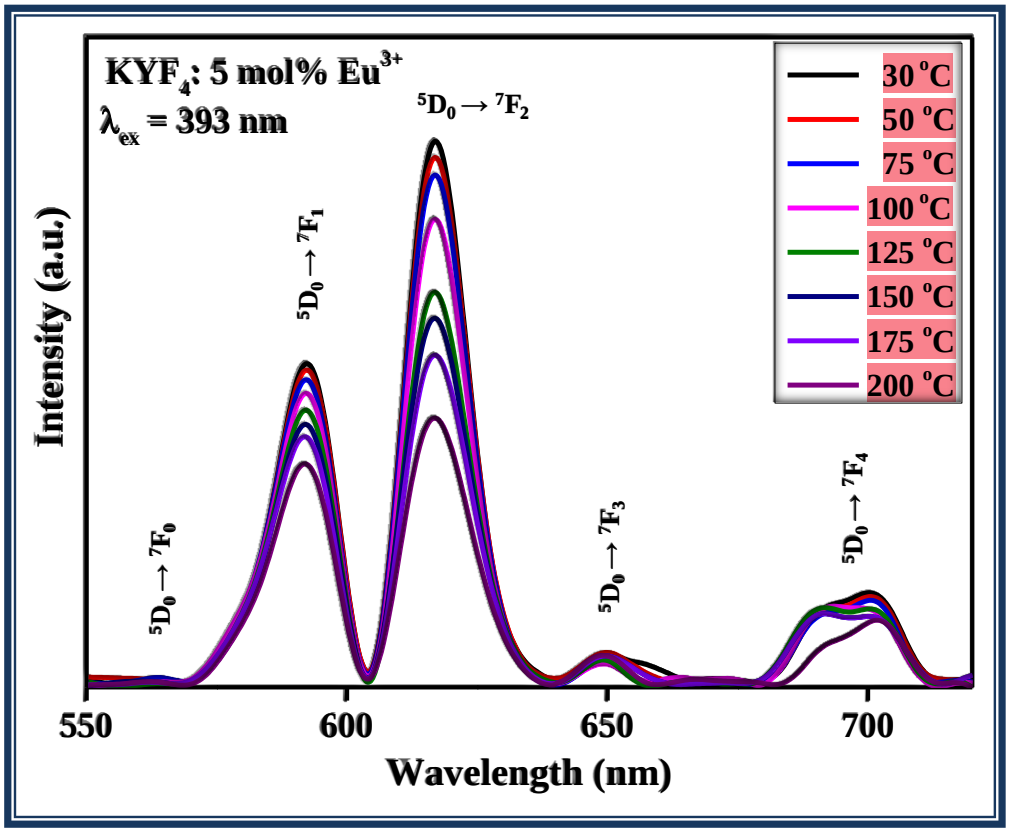

Figure: 6.7. *Thermal stability of KYF_4: 5 mol% Eu^{3+} (393 nm excitation).*

where I_0 and I_T pertains to intensity of emission at RT and at some other temperature T in Kelvin respectively. C and K_B denotes the arbitrary and Boltzmann constants respectively. To estimate ΔE a graph has been plotted between $ln[(I_o/I_T) - 1]$ vs $1/K_B\ T$ as shown in Fig. 3.8. The slope of the graph (0.309) plotted in Fig.3.8 gives activation energy of the as prepared phosphor. Therefore, temperature dependent PL studies conducted on 5 mol% of Eu doped KYF_4[186–188] nanophosphor reveals the activation energy equal to 0.309 eV. This value obtained for the as prepared nanophosphor is relatively high when compared with the values reported in literature for other phosphors [55, 56]. At the end, thermal dependency studies

conducted on 5 mol% of Eu^{3+} doped KYF_4 nanophosphors allows us to contemplates that the as prepared nanophosphors are possessing good thermal stability.

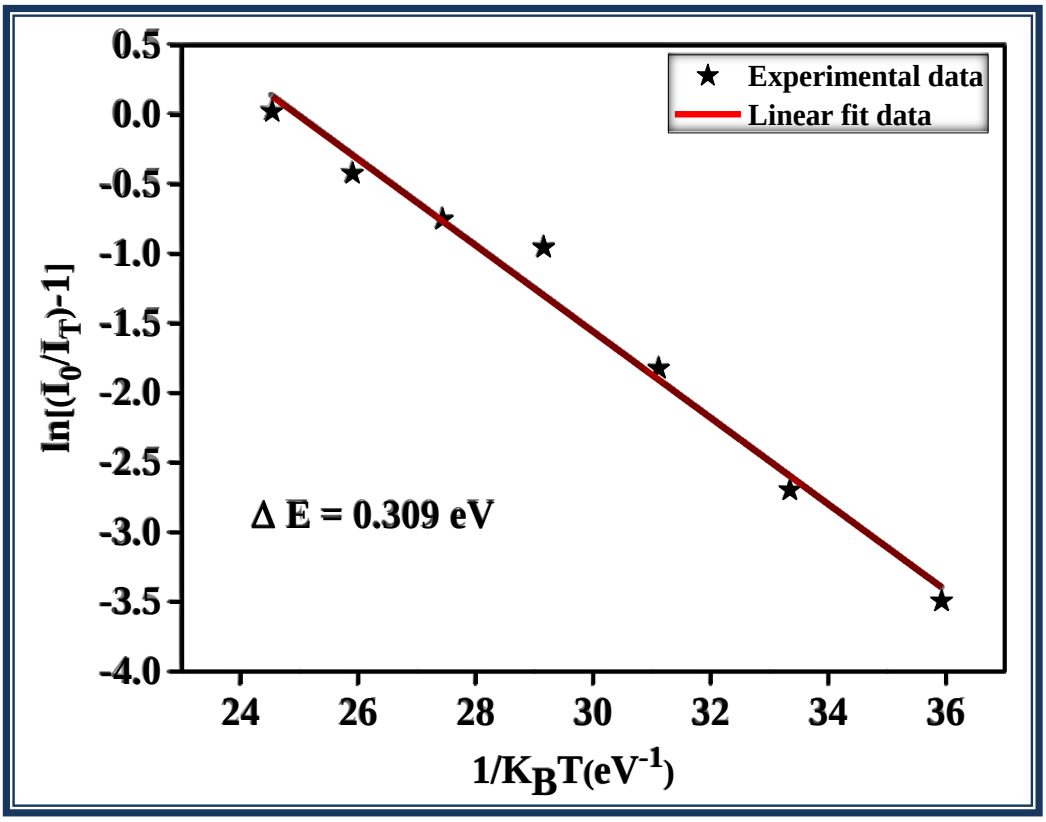

Figure: 6.8. *Activation energy of KYF_4: 5 mol% Eu^{3+} (393 nm excitation).*

6.3.4. The UC PL studies of KYF_4:Eu^{3+}nanophosphors.

Under 800 nm spitfire femtosecond laser excitation, strong red emission from Eu^{3+} doped KYF_4 was easily visible to the naked eye. Fig.3.9 depicts the UC emission spectra of *x* mol% Eu^{3+} (*x* = 1 to 5%) doped KYF_4 nanophosphors. The PL spectra show lower order transitions $^5D_0 \rightarrow {}^7F_0$, $^7F_1$, $^7F_2$, $^7F_3$, $^7F_4$ corresponding to the peaks 576, 590, 612, 650, 700 nm respectively along with higher order transitions $^5D_1 \rightarrow {}^7F_0$, $^7F_1$, $^7F_2$ corresponds to the peaks 523 531, 552 nm, respectively. Higher order transitions are only because of low phonon energies in the host lattice, which ultimately helps in patronizing the radiative probabilities of the sample. The hosts such as $AREF_4$ (A = Na, K) contains relatively low phonon energies and hence the europium

ions excited to higher $^5D_2$ level deactivate to the lower energies levels such as $^5D_1$ and $^5D_0$ through non-radiative multi-phonon relaxation process [189]7].

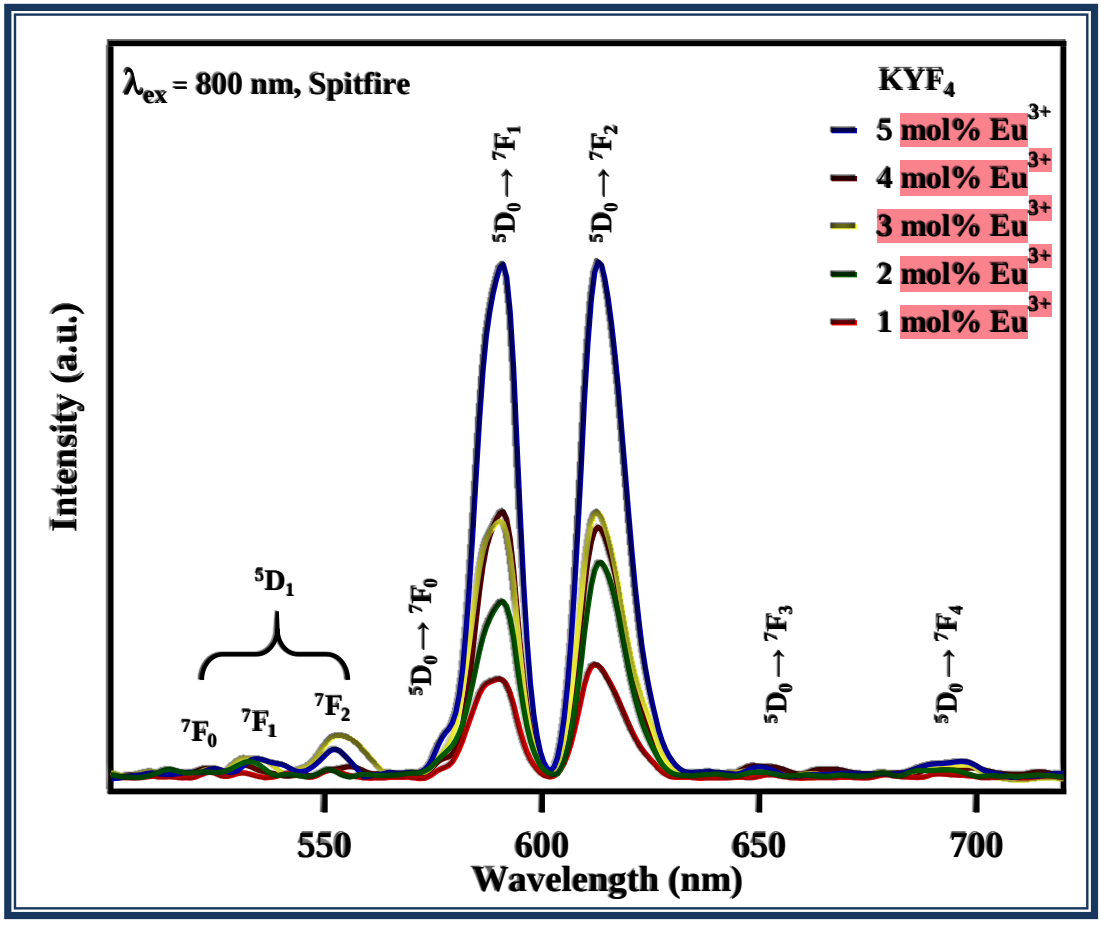

Figure: 6.9. *UC PL spectra of KYF_4: x mol% Eu^{3+}nanoparticles (x = 0 - 5%) under 800 nm spitfire femtosecond laser excitation.*

In case of Eu doped phosphors/glasses, it is not possible to obtain visible emission through a single photon absorption process from infrared pumping. However, in such Eu doped matrices, visible emission is possible through up-conversion process. Fig. 3.10 shows a typical energy level diagram of Eu in a host matrix. A multiphoton UC process (800 nm excitation in the present case) excites the electrons to 5d level Eu^{3+} and produces visible emission as shown in Fig.10. In the energy level diagram of Eu as shown in Fig.3.10, there is no any intermediate state around the 12500 cm^{-1} which corresponds to the 800 nm photon between the ground state

and luminescent excited state for Eu^{3+}. Therefore, single photon NIR excitation cannot produce any visible emission in case of Eu doped matrix. However, under continuous excitation of 800 nm photons, visible emission is possible as shown in Fig.3.9.

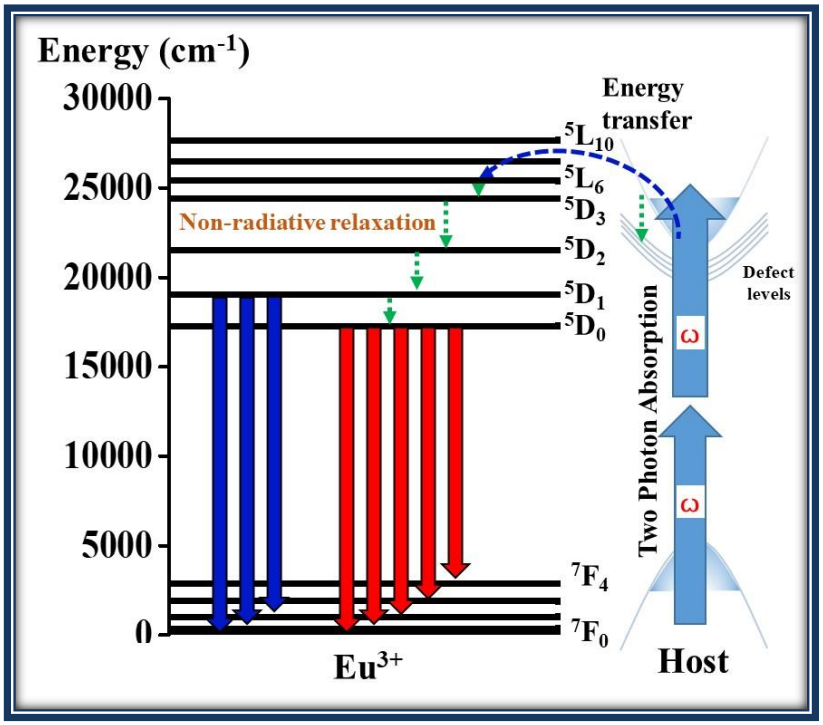

Figure: 6.10. *Schematic energy level diagram and UC mechanism of Eu^{3+} ion in KYF_4 doped with x mol% Eu^{3+} (x = 1, 2, 3, 4, 5) pumped by 800 nm spitfire femtosecond laser.*

When electrons are pumped from ground state to higher level $^7F_0 \rightarrow {}^5L_6$ via two photon absorption (as shown in Fig. 3.10), the electrons at $^5L_6$ level non-radiatively relax to $^5D_3$, $^5D_2$, $^5D_1$ and $^5D_0$ levels and radiatively transfers energy to the ground states ^7F_J (J = 0 - 4). As a result, the characteristic UC luminescence emission of Eu^{3+} occurs as depicted in Fig.10 [190]. Thus, a two-photon absorption is responsible for the up-conversion under 800 nm femtosecond laser excitation.

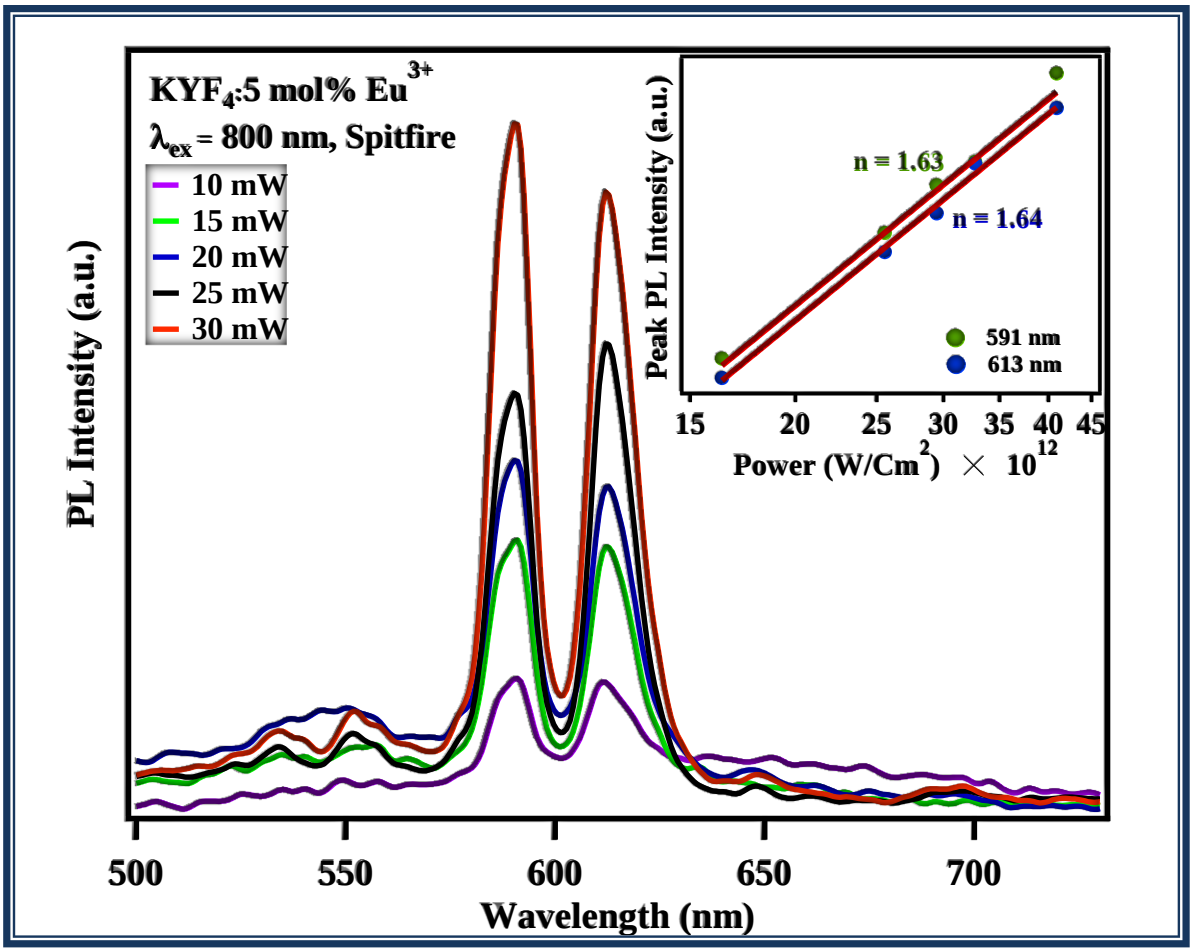

Figure: 6.11. *Powder dependent UC spectra of KYF_4: x mol% Eu^{3+} nanoparticles (x = 5%) under 800 nm spitfire femtosecond laser excitation. The inset figure shows the log-log dependence of UC PL intensity ($^5D_0 \rightarrow {}^7F_1, {}^5D_0 \rightarrow {}^7F_2$) on pump power.*

To have a further confirmation for two-photon excitation process, power dependence studies have been carried out on 5 mol% Eu^{3+} doped KYF_4 under 800 nm femtosecond spitfire laser excitation and is shown in Fig.3.11. Because of multiphoton involvement, the relationship between UC emission intensity of $^5D_0 \rightarrow {}^7F_1$ and $^5D_0 \rightarrow {}^7F_2$ transitions and the pump power of the incident laser was analyzed through the following equation:

$$I \alpha P^n$$

here I is up-conversion emission intensity, P is the pump power of the laser (femtosecond one), n denotes photon number [191][192]. The inset of Fig. 3.11. shows the log-log dependence of UC luminescence intensity of $^5D_0 \rightarrow {}^7F_1$, $^5D_0 \rightarrow {}^7F_2$ peaks on pump power. From the inset figure, it can be seen that the slope is below or nearby 2 (n = 1.64) this may be because of contribution of cross-relaxation process in the multiphoton process. This suggests that the energy transfer involved in the up-conversion energy transfer process in the as prepared phosphors is through two photon process. Two photon luminescence of KYF_4 doped with *x* mol% Eu^{3+} (*x* = 1, 2, 3, 4, 5) is a general phenomenon. The calculated CIE color coordinates of UC KYF_4 doped with different concentration of Eu^{3+} also lies in red region as shown in Fig. 6.12.

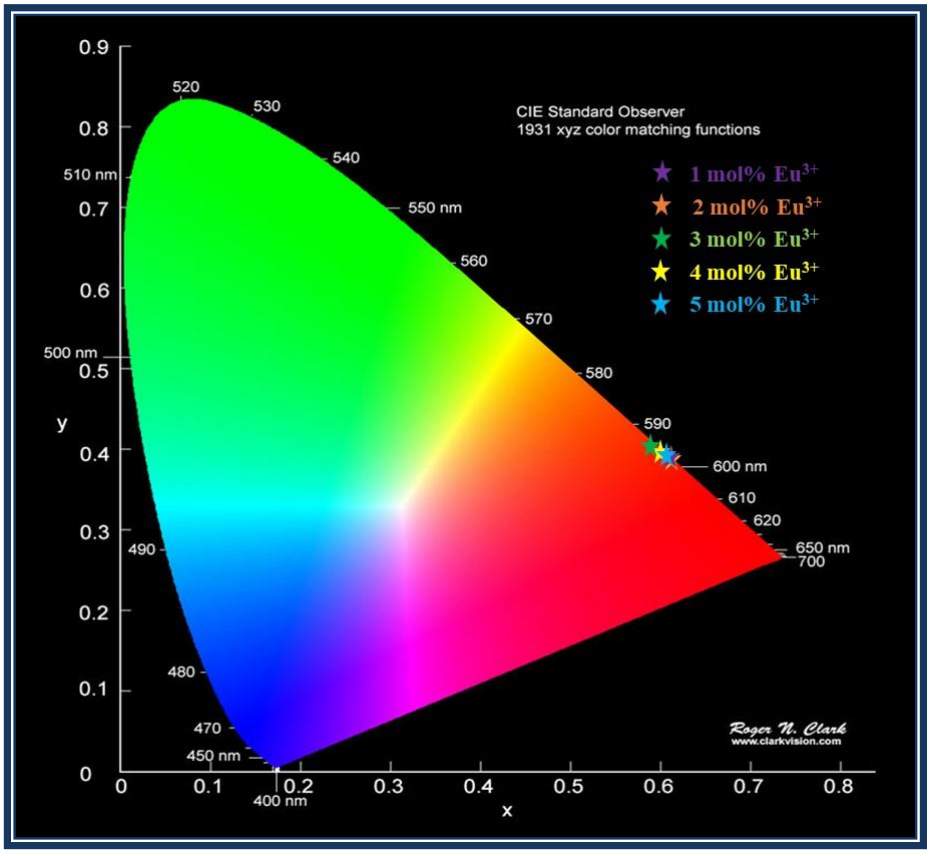

Figure: 6.12. *CIE diagram of UC KYF_4: x mol% Eu^{3+} (x = 0 - 5%) nanophosphor under 800 nm spitfire femtosecond laser excitation.*

6.4. Conclusions

Uniform cubic-phase Eu^{3+} ions doped KYF_4 nanophosphors were synthesized via a wet chemical route method. The particle size and phase crystallinity of *x* mol% of Eu^{3+} (*x* = 0 to 5) doped KYF_4 phosphors was examined by powder XRD at the room temperature. The average crystal size estimated from the Debye-Scherrer analysis was in the range of 3 - 4 nm. The SEM and elemental mapping show that all the elements potassium, yttrium, fluorine and europium are uniformly distributed in the crystal structure. The UC of as prepared samples show strong emission peaks at 576, 590, 612, 650, 700 nm which can be attributed to $^5D_0 \rightarrow {}^7F_j$ (J = 0 - 4) transitions under 800 nm laser excitation. This UC phenomenon can be only possible by two-photon simultaneous absorption process. The same visible peaks were observed through DS studies under 393 nm and 405 nm excitation. The powder dependence studies conducted on UC as well as DS studies clearly reveal the excitation process as two photon and single photon respectively. The smaller sizes of the KYF_4 UCNPs (3 - 4 nm) and their ability to emit visible red emission enhances the scope of the as prepared phosphors in various photonic applications. Thermal dependence studies conducted on 5 mol% of Eu^{3+} doped KYF_4 nanophosphors reveals thermal stability and superiority of the as prepared phosphors. Thus, the interesting results obtained finally allows us to contemplate that the as prepared UCNPs are useful for bio-imaging (through UC process) as well as solid state lighting applications (through DS process).

Chapter 7

Summary, Future Scope and Social Impact of the Research Work

This dissertation's seventh chapter provides an overview of the entire research endeavor and the conclusions, social impact derived from the data. This chapter also examines the study's future directions and how it may be applied to guide future research initiatives.

7.1. Conclusions

Glass science and technology experts have prepared a range of glasses utilizing different glass formers and network formers, and they have examined the spectroscopic characteristics of these glasses. The goals of this thesis were outlined in chapter 1 and included creating high-quality optical glasses doped with specific RE ions and maximizing the environment for a variety of photonic uses. Glasses were effectively prepared with the use of single and co-doped RE ions, such as Dy^{3+}, Sm^{3+}, Eu^{3+} doping the melt quenching process. The many characterization methods that we employed in our research, as well as the melt-quenching method, were covered in detail in chapter 2.

In 3rd chapter, Dy^{3+} doped AZABS glasses were prepared using the melt quench technique. Various morphological and photoluminescence studies were conducted on the as-prepared glass samples. Under 350 nm excitation, the glass samples show sharp bands related to transitions from the energy level $^4F_{9/2}$ to the levels $^6H_{15/2}$ (482 nm), $^6H_{13/2}$ (575 nm) and $^6H_{11/2}$ (665nm). Dexter theory analysis showed that the energy transfer between the dopant ions was of dipole-dipole nature. Temperature-dependent photoluminescence studies show that these AZABS glass samples have excellent thermal stabilities. Decay kinetics of the as-prepared glass samples

indicate high lifetimes. Such sharp luminescence intensities under UV excitation coupled with high lifetimes, superior thermal stabilities of luminescence intensities and positive results from colorimetric calculations prove that Dy^{3+} doped AZABS glasses are suitable candidates for applications in w-LEDs and solid-state lighting.

Chapter 4 describes Sm^{3+} doped AZABS glasses have been prepared via quick melt quench technique. To understand the optical and physical characteristics of the as prepared glasses, various characterizations were undertaken. 0.25 mol% Sm^{3+} doped glass showed the highest luminescence intensity under 402 nm excitation and was subsequently chosen for all the optical studies. In the absorption analysis, $^6H_{5/2} \rightarrow {}^6P_{3/2}$, $^4I_{11/2}$, $^6F_{11/2}$, $^6F_{9/2}$, $^6F_{7/2}$, $^6F_{5/2}$, $^6F_{3/2}$, $^6H_{15/2}$ and $^6F_{1/2}$ bands were seen. This data was then utilized to calculate the direct optical band gap of the 0.25 mol% Sm^{3+} doped AZABS glass. The glass shows sharp excitation and emission bands. In the emission spectrum under 402 nm excitation, three bands corresponding to $^4G_{5/2} \rightarrow {}^6H_{5/2}$, $^4G_{5/2} \rightarrow {}^6H_{7/2}$ and $^4G_{5/2} \rightarrow {}^6H_{9/2}$ transitions can be seen. Dexter's analysis of the glass shows that lanthanide interactions are dipole-dipole in nature. These glasses have high thermal stabilities as could be seen from the high value of activation energy obtained from temperature dependent PL data. On the basis of these results along with the fact that these glasses have high lifetimes for the 599 nm emission, we propose to utilise the Sm^{3+} doped AZABS glasses for SSL and w-LEDs applications.

Chapter 5 explain about AZABS glasses doped with *x mol%* Eu^{3+} ions (x = 0.1 to 2.5 mol %) were synthesized via conventional melt quenching technique and investigated using XRD, absorption, PL excitation & emission, temperature dependent PL and PL decay spectral analysis. Amorphous nature of the as synthesized undoped glass has been confirmed from the XRD spectrum. The DSC and TGA shows the thermal stability and aggregate weight loss of an

undoped glass respectively. The total loss of mass observed (16.80%) for and undoped glass indicates its thermal stability at high temperatures. The absorption spectral features recorded for the as prepared glasses are used to estimate optical band gap and found to be in the range from 2.98 to 3.06 eV. The sharp excitation bands observed in the PLE spectra reveals the feasibility of using commercially available UV red LEDs as an excitation source. The R/O ratio observed in the range 3.62 to 3.92 suggests that the Eu^{3+} ions are present at a low symmetry site. Within the Eu^{3+} ions dopant range (0.5 to 2.5 mol%) the AZABS glass containing 2.5 mol% of Eu^{3+} ions possess higher covalency among all the as prepared AZABS glasses. Emission spectral features are subjected to J-O analysis to understand the nature of bonding between the doped RE ions and the surrounding ligands along with the radiative properties of the as prepared glasses. Relatively higher Ω_2 J-O intensity parameter obtained for 2.5 mol% Eu^{3+} in AZABS glass indicates relatively high covalency and low symmetry. This information is in consonance with the result of red to orange (R/O) intensity ratios estimated for as prepared AZABS glasses. The CIE coordinates of all as prepared glasses were located in the red region. The delay profile of the $^5D_0$ level shows bi-exponential nature of all given concentration of europium ions and found that the lifetime of 0.5 mol% Eu^{3+} is 1.98 ms for $^5D_0$ is relatively high. Temperature dependent study conducted on 2.5 mol% of Eu^{3+} doped AZABS glass reveals its thermal stability. All the aforementioned results observed for thermally stable Eu^{3+} doped AZABS glasses finally allows us to contemplate the potentiality of 2.5 mol% Eu^{3+} in AZABS glass for the fabrication of visible photonic devices such as solid-state lightening devices (red component in w-LEDs) and visible red lasers.

6th chapter includes the uniform cubic-phase Eu^{3+} ions doped KYF_4 nanophosphors were synthesized via a wet chemical route method. The particle size and phase crystallinity of *x* mol% of Eu^{3+} (x = 0 to 5) doped KYF_4 phosphors was examined by powder XRD at the room

temperature. The average crystal size estimated from the Debye-Scherrer analysis was in the range of 3 - 4 nm. The SEM and elemental mapping show that all the elements potassium, yttrium, fluorine and europium are uniformly distributed in the crystal structure. The UC of as prepared samples show strong emission peaks at 576, 590, 612, 650, 700 nm which can be attributed to $^5D_0 \rightarrow {}^7F_j$ (J = 0 - 4) transitions under 800 nm laser excitation. This UC phenomenon can be only possible by two-photon simultaneous absorption process. The same visible peaks were observed through DS studies under 393 nm and 405 nm excitation. The powder dependence studies conducted on UC as well as DS studies clearly reveal the excitation process as two photon and single photon respectively. The smaller sizes of the KYF_4 UCNPs (3 - 4 nm) and their ability to emit visible red emission enhances the scope of the as prepared phosphors in various photonic applications. Thermal dependence studies conducted on 5 mol% of Eu^{3+} doped KYF_4 nanophosphors reveals thermal stability and superiority of the as prepared phosphors. Thus, the interesting results obtained finally allows us to contemplate that the as prepared UCNPs are useful for bio-imaging (through UC process) as well as solid state lighting applications (through DS process).

The above-mentioned noteworthy results all attest to the potential utility of the RE doped AZABS glasses and KYF_4 nanophosphors developed in the thesis for photonic applications, including solid-state lasers, LED lighting, bio-photonics, and optical amplifiers.

7.2. Scope of Future Work

A lot of research has been done on luminescent glass, and further research can be done by using the thesis work as a foundation. Some of the research projects that will be undertaken in the future include: -

- To improve the luminous characteristics of our glass substrate by adjusting the combination of distinct co-doped RE ions.
- To evaluate the prepared materials' efficacy in comparison to materials that are used commercially.
- To use prepared glasses and fabricate efficient w-LEDs.
- To increase the glass's usefulness for additional potential uses, like temperature sensors, lasers, and optical fiber applications.
- To analyze the biocompatible characteristics of prepare nanophosphor and their utility in biophotonic devices.

7.3. Social Impact

The as prepare, rare earth (Dy^{3+}, Sm^{3+} and Eu^{3+}) doped AZABS glasses can be directly utilized in advance photonic devices like WLEDs, lasers, optical fibers, and displays, have a significant positive social impact owing to their exceptional properties. Excellent luminescence characteristics under UV excitation coupled with high lifetimes, superior thermal stabilities of luminescence intensities and positive results from colorimetric calculations prove that Dy^{3+} doped AZABS glasses are suitable candidates for applications in w-LEDs and solid-state lighting. Also, Dy^{3+} doped AZABS glasses can be overcome the numerous shortcomings of commercially used phosphor converted w-LEDs. The thermally stable Eu^{3+} doped AZABS glasses allow us to contemplate the potentiality of 2.5 mol% Eu^{3+} in AZABS glass for the fabrication of visible photonic devices such as solid-state lightening devices (red component in w-LEDs) and visible red lasers. Eu^{3+} doped AZABS glasses can enhance the CCT and CRI of commercially used YAG:Ce^{3+} in coated w-LEDs and also functioned as incapsulating agent from external environment.

The smaller sizes of the KYF_4 UCNPs (3 - 4 nm) and their ability to emit visible red emission enhances the scope of the as prepared phosphors in various photonic applications. Thermal dependence studies conducted on 5 mol% of Eu^{3+} doped KYF_4 nanophosphors reveals thermal stability and superiority of the as prepared phosphors. Thus, the interesting results obtained finally allows us to contemplate that the as prepared UCNPs are useful for bio-imaging (through UC process) as well as solid state lighting applications (through DS process). The prepared Eu^{3+} doped KYF_4 nanophosphors can be potential candidates for bio imaging to detect the cancer cell and targeted drug delivery. Owing these exceptional luminescence characteristics, Eu^{3+} doped KYF_4 nanophosphors could play vital role in disease detections, which can be socially benefits for people across the world.

CHAPTER 7

References

[1] M. Rodríguez Chialanza, R. Faccio, H. Bentos Pereira, R. Marotti, Opt Mater (Amst) 123 (2022) 111890.

[2] B.P. Choudhary, N.B. Singh, (2023) 79–112.

[3] M. Giordano, D. Leporini, M.P. Tosi, (1996) 1–392.

[4] J.D. Musgraves, J. Hu, L. Calvez, (2019) 1851.

[5] J.L. Mass, R.E. Stone, M.T. Wypyski, Prehistory and History of Glassmaking Technology (1998) 121–145.

[6] D. Crossley, The Prehistory and History of Glassmaking Technology (1998) 167–179.

[7] H. Wen, G. Jia, C.-K. Duan, P.A. Tanner, Physical Chemistry Chemical Physics 12 (2010) 9933–9937.

[8] H. Wu, X. Zhang, C. Guo, J. Xu, M. Wu, Q. Su, IEEE Photonics Technology Letters 17 (2005) 1160–1162.

[9] H. Wen, B.M. Cheng, P.A. Tanner, RSC Adv 7 (2017) 26411–26419.

[10] P. Vani, G. Vinitha, M.I. Sayyed, M.M. AlShammari, N. Manikandan, Nuclear Engineering and Technology 53 (2021) 4106–4113.

[11] K. Maheshwari, Ravita, A. Prasad, Y. Tayal, A.S. Rao, Opt Mater (Amst) 140 (2023).

[12] S. Kumar Ray, Y.K. Kshetri, S. Wohn Lee -, P. Linna Guo, Y. Wang, J. Zhang, al -, nanotubes Zepeng Li, J. Wang, L. Wang, E. Erol, N. Vahedigharehchopogh, O. Kıbrıslı, elikbilek Ersundu, A. Erç in Ersundu, Journal of Physics: Condensed Matter 33 (2021) 483001.

[13] Y. Wang, W. Zheng, Y. Lu, P. Li, S. Xu, J. Zhang, J Lumin 237 (2021) 118152.

[14] L.P. Naranjo, N.T.C. Oliveira, L.R.P. Kassab, C.B. de Araújo, J Lumin 238 (2021) 118225.

[15] X. Li, J. Cao, Y. Wei, Z. Yang, H. Guo, Journal of the American Ceramic Society 98 (2015) 3824–3830.

[16] C.B. Annapurna Devi, S. Mahamuda, M. Venkateswarlu, K. Swapna, A. Srinivasa Rao, G. Vijaya Prakash, Opt Mater (Amst) 62 (2016) 569–577.

[17] B.N.K. Reddy, B.D. Raju, K. Thyagarajan, R. Ramanaiah, Y.D. Jho, B.S. Reddy, Ceram Int 43 (2017) 8886–8892.

[18] K. Jha, M. Jayasimhadri, Journal of American Ceramic Society (2017) 1402–1411.

[19] A.G. Clare, P.F. Wachtel, J.D. Musgraves, Springer Handbooks (2019) 595–616.

[20] A. Zakery, S.R. Elliott, Springer Series in Optical Sciences 135 (2007) 1–193.

[21] Optical Nonlinearities in Chalcogenide Glasses and Their Applications (2007) 1–28.

[22] F. N, A. G, YMER Digital 21 (2022) 111–126.

[23] L.D. Pye, R. Locker, M.J. Plodinec, Materials Science Research 15 (1983) 627–637.

[24] M. Kuwik, J. Pisarska, W.A. Pisarski, Materials 13 (2020) 1–20.

[25] R. Baños, F. Manzano-Agugliaro, F.G. Montoya, C. Gil, A. Alcayde, J. Gómez, Renewable and Sustainable Energy Reviews 15 (2011) 1753–1766.

[26] Introduction to Glass Science and Technology Second Edition, n.d.

[27] L.U. Khan, Z.U. Khan, Handbook of Materials Characterization (2018) 345–404.

[28] J. Zhou, Q. Liu, W. Feng, Y. Sun, F. Li, Chem Rev 115 (2014) 395–465.

[29] G. Blasse, B.C. Grabmaier, (1994).

[30] H.K. Yang, J.H. Jeong, Society 12 (2010) 226–230.

[31] A. Escudero, M.E. Calvo, S. Rivera-ferna, (2013).

[32] P. Yasaka, J. Kaewkhao, in: Proceedings - 2015 4th International Conference on Instrumentation, Communications, Information Technology and Biomedical

Engineering, ICICI-BME 2015, Institute of Electrical and Electronics Engineers Inc., 2016, pp. 4–15.

[33] S. Gai, C. Li, P. Yang, J. Lin, Chem Rev 114 (2014) 2343–2389.

[34] Luminescence: Phenomena, Materials and Applications & Special Attention to Borate Host Materials, n.d.

[35] D. Chen, Z. Wan, Y. Zhou, X. Zhou, Y. Yu, J. Zhong, M. Ding, Z. Ji, ACS Appl Mater Interfaces 7 (2015) 19484–19493.

[36] C. Feldmann, T. Justel, C.R. Ronda, P.J. Schmidt, Adv Funct Mater 13 (2003) 511–516.

[37] B.R. Judd, J Chem Phys 44 (1966) 839–840.

[38] G.S. Opelt, J Chem Phys 37 (1962) 511–520.

[39] X. Wang, Q. Liu, Y. Bu, C.S. Liu, T. Liu, X. Yan, RSC Adv 5 (2015) 86219–86236.

[40] G.C. Righini, F. Enrichi, L. Zur, M. Ferrari, J Phys Conf Ser 1221 (2019) 012028.

[41] B. Hou, M. Jia, P. Li, G. Liu, Z. Sun, Z. Fu, Inorg Chem 58 (2019) 7939–7946.

[42] V.B. Pawade, H.C. Swart, S.J. Dhoble, Renewable and Sustainable Energy Reviews 52 (2015) 596–612.

[43] N. Yao, J. Huang, K. Fu, X. Deng, M. Ding, X. Xu, RSC Adv 6 (2016) 17546–17559.

[44] T.H. Kim, W. Wang, Q. Li, Front Chem Sci Eng 6 (2012) 13–26.

[45] G. Blasse, Philips Res. Rep. 24 (1969) 131–144.

[46] L.G. Van Uitert, J Electrochem Soc 114 (1967) 1048–1053.

[47] Y. Tian, B. Chen, B. Tian, R. Hua, J. Sun, L. Cheng, H. Zhong, X. Li, J. Zhang, Y. Zheng, T. Yu, L. Huang, Q. Meng, J Alloys Compd 509 (2011) 6096–6101.

[48] J.A. Duffy, M.D. Ingram, J Non Cryst Solids 21 (1976) 373–410.

[49] M. Kumar, A.S. Rao, Opt Mater (Amst) 109 (2020) 110356.

[50] Z. Boruc, B. Fetlinski, M. Kaczkan, S. Turczynski, D. Pawlak, M. Malinowski, J Alloys Compd 532 (2012) 92–97.

[51] B. Tian, B. Chen, Y. Tian, J. Sun, X. Li, J. Zhang, H. Zhong, L. Cheng, R. Hua, Journal of Physics and Chemistry of Solids 73 (2012) 1314–1319.

[52] R.Y. Yang, Y.M. Peng, H.L. Lai, C.J. Chu, B. Chiou, Y.K. Su, Opt Mater (Amst) 35 (2013) 1719–1723.

[53] B. Szpikowska-Sroka, N. Pawlik, T. Goryczka, M. Bańczyk, W.A. Pisarski, J Lumin 188 (2017) 400–408.

[54] L.J. Curtis, H.G. Berry, J. Bromander, Phys Scr 2 (2007) 216–220.

[55] B.C. Jamalaiah, J. Suresh Kumar, A. Mohan Babu, L. Rama Moorthy, K. Jang, H.S. Lee, M. Jayasimhadri, J.H. Jeong, H. Choi, J Lumin 129 (2009) 1023–1028.

[56] D. Haranath, V. Shanker, H. Chander, P. Sharma, Mater Chem Phys 78 (2002) 6–10.

[57] M.K. Sahu, M. Jayasimhadri, J Lumin 227 (2020) 117570.

[58] H. Kaur, M. Jayasimhadri, Ceram Int 45 (2019) 15385–15393.

[59] K. Jha, A.K. Vishwakarma, M. Jayasimhadri, D. Haranath, K. Jang, J Non Cryst Solids 553 (2021) 120516.

[60] N. Deopa, A.S. Rao, Opt Mater (Amst) 72 (2017) 31–39.

[61] A. Kumar, Anu, M.K. Sahu, Ravita, S. Dahiya, N. Deopa, A. Malik, R. Punia, A.S. Rao, J Lumin 244 (2022) 118676.

[62] S. Kaur, A.S. Rao, M. Jayasimhadri, Ceram Int 43 (2017) 7401–7407.

[63] S.B. Mallur, T.C. Khoo, S. Rijal, O.R. Huff, P.K. Babu, Mater Chem Phys 258 (2021) 123886.

[64] R.A. Talewar, S. Mahamuda, A. Vyas, A.S. Rao, S. V. Moharil, J Alloys Compd 775 (2019) 810–817.

[65] R.A. Talewar, S. Mahamuda, K. Swapna, A.S. Rao, J Alloys Compd 771 (2019) 980–986.

[66] Y. Tayal, A.S. Rao, Opt Mater (Amst) 107 (2020) 110070.

[67] A.A. El-Maaref, K.S. Shaaban, M. Abdelawwad, Y.B. Saddeek, Opt Mater (Amst) 72 (2017) 169–176.

[68] C. Zuo, Z. Zhou, L. Zhu, A. Xiao, Y. Chen, Mater Res Bull 83 (2016) 155–159.

[69] J. Zarzycki, Science (1979) 267 (1995) 1887.

[70] R.A. Talewar, S. Mahamuda, K. Swapna, M. Venkateswarlu, A.S. Rao, Mater Res Bull 105 (2018) 45–54.

[71] M. Wagner, Thermal Analysis in Practice (2017) 1–349.

[72] A. Nithya, H.L. Jeevakumari, K. Rokesh, K. Ruckmani, K. Jeganathan, K. Jothivenkatachalam, Journal of Photochemistry and Photobiology B: Biology 153 (2015) 412–422.

[73] S. Vyazovkin, N. Koga, C. Schick, (n.d.).

[74] B. Cullity, Elements of X-Ray Diffraction, Second edition., Addison-Wesley Publishing Company Inc., Reading MA, 1978.

[75] H.M. Moghaddam, S. Nasirian, Nanoscience Methods 1 (2012) 201–212.

[76] J. McKittrick, L.E. Shea-Rohwer, Journal of the American Ceramic Society 97 (2014) 1327–1352.

[77] G. Keresztury, Handbook of Vibrational Spectroscopy (2006).

[78] R.F. Egerton, Physical Principles of Electron Microscopy: An Introduction to TEM, SEM, and AEM (2005) 1–202.

[79] G. Wypych, Handbook of UV Degradation and Stabilization: Second Edition (2015) 1–419.

[80] G. Blasse, A. Bril, Appl Phys Lett 11 (1967) 53–55.

[81] J.R. Lakowicz, Principles of Fluorescence Spectroscopy (1983) 1–18.

[82] M.K. Singh, M.S. Mehata, Optical Materials 109 (2020).

[83] K. Wakabayashi, Y. Yamaguchi, T. Sekiya, S. Kurita, Journal of Luminescence 112 (2005) 50–53.

[84] D. V. O'Connor, D. (David) Phillips, (1984) 288.

[85] K. Swapna, S. Mahamuda, A.S. Rao, T. Sasikala, P. Packiyaraj, L.R. Moorthy, G.V. Prakash, Journal of Luminescence 156 (2014) 80–86.

[86] K. Annapoorani, K. Marimuthu, Journal of Non-Crystalline Solids 463 (2017) 148–157.

[87] S. Arunkumar, K. Marimuthu, AIP Conference Proceedings 1447 (2012) 573–574.

[88] S. Mahamuda, K. Swapna, M. Venkateswarlu, A. Srinivasa Rao, S. Shakya, G. Vijaya Prakash, Journal of Luminescence 154 (2014) 410–424.

[89] S. Mahamuda, K. Swapna, A. Srinivasa Rao, T. Sasikala, L. Rama Moorthy, Physica B: Condensed Matter 428 (2013) 36–42.

[90] A.K. Vishwakarma, M. Jayasimhadri, Journal of Luminescence 176 (2016) 112–117.

[91] C.B. Annapurna Devi, S. Mahamuda, M. Venkateswarlu, K. Swapna, A. Srinivasa Rao, G. Vijaya Prakash, Optical Materials 62 (2016) 569–577.

[92] N. Deopa, A.S. Rao, S. Mahamuda, M. Gupta, M. Jayasimhadri, D. Haranath, G.V. Prakash, Journal of Alloys and Compounds 708 (2017) 911–921.

[93] R. Bajaj, M. Gupta, R. Nagarajan, A.S. Rao, G.V. Prakash, (2020) 10058–10068.

[94] N. Deopa, A.S. Rao, Journal of Luminescence 192 (2017) 832–841.

[95] K. Jha, M. Jayasimhadri, Journal of Alloys and Compounds 688 (2016) 833–840.

[96] N. Deopa, A.S. Rao, S. Mahamuda, M. Gupta, M. Jayasimhadri, D. Haranath, G.V. Prakash, Journal of Alloys and Compounds 708 (2017) 911–921.

[97] K. Jha, A.K. Vishwakarma, M. Jayasimhadri, D. Haranath, Journal of Alloys and Compounds 719 (2017) 116–124.

[98] H. Masai, Y. Yamada, Y. Suzuki, K. Teramura, Y. Kanemitsu, T. Yoko, Scientific Reports 3 (2013) 1–7.

[99] Y. Zhang, C. Lu, L. Sun, Z. Xu, Y. Ni, 44 (2009) 179–183.

[100] N. Deopa, A.S. Rao, Optical Materials 72 (2017) 31–39.

[101] H. Gui, C. Li, C. Lin, Q. Zhang, Z. Luo, L. Han, J. Liu, T. Liu, A. Lu, Journal of the European Ceramic Society 39 (2019) 1397–1410.

[102] N.F. YUSOF, K.H.K. BULAT, N.A. BADARULZAMAN, M.A.A.M. NOR, International Journal of Current Research in Science, Engineering & Technology 1 (2018) 130.

[103] N. Deopa, S. Saini, S. Kaur, A. Prasad, A.S. Rao, Journal of Rare Earths 37 (2019) 52–59.

[104] M.H.A. Mhareb, M. Alqahtani, F. Alshahri, Y.S.M. Alajerami, N. Saleh, N. Alonizan, M.I. Sayyed, M.G.B. Ashiq, T. Ghrib, S.I. Al-Dhafar, T. Alayed, M.A. Morsy, Journal of Non-Crystalline Solids 541 (2020) 120090.

[105] J. Rajagukguk, Fitrilawati, B. Sinaga, J. Kaewkhao, Spectrochimica Acta - Part A: Molecular and Biomolecular Spectroscopy 223 (2019) 117342.

[106] K. Swapna, S. Mahamuda, A. Srinivasa Rao, M. Jayasimhadri, T. Sasikala, L. Rama Moorthy, Ceramics International 39 (2013) 8459–8465.

[107] N. Kiran, A. Suresh Kumar, Journal of Molecular Structure 1054–1055 (2013) 6–11.

[108] A.M. Babu, B.C. Jamalaiah, J.S. Kumar, T. Sasikala, L.R. Moorthy, Journal of Alloys and Compounds 509 (2011) 457–462.

[109] W.T. Carnall, P.R. Fields, K. Rajnak, The Journal of Chemical Physics 49 (1968) 4424–4442.

[110] P. Rekha Rani, M. Venkateswarlu, S. Mahamuda, K. Swapna, N. Deopa, A.S. Rao, Journal of Alloys and Compounds 787 (2019) 503–518.

[111] H. George, N. Deopa, S. Kaur, A. Prasad, M. Sreenivasulu, M. Jayasimhadri, A.S. Rao, Journal of Luminescence 215 (2019).

[112] S. Kaur, M. Jayasimhadri, A.S. Rao, Journal of Alloys and Compounds 697 (2017) 367–373.

[113] A.K. Vishwakarma, M. Jayasimhadri, Journal of Alloys and Compounds 683 (2016) 379–386.

[114] M. Reddi Babu, N. Madhusudhana Rao, A. Mohan Babu, N. Jaidass, C. Krishna Moorthy, L. Rama Moorthy, Optik 127 (2016) 3121–3126.

[115] C.R. Kesavulu, H.J. Kim, S.W. Lee, J. Kaewkhao, N. Chanthima, Y. Tariwong, Journal of Alloys and Compounds 726 (2017) 1062–1071.

[116] L. Mishra, A. Sharma, A.K. Vishwakarma, K. Jha, M. Jayasimhadri, B. V Ratnam, K. Jang, A.S. Rao, R.K. Sinha, Journal of Luminescence 169 (2016) 121–127.

[117] D.L. Dexter, The Journal of Chemical Physics 21 (1953) 836–850.

[118] D.L. Dexter, J.H. Schulman, The Journal of Chemical Physics 22 (1954) 1063–1070.

[119] K. Linganna, C.S. Rao, C.K. Jayasankar, Journal of Quantitative Spectroscopy and Radiative Transfer 118 (2013) 40–48.

[120] M.K. Sahu, M. Jayasimhadri, Journal of Luminescence 227 (2020) 117570.

[121] A. Prasad, A.S. Rao, M. Gupta, G.V. Prakash, Materials Chemistry and Physics 219 (2018) 13–21.

[122] A. Prasad, A.S. Rao, G.V. Prakash, Journal of Molecular Structure 1205 (2020) 127647.

[123] C.S. McCamy, Color Research & Application 17 (1992) 142–144.

[124] L. Wang, M. Xu, H. Zhao, D. Jia, New Journal of Chemistry 40 (2016) 3086–3093.

[125] D. Xu, Z. Yang, J. Sun, X. Gao, J. Du, Journal of Materials Science: Materials in Electronics 27 (2016) 8370–8377.

[126] M.K. Sahu, J. Mula, Journal of the American Ceramic Society 102 (2019) 6087–6099.

[127] R. Bajaj, A.S. Rao, G.V. Prakash, Journal of Alloys and Compounds 885 (2021) 160893.

[128] P. Manasa, F. Ran, C. Basavapoornima, S.R. Depuru, C.K. Jayasankar, Journal of Luminescence 223 (2020) 117210.

[129] L. Han, Q. Zhang, J. Song, Z. Xiao, Y. Qiang, X. Ye, W. You, A. Lu, Journal of Luminescence 221 (2020) 117041.

[130] A.S. Asyikin, M.K. Halimah, A.A. Latif, M.F. Faznny, S.N. Nazrin, Journal of Non-Crystalline Solids 529 (2020) 119777.

[131] Ravina, Naveen, Sheetal, V. Kumar, S. Dahiya, N. Deopa, R. Punia, A.S. Rao, Journal of Luminescence 229 (2021).

[132] S. Mohan, S. Kaur, D.P. Singh, P. Kaur, Optical Materials 73 (2017) 223–233.

[133] A. Prasad, A.S. Rao, G.V. Prakash, Optik - International Journal for Light and Electron Optics 208 (2020) 164538.

[134] R.S. Yadav, S.B. Rai, Journal of Alloys and Compounds 700 (2017) 228–237.

[135] A. Muley, S.B. Dhoble, P. Ramesh, R. Sagar, S.J. Dhoble, Progress in Solid State Chemistry 66 (2022) 100347.

[136] R.H. A. Bergh, G. Craford, A. Duggal, Physics Today 54 (2001) 42–47.

[137] V. Singh, A. Prasad, S. Kaur, A.S. Rao, N. Ravi, V.K. Kummara, Optik 242 (2021) 167263.

[138] X. Zhao, L. Fan, T. Yu, Z. Li, Z. Zou, Optics Express 21 (2013) 31660.

[139] S. Kaur, V. Katyal, V. Plakkot, N. Deopa, A. Prasad, A.S. Rao, Journal of Non-Crystalline Solids 572 (2021) 121106.

[140] N. Deopa, A.S. Rao, M. Gupta, G.V. Prakash, Optical Materials 75 (2018) 127–134.

[141] S.A. Saleem, B.C. Jamalaiah, M. Jayasimhadri, A.S. Rao, K. Jang, L.R. Moorthy, Journal of Quantitative Spectroscopy and Radiative Transfer 112 (2011) 78–84.

[142] P. Manasa, C.K. Jayasankar, Optical Materials 62 (2016) 139–145.

[143] A. Khanna, A. Saini, B. Chen, F. González, C. Pesquera, Journal of Non-Crystalline Solids 373–374 (2013) 34–41.

[144] M. Vijayakumar, K. Marimuthu, Journal of Luminescence 178 (2016) 414–424.

[145] S. Xu, H. Ma, D. Fang, Z. Zhang, Z. Jiang, Journal of Luminescence 117 (2006) 135–140.

[146] N. Deopa, B. Kumar, M.K. Sahu, P.R. Rani, A.S. Rao, Journal of Non-Crystalline Solids 513 (2019) 152–158.

[147] N. Deopa, A.S. Rao, Optical Materials 72 (2017) 31–39.

[148] R. Bajaj, A. Prasad, A.V.S. Yeswanth, P. Rohilla, S. Kaur, Journal of Materials Science: Materials in Electronics 33 (2021) 4782–4793.

[149] A. Rupesh Kumar, T.G.V.M. Rao, N. Veeraiah, M. Rami Reddy, Optical Materials 35 (2013) 402–406.

[150] N. Deopa, S. Saini, S. Kaur, A. Prasad, A.S. Rao, Journal of Rare Earths 37 (2019).

[151] J. Rajagukguk, J. Kaewkhao, M. Djamal, R. Hidayat, Suprijadi, Y. Ruangtaweep, Journal of Molecular Structure 1121 (2016) 180–187.

[152] B.C. Jamalaiah, M.V.V. Kumar, K.R. Gopal, Optical Materials 33 (2011) 1643–1647.

[153] R.S. Yadav, Y. Dwivedi, S.B. Rai, SPECTROCHIMICA ACTA PART A: MOLECULAR AND BIOMOLECULAR SPECTROSCOPY 96 (2012) 148–153.

[154] R.S. Yadav, Journal of Alloys and Compounds 931 (2023) 167579.

[155] R.S. Yadav, S.B. Rai, Optics and Laser Technology 111 (2019) 169–175.

[156] N. Baig, R.S. Yadav, N.S. Dhoble, V.L. Barai, S.J. Dhoble, Journal of Luminescence 215 (2019) 116645.

[157] R. Bajaj, A.S. Rao, G.V. Prakash, Journal of Non-Crystalline Solids 575 (2022) 121184.

[158] I.I. Pm, W.T. Carnall, P.R. Fields, K. Rajnak, The Journal of Chemical Physics 4412 (1968).

[159] S. Mahamuda, K. Swapna, M. Venkateswarlu, A. Srinivasa Rao, S. Shakya, G. Vijaya Prakash, Journal of Luminescence 154 (2014) 410–424.

[160] T. Suhasini, J.S. Kumar, T. Sasikala, K. Jang, H. Sueb, M. Jayasimhadri, J. Hyun, S. Soo, L.R. Moorthy, Optical Materials 31 (2009) 1167–1172.

[161] P. Rohilla, A.S. Rao, Materials Research Bulletin 150 (2022) 111753.

[162] E. Rai, R. Sagar, D. Kumar, A. Kumar, V. Janardhan, S. Bahadur, Solid State Sciences 129 (2022) 106904.

[163] C.S. McCamy, Color Research & Application 17 (1992) 142–144.

[164] W. Feng, C. Han, F. Li, (2013) 5287–5303.

[165] M. Haase, H. Schäfer, (2011) 5808–5829.

[166] F. Wang, X. Liu, F. Wang, (2009) 976–989.

[167] F. Wang, Y. Han, C.S. Lim, Y. Lu, J. Wang, J. Xu, H. Chen, C. Zhang, M. Hong, X. Liu, Nature 463 (2010) 1061–1065.

[168] Z. Wang, J. Hao, H.L.W. Chan, G. Law, W. Wong, K. Wong, M.B. Murphy, T. Su, Z.H. Zhang, S.Q. Zeng, (2011) 2175–2181.

[169] 5 (2013).

[170] D. Nunes, A. Pimentel, M. Matias, A. Ara, F. Silva, S. Garcia, A. Carvalho, E. Fortunato, R. Martins, (n.d.).

[171] C. Li, J. Yang, Z. Quan, P. Yang, D. Kong, J. Lin, (2007) 4933–4942.

[172] R. Liu, D. Tu, Y. Liu, H. Zhu, R. Li, W. Zheng, E. Ma, X. Chen, Nanoscale 4 (2012) 4485–4491.

[173] A. Manuscript, (2013).

[174] H. Wang, C. Duan, P.A. Tanner, (2008) 16651–16654.

[175] L. Wang, X. Li, Z. Li, W. Chu, R. Li, K. Lin, H. Qian, Y. Wang, C. Wu, J. Li, D. Tu, Q. Zhang, L. Song, J. Jiang, (2015) 5528–5533.

[176] B.J. Zeng, J. Su, Z. Li, R. Yan, (2005) 2119–2123.

[177] A. Prasad, A.S. Rao, M. Gupta, G.V. Prakash, Materials Chemistry and Physics 219 (2018) 13–21.

[178] Q. Chen, C. Wang, L. Cheng, W. He, Z. Cheng, Z. Liu, Biomaterials 35 (2014) 2915–2923.

[179] S. Ahmad, S. Das, R. Nagarajan, G. Vijaya Prakash, Optical Materials 36 (2013) 396–401.

[180] S. Das, A. Amarnath Reddy, S. Ahmad, R. Nagarajan, G. Vijaya Prakash, Chemical Physics Letters 508 (2011) 117–120.

[181] L. Yang, K. Kamada, M. Yamashita, T. Akai, (2018) 3–8.

[182] S. Kaur, A.S. Rao, M. Jayasimhadri, Journal of Luminescence 202 (2018) 461–468.

[183] S. Kaur, A.S. Rao, M. Jayasimhadri, B. Sivaiah, D. Haranath, Journal of Alloys and Compounds 802 (2019) 129–138.

[184] A. Manuscript, (2018).

[185] J. Liang, P. Du, H. Guo, L. Sun, B. Li, X. Huang, Dyes and Pigments 157 (2018) 40–46.

[186] D. Xu, Z. Yang, J. Sun, X. Gao, J. Du, Journal of Materials Science: Materials in Electronics 27 (2016) 8370–8377.

[187] K. Li, M. Shang, H. Lian, J. Lin, Inorg Chem 54 (2015) 7992–8002.

[188] P. Li, M. Peng, X. Yin, Z. Ma, G. Dong, Q. Zhang, J. Qiu, Opt Express 21 (2013) 18943–18948.

[189] S. Ahmad, G.V. Prakash, R. Nagarajan, (2012).

[190] J.A. Phys, 063511 (2014) 1–5.

[191] A. You, M.A.Y. Be, I. In, 2076 (2004) 10–13.

[192] D. Wang, H. Fan, Z. Chen, X. Wan, S. Tie, 657 (2016) 115–121.